KAUNAS UNIVERSITY OF TECHNOLOGY

MOHAMMAD SHAHBAKHTI

ASSESSING CONSCIOUSNESS LEVELS USING A SINGLE FRONTAL ELECTROENCEPHALOGRAM CHANNEL

Doctoral dissertation
Technological Sciences, Electrical and Electronics Engineering (T 001)

Kaunas, 2024

The dissertation has been prepared at the Biomedical Engineering Institute of Kaunas University of Technology in 2020-2024. The research has been sponsored by the Research Council of Lithuania.

Research supervisor:
Prof. Dr. Vaidotas MAROZAS (Kaunas University of Technology, Technological Sciences, Electrical and Electronics Engineering, T 001).

Edited by: English language editor Dr. Armandas Rumšas (Publishing House *Technologija*), Lithuanian language editor Aurelija Gražina Rukšaitė (Publishing House *Technologija*).

Dissertation Defence Board of Electrical and Electronics Engineering Science Field:
Prof. Dr. Elena JASIŪNIENĖ (Kaunas University of Technology, Technological Sciences, Electrical and Electronics Engineering, T 001) – **chairperson**;
Prof. Dr. Piotr DURKA (University of Warsaw, Poland, Technological Sciences, Electrical and Electronics Engineering, T 001);
Prof. Dr. Dangirutis NAVIKAS (Kaunas University of Technology, Technological Sciences, Electrical and Electronics Engineering, T 001);
Prof. Dr. Aušra SAUDARGIENĖ (Lithuanian University of Health Sciences, Natural Sciences, Biophysics, N 011, Informatics, N 009);
Prof. Dr. Algimantas VALINEVIČIUS (Kaunas University of Technology, Technological Sciences, Electrical and Electronics Engineering, T 001).

The dissertation defence will be held on 22 October 2024, at 10 a.m. in a public meeting of the Dissertation Defence Board of the Electrical and Electronics Engineering Science Field at the Rectorate hall of Kaunas University of Technology.

Address: K. Donelaičio 73-402, Kaunas, LT-44249, Lithuania.
Phone: (+370) 608 28 527; e-mail: doktorantura@ktu.lt.

The dissertation was sent on 20 September 2024.
The dissertation is available on the internet http://ktu.edu and at the library of Kaunas University of Technology (Gedimino 50, LT-44239 Kaunas, Lithuania).

KAUNO TECHNOLOGIJOS UNIVERSITETAS

MOHAMMAD SHAHBAKHTI

SĄMONĖS LYGIŲ ĮVERTINIMAS NAUDOJANT VIENĄ FRONTALINĮ ELEKTROENCEFALOGRAMOS KANALĄ

Daktaro disertacija
Technologijos mokslai, elektros ir elektronikos inžinerija (T 001)

2024, Kaunas

Disertacija rengta 2020–2024 metais Kauno technologijos universiteto Biomedicininės inžinerijos institute. Mokslinius tyrimus rėmė Lietuvos mokslo taryba.

Mokslinis vadovas:
prof. dr. Vaidotas MAROZAS (Kauno technologijos universitetas, technologijos mokslai, elektros ir elektronikos inžinerija, T 001).

Redagavo: anglų kalbos redaktorius dr. Armandas Rumšas (leidykla „Technologija“), lietuvių kalbos redaktorė Aurelija Gražina Rukšaitė (leidykla „Technologija“).

Elektros ir elektronikos inžinerijos mokslo krypties disertacijos gynimo taryba:
prof. dr. Elena JASIŪNIENĖ (Kauno technologijos universitetas, technologijos mokslai, elektros ir elektronikos inžinerija, T 001) – **pirmininkė**;
prof. dr. Piotr DURKA (Varšuvos universitetas, Lenkija, technologijos mokslai, elektros ir elektronikos inžinerija, T 001);
prof. dr. Dangirutis NAVIKAS (Kauno technologijos universitetas, technologijos mokslai, elektros ir elektronikos inžinerija, T 001);
prof. dr. Aušra SAUDARGIENĖ (Lietuvos sveikatos mokslų universitetas, gamtos mokslai, biofizika, N 011, informatika, N 009);
prof. dr. Algimantas VALINEVIČIUS (Kauno technologijos universitetas, technologijos mokslai, elektros ir elektronikos inžinerija, T 001).

Disertacija bus ginama viešame Elektros ir elektronikos inžinerijos mokslo krypties disertacijos gynimo tarybos posėdyje 2024 m. spalio 22 d. 10 val. Kauno technologijos universiteto Rektorato salėje.

Adresas: K. Donelaičio g. 73-402, Kaunas, LT-44249, Lietuva.
Tel. (+370) 608 28 527; el. paštas doktorantura@ktu.lt.

Disertacija išsiųsta 2024 m. rugsėjo 20 d.
Su disertacija galima susipažinti interneto svetainėje http://ktu.edu ir Kauno technologijos universiteto bibliotekoje (Gedimino g. 50, LT-44239 Kaunas, Lietuva).

In loving memory of my dear mother, whose unwavering support and enduring love continue to inspire me, though she is no longer with me.

— Rest in Peace Maman Narges

TABLE OF CONTENTS

List of Abbreviations **8**

List of Figures **9**

List of Tables **13**

INTRODUCTION **15**

1. EEG ARTIFACT REMOVAL **22**
1.1. Electrical Shift and Linear Trends 22
1.1.1. The proposed SWT-kurtosis algorithm 24
1.1.2. Data 27
1.1.3. Results 29
1.1.4. Discussion 30
1.2. Eye Blinks 33
1.2.1. The proposed VME-DWT algorithm 34
1.2.2. Data 39
1.2.3. Results 40
1.2.4. Discussion 44
1.3. Conclusions of the Chapter 45

2. SLEEP ASSESSMENT **47**
2.1. Discrimination of Wakefulness from Sleep Stage I 47
2.1.1. The proposed algorithm 48
2.1.2. Data 52
2.1.3. Results 54
2.1.4. Discussion 56
2.2. Conclusions of the Chapter 58

3. DRIVER FATIGUE DETECTION **59**
3.1. The Influence of Eye Blink Artifacts on Prefrontal EEG Signals for Detection of Driver Fatigue 59
3.1.1. The proposed algorithm for simultaneous eye blink characterization and elimination 60
3.1.2. Data 65
3.1.3. Results 65
3.1.4. Discussion 68
3.2. Fusion of EEG and Eye Blink Analysis using a Single Fp1 Channel . . . 69
3.2.1. The proposed algorithm 71
3.2.2. Data 77
3.2.3. Results 77

3.2.4. Discussion 81
3.3. Conclusions of the Chapter 83

4. DEPTH OF ANESTHESIA MONITORING 84
4.1. Entropy-based DoA Monitoring 85
4.1.1. The proposed entropy-based algorithm for DoA monitoring . . . 86
4.1.2. Data 89
4.1.3. Results 89
4.1.4. Discussion 91
4.2. Parameter-Free Feature Set for DoA Monitoring 92
4.2.1. The proposed algorithm 93
4.2.2. Data 96
4.2.3. Results 97
4.2.4. Discussion 100
4.3. Conclusions of the Chapter 102

5. CONCLUSIONS 103

6. SANTRAUKA 105

REFERENCES 134

CURRICULUM VITAE 152

LIST OF PUBLICATIONS ON THE DOCTORAL THESIS SUBJECT 153

LIST OF PUBLICATIONS WHICH ARE NOT DIRECTLY RELATED TO THE TOPIC OF DOCTORAL DISSERTATION 156

ACKNOWLEDGMENTS 158

List of Abbreviations

ABA	Average blink amplitude
ABD	Average blink distance
Acc	Accuracy
AppEn	Approximate entropy
AWICA	Automatic wavelet-independent component analysis
BIS	Bispectral index
BR	Blink rate
CC	Correlation coefficient
DispEn	Dispersion entropy
DoA	Depth of anesthesia
DWT	Discrete wavelet transform
EAWICA	Enhanced automatic wavelet-independent component analysis
EEG	Electroencephalography
ESLT	Electrical shifts and linear trends
FuzzEn	Fuzzy entropy
HFD	Higuchi's fractal dimension
KFD	Katz's fractal dimension
LeEn	Log energy entropy
MAE	Mean absolute error
MAICA	Moving average independent component analysis
MSD	Moving standard deviation
NCA	Neighborhood component analysis
NRMSE	Normalized root mean square error
PCA	Principal component analysis
RBP	Relative band power
RF	Random forest
RRMSE	Relative root mean square error
SampEn	Sample entropy
SE	Shannon entropy
Sen	Sensitivity
SlopEn	Slope entropy
SNR	Signal-to-noise ratio
Spe	Specificity
SpEn	Spectral entropy
SVM	Support vector machine
SWT	Stationary wavelet transform
VME	Variational mode extraction

List of Figures

1 EEG electrode placement based on the 10-10 system, adopted from [15]. 16
2 Placement of NeuroSky's MindWave headset electrodes according to the 10-20 international system, adopted from [16,17]. 17

1.1 Example on artifacts in EEG signals, adopted from [28]. 22
1.2 The visual presentation of Daubechies 1 wavelet function. 24
1.3 EEG signals: contaminated (**a**), artifact-free (**b**) and the corresponding distributions (**c**). k is the kurtosis value. 25
1.4 Examples of artifact-free EEG (**a**), ESLT artifact (**b**), white noise (**c**), and contaminated EEG signal (**d**). 28
1.5 Mean$\pm$standard deviation of CC **(a)** and NRMSE **(b)** between the ESLT-free and filtered EEG signals for different T values of the development data. 29
1.6 Examples of contaminated (**a**), and EEG signals filtered by the SWT-kurtosis (**b**), AWICA (**c**), and EAWICA (**d**) algorithms. 30
1.7 Beeswarm plot of CC (**a**), NRMSE (**b**) and PSNR (**c**) between the ESLT-free and the filtered EEG signals for the SWT-kurtosis, AWICA, and EAWICA algorithms. μ and σ stand for mean and SD. 31
1.8 Examples of real contaminated EEG signals (**a**) and the corresponding filtered EEG signals by the proposed SWT-kurtosis (**b**), AWICA (**c**), and EAWICA (**d**) algorithms. 32
1.9 The block diagram of the proposed algorithm. 35
1.10 Examples of a contaminated EEG with a double eye blink **(a)**, extracted VME mode with detected eye blink peaks **(b)**, formed the artifactual window on VME mode **(c)**, and EEG with projected artifactual interval **(d)**. 36
1.11 Examples of eye blink-free **(a)** and contaminated **(b)** EEG signals with the corresponding distributions. S indicates the skewness value. . . . 37
1.12 Examples of contaminated EEG signals with different SNRs **(a)**, the corresponding desired mode extracted by VME **(b)**, the true positive rate **(c)**, and the false positive rate per interval **(d)**. 40
1.13 The mean$\pm$standard deviation of CC **(a)** and RRMSE **(b)** between the eye blink-free and filtered EEG signals. 41
1.14 Examples of contaminated **(a)**, and filtered EEG signals by the VME-DWT **(b)**, DWT **(c)**, and AVMD **(d)** algorithms. 42
1.15 Boxplots of CC **(a)** and RRMSE **(b)** between the eye blink-free and filtered EEG signals for all algorithms. 42
1.16 Columns with examples of real contaminated EEG signal from [71] **(a)**, [72] **(b)**, [73] **(c)**, [74] **(d)**, and below the corresponding filtered EEG signals. 43

2.1 Block diagram of the proposed algorithm for classification of awake and sleep Stage I cases using a single EEG channel. 49
2.2 An example of decomposed EEG signal into its sub-bands by DWT. . 50
2.3 Boxplots of the proposed features in different EEG bands: HFD **(a)**, KFD **(b)**, BubbEn **(c)** , and DispEn **(d)**. 55
2.4 The comparison between Acc, Sen, and Spe values (mean$\pm$standard deviation) for both feature sets using Sleep Telemetry **(a)**, DREAMS **(b)**, DCSM **(c)**, and MESA **(d)** databases. 56
2.5 The ROC curves and the corresponding AUC values using both feature sets for Sleep Telemetry **(a)**, DREAMS **(b)**, DCSM **(c)** , and MESA **(d)** databases. 57

3.1 Block diagram of the proposed algorithm for simultaneous eye blink feature extraction and elimination to improve the quality of driver's status monitoring. Blocks in the green dashed line (circle A) show the steps of the proposed algorithm for eye blink detection (red-colored) and filtering (light blue-colored) from EEG, and blocks in dark blue dashed lines (circle B) demonstrate the procedure of driver fatigue detection by using blink and filtered EEG band power features by SVM (purple-colored). 61
3.2 Eye blink interval detection from Fp1 channel with one **(a)** and two **(b)** blink events. 62
3.3 Examples of EEG signals in alert **(a)** and fatigue **(b)** states. 63
3.4 Examples of two-channel EEG configuration (Fp1 and Fp2) with the corresponding filtered signals in fatigue **(a)** and alert **(b)** states. 66
3.5 The quality improvement of driver fatigue detection when using BR and BA before and after eye blink removal by the proposed algorithm. EB indicates eye blink. 67
3.6 Block diagram of the proposed method for classifying the fatigue and alert driving by using a single Fp1 EEG channel. 71
3.7 An example for EBIs detection from an Fp1 EEG channel. EEG signal **(a)**, the MSD of EEG signal with the local maxima that exceeds Th_1 **(b)**, the MSD with the potential eye blink highest peaks **(c)**, the potential eye blink highest peaks of MSD projected to the EEG **(d)**, the corrected location of the highest eye blink peaks in EEG **(e)**, and the identified EBIs in EEG **(f)**. 73
3.8 An example for extraction of the blink-related features from an Fp1 EEG channel. M stands for the locations of four (i=4) blinks. 74
3.9 The contaminated EEG (dark below) and its corresponding MSDs with different window sizes (green). 78
3.10 Results for EBIs detection and filtering. Database A **(a)-(b)**, and Database B **(c)-(d)**. 79

3.11 Classification results for the detection of driver fatigue by all models. Database A **(a)-(b)**, Database B **(c)-(d)**. 80

4.1 The block diagram of DoA monitoring using different entropy metrics. 86
4.2 Scatter plots between reference and estimated DoA index values for different entropy metrics. 90
4.3 Scatter plots and histograms of AE between reference and estimated DoA index values by employing fused FuzzEn. 91
4.4 The block diagram of the proposed algorithm for DoA monitoring. . . 94
4.5 The selected features (green) by the NCA, categorized based on each sub-band. 98
4.6 An example on how RF (dark blue) **(a)** and SVM (purple) **(b)** follows the trend of references DoA index values (light gray) for one subject from Database II. 99

6.1 EEG elektrodų išdėstymas pagal 10–10 sistemą, adaptuota iš [15] . . . 106
6.2 „NeuroSky“ MindWave ausinių elektrodų išdėstymas pagal 10-20 tarptautinę sistemą, adaptuota iš [16,17] 107
6.3 Tikrų užterštų EEG signalų **(a)** ir filtruotų EEG signalų pavyzdžiai pagal siūlomus SWT kurtozės **(b)**, AWICA **(c)** ir EAWICA **(d)** algoritmus 112
6.4 Stulpeliuose pateikti tikro užteršto EEG signalo pavyzdžiai iš [71] **(a)**, [72] **(b)**, [73] **(c)**, [74] **(d)**, o žemiau – atitinkami filtruoti EEG signalai 115
6.5 Siūlomo budrumo ir I miego stadijos atvejų klasifikavimo, naudojant vieną EEG kanalą, algoritmo blokinė schema 117
6.6 SVM gautų Acc, Sen ir Spe verčių (vidurkis $\pm$ SD) palyginimas, abiem funkcijų rinkiniams naudojant miego telemetrijos **(a)**, DREAMS **(b)**, DCSM **(c)** ir MESA **(d)** duomenų bazes 118
6.7 Siūlomo algoritmo, skirto tuo pačiu metu išskirti ir pašalinti akių mirkčiojimo funkcijas, siekiant pagerinti vairuotojo būklės stebėjimo kokybę, blokinė schema. Blokeliuose, pažymėtuose žaliomis brūkšninėmis linijomis (apskritimas A), parodyti siūlomo akių mirkčiojimo aptikimo (raudona spalva) ir filtravimo (žydra spalva) iš EEG algoritmo etapai, o blokeliuose, pažymėtuose tamsiai mėlynomis brūkšninėmis linijomis (apskritimas B), – vairuotojo nuovargio aptikimo procedūra naudojant mirkčiojimo ir filtruotų EEG juostų galios funkcijas pagal SVM (violetinė spalva) 121
6.8 Vairuotojo nuovargio aptikimo naudojant BR ir BA kokybės pagerėjimas prieš ir po akių mirkčiojimo pašalinimo siūlomu algoritmu. EB reiškia akių mirkčiojimą 121
6.9 Siūlomo metodo, skirto nuovargiui ir budriam vairavimui klasifikuoti, naudojant vieną Fp1 EEG kanalą, blokinė schema 123
6.10 Klasifikavimo rezultatai, nustatant vairuotojo nuovargį pagal visus modelius. A duomenų bazė **(a)-b)**, B duomenų bazė **(c)-d)** 125

6.11 DoA stebėjimo, naudojant skirtingus entropijos rodiklius, blokinė diagrama 127
6.12 AE sklaidos diagramos ir histogramos tarp atskaitos ir apskaičiuotų DoA indekso verčių, naudojant sulietą FuzzEn 128
6.13 Siūlomo DoA stebėsenos algoritmo blokinė schema 130
6.14 NKI pasirinktos funkcijos (žalios), suskirstytos į kategorijas pagal kiekvieną pojuostę 130
6.15 Pavyzdys, kaip atsitiktinio miško (tamsiai mėlyna) **(a)** ir SVM (violetinė) **(b)** modeliai atkartoja vieno II duomenų bazės tiriamojo DoA indekso verčių tendenciją (šviesiai pilka) 131

List of Tables

1.1 Finest artifact marker values for AWICA and EAWICA algorithms. . . 26
1.2 Data description for developing and testing the proposed SWT-kurtosis algorithm. 27
1.3 A brief description of the employed databases for real EEG data analysis. 40
1.4 Percentage of TPR and FPR of VME-DWT for eye blink detection. . . 41
1.5 Percentage of TPR and FPR of VME-DWT for eye blink detection in four real EEG databases. 43
1.6 CC and RRMSE comparison (mean±standard deviation) between the eye blink-free intervals of contaminated and filtered EEG signals for real data. 44

2.1 Description of the used databases in summary. 53
2.2 The average training-validation results of the SVM classifier for all databases using both feature sets. 55

3.1 Mean±standard deviation of Sen, Spe, and Acc for the blink and EEG band power features of raw and filtered EEG signals. 67
3.2 The comparison between eye blink detection methods in terms of mean ± standard deviation of CSI values. 79
3.3 The weighted features by using NCA, (selected features are in bold). . 80
3.4 The comparison between the proposed and state-of-the-art methods. LOSOCV and LOOCV stand for leave-one-subject-out and leave-one-out cross-validation, respectively. 81

4.1 The values of parameters for the other entropy metrics. SD stands for standard deviation. 88
4.2 The performance of each entropy for regressing the DoA index values. 90
4.3 The MAE and CC obtained for the random sampling approach using both Databases. 98
4.4 The MAE and CC obtained for the LOSOCV approach using both Databases. 98
4.5 The comparison between the proposed and state-of-the-art algorithms. LR and LOSOCV represent the linear regression and leave-one-subject-out cross-validation, respectively. 99

6.1 Užterštų ir filtruotų EEG signalų bei užterštų ir filtruotų realių duomenų akių nemirkčiojimo intervalų CC ir RRMSE palyginimas (vidurkis ± SD) (CC ir RRMSE reiškia koreliacijos koeficientą ir santykinę vidutinę kvadratinę paklaidą) 115
6.2 Naudojamų duomenų bazių aprašymo santrauka 117
6.3 Svertinės funkcijos, naudojant NCA (pasirinktos funkcijos paryškintos) 124

6.4 Kiekvienos entropijos rezultatai, regresuojant DoA indekso reikšmes . 127

INTRODUCTION

Relevance of the research

Consciousness refers to the state of being aware of and able to experience sensations, thoughts, and one's environment, which encompasses the subjective aspects of human experience, including perception, self-awareness, and the ability to process information [1]. Consciousness is a multifaceted construct, spanning a continuum from wakefulness, characterized by responsiveness to external stimuli and cognitive engagement, to altered states where individuals may experience a decreased cognitive function or difficulty being easily aroused [2]. As an individual transits from wakefulness into altered states of consciousness, e.g., fatigue, sleep, and anesthesia, consciousness undergoes dynamic shifts associated with distinct neural patterns and subjective experiences [3]. Thus, analyzing the consciousness level holds paramount significance in contexts such as, but not limited to, sleep assessment, fatigue detection, and the depth of anesthesia monitoring, with far-reaching implications for practical and medical applications.

Within the sleep assessment domain, sleep quality is intricately tied to the consciousness level experienced during rest, offering insights into the depth and character of an individual's rejuvenating repose [4]. According to a recent study, almost 25% of the European Union's population suffers from some form of sleep disorder, which adversely influences physical and mental health [5]. The associated treatment costs and the inefficiency of individuals due to poor sleep quality further underscore the importance of addressing sleep-consciousness-related issues.

Fatigue detection is another critical application where consciousness analysis becomes indispensable. Fatigue significantly impairs the cognitive function and alertness [6]. Globally, it is estimated that 14–20% of road accidents occur due to driver fatigue [7]. Just in the United States, a study by the AAA Foundation for Traffic Safety approximated that, annually, more than 328,000 crashes are caused by driver fatigue, of which 109,000 result in an injury and about 6,400 are fatal [8]. Analyzing consciousness levels facilitates the early detection of fatigue-related changes, enabling timely interventions to prevent accidents. By examining the intricate interplay between consciousness and fatigue, researchers can develop advanced driver monitoring systems that enhance road safety.

In the medical field, monitoring the depth of anesthesia is vital for ensuring patient safety during surgical procedures. Analyzing different consciousness levels aids anesthesiologists in maintaining an optimal balance between keeping patients unconscious and minimizing potential side effects. This delicate balance not only contributes to successful surgeries but also prevents complications associated with insufficient or excessive anesthesia [9, 10]. In addition, continuous monitoring of

consciousness levels during anesthesia can provide economic benefits by preventing the wastage of anesthetics, which has been identified as a significant contributor to the overall cost of anesthesia procedures [11]. Thus, such a monitoring benefits the patient and promotes the efficient use of resources in the healthcare system.

Brain, with its intricate neural networks and complex interactions, is the central hub for generating conscious experiences [12]. Neuroscientific evidence consistently correlates specific brain activities with conscious phenomena, thereby highlighting the brain's pivotal role. Studies involving brain injuries, neuroimaging, and neural stimulation affirm the brain as the biological substrate of consciousness [13]. Electroencephalography (EEG) is paramount for analyzing levels of consciousness, providing real-time insights into brain states with high temporal resolution [14]. Its non-invasive nature, portability, and cost-effectiveness make EEG indispensable for studying the dynamics of consciousness across various contexts, from medical applications to cognitive research.

EEG electrodes are strategically placed on the scalp according to standard systems, like the 10-20 and 10-10 systems, which ensure consistent and reproducible measurements. Named based on their underlying brain regions, these electrodes cover critical areas including the frontal (F), temporal (T), parietal (P), occipital (O), and central (C) regions. The positioning follows a systematic nomenclature: odd numbers (1, 3, 5, 7) signify locations on the left hemisphere, while even numbers (2, 4, 6, 8) denote positions on the right. Electrodes placed along the midline of the scalp are labelled with the letter 'z' (zero), such as Fz (frontal midline), Cz (central midline), and Pz (parietal midline) (Fig. 1) [15].

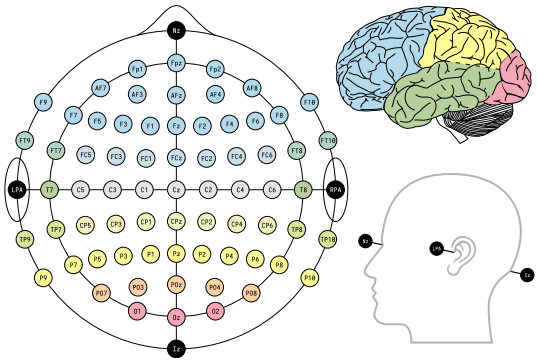

Fig. 1. EEG electrode placement based on the 10-10 system, adopted from [15].

The gap in current research and the potential strategy

While the literature has shown promising results in studying consciousness levels by using EEG, a significant portion of these studies have focused on employing multichannel recordings. This approach adds complexity to wearable instrumentation

and poses challenges for long-term recordings. Furthermore, this configuration not only limits the scalability of EEG studies but also hinders practical applications in real-life scenarios. The intricate setup process and the need for expert oversight make widespread use beyond controlled research environments impractical. Moreover, conventional multichannel EEG systems are prohibitively expensive, making them largely inaccessible for daily use by most individuals. In essence, the focus on multichannel EEG recordings may inadvertently restrict the translation of findings from the laboratory to the real-life scenarios. For EEG-based consciousness level studies to have meaningful applications in daily life, exploring a more affordable, simpler, and user-friendly configuration that can be seamlessly integrated into people's routines is crucial.

A possible remedy to overcome the presently discussed issues is the employment of low-cost portable single frontal channel EEG headbands. These devices offer significant advantages over conventional ones in terms of accessibility, usability, affordability, and real-world applications. By being lightweight and user-friendly, these devices provide a simplified yet effective means of monitoring the brain activity, thereby making the EEG technology more accessible to a broader population. Their affordability makes them particularly appealing for widespread adoption, opening up opportunities for individuals to monitor their cognitive states at home or in various daily-life settings. Furthermore, the simplicity of a single frontal channel design not only reduces the overall cost but also mitigates challenges associated with complex installations and expert oversight, facilitating easy deployment by users with minimal training. Furthermore, recording EEG from the frontal cortex can be more convenient since it is a non-hair-bearing area, i.e., less susceptible to noise, and can provide the user with more comfort by allowing them to use the headrest during the daily life. An example of such a system is NeuroSky's MindWave headset, which offers a user-friendly interface for educational and research purposes, enabling the study of brainwave patterns in diverse environments (Fig. 2) [16, 17].

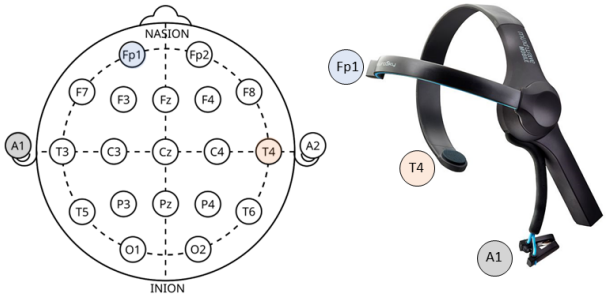

Fig. 2. Placement of NeuroSky's MindWave headset electrodes according to the 10-20 international system, adopted from [16,17].

Scientific-technological problem: Despite the advantages of low-cost wearable EEG systems mentioned above, the limited spatial coverage of a single frontal channel may reduce the richness and specificity of the recorded brain signals, potentially compromising the comprehensiveness of the neural activity information related to different consciousness levels.

Research question: How can the limitation of spatial coverage in single frontal channel EEG recordings be compensated for capturing changes in consciousness levels?

Working hypothesis: Decomposing a single frontal EEG signal into its sub-bands and applying nonlinear analysis may compensate the spatial coverage limitation by capturing distinct complex dynamics associated with changes in consciousness levels.

Research object

This research focuses on the development and investigation of signal processing algorithms for characterizing consciousness levels in sleep assessment, fatigue detection, and anesthesia monitoring using a single frontal EEG channel.

The aim of the research

This doctoral thesis aims to propose methods for monitoring different levels of consciousness using low-cost portable EEG devices, with a focus on real-life applications.

The objectives of the research

1. To develop algorithms to eliminate electrical shifts, linear trends, and eye blink artifacts commonly appearing in EEG data recorded by low-cost portable devices.
2. To develop an algorithm for discrimination between wakefulness and sleep Stage I by using a single frontal EEG channel, thereby enabling the estimation of sleep onset latency, pivotal for assessing the sleep quality.
3. To develop algorithms specifically tailored for the detection of driver fatigue by using current commercial low-cost portable EEG devices.
4. To develop algorithms for monitoring the depth of anesthesia by using commercially available low-cost portable EEG devices.

Scientific novelty

Firstly, this doctoral thesis proposes two new low-complexity algorithms specifically developed to eliminate common artifacts in short segments of single-channel EEG recordings. Unlike existing methods, these algorithms are

optimized for semi-real-time use in portable EEG devices, ensuring robust data analysis within brief time windows, which is crucial for enhancing the reliability of EEG analysis in real-world applications.

Secondly, this thesis introduces a novel perspective on the role of eye blink artifacts in prefrontal EEG signals for detecting driver fatigue. This is the first study to demonstrate that eye blink artifacts can have both beneficial and detrimental effects on EEG signals, challenging the traditional view that these artifacts are merely noise. Understanding these dual effects could lead to improved algorithms for driver fatigue detection, making the findings significant for enhancing the accuracy of EEG-based fatigue monitoring.

Thirdly, this thesis explores the use of nonlinear analysis of EEG sub-bands to classify different levels of consciousness for sleep assessment, driver fatigue detection, and depth of anesthesia monitoring. By applying this analysis with the channel configurations of commercial portable EEG devices, the thesis provides new insights into the real-life applications of these technologies.

In contrast to the majority of studies that utilized only one database for algorithm development and testing, this thesis utilizes multiple databases for both stages. This is particularly significant when incorporating nonlinear features such as sample entropy (SampEn), which necessitate parameter tuning before computation. Addressing the critical issue of the interchangeability of tuned nonlinear features across different databases is essential for ensuring the generality of the proposed method, a consideration often overlooked in the current state-of-the-art methods.

Practical significance

The outcomes of this thesis have practical implications as follows:

1. The proposed artifact reduction algorithms can facilitate improving the data quality for portable EEG-based algorithms that analyze the consciousness levels during daily activities. In addition, the proposed algorithms with their adjusted parameters can be used for improving the quality of EEG signals for other applications.

2. The proposed feature set for discriminating wakefulness for sleep Stage I has the potential to be used for estimation of the sleep onset latency, which is of great importance index for assessing the quality of sleep and insomnia detection.

3. The proposed algorithms for driver fatigue detection allow for the extraction of eye blink features while simultaneously eliminating them from EEG signals. These algorithms are compatible with both single and multi-channel EEG systems and can be utilized in a range of EEG applications, particularly those requiring concurrent analysis of brain activity and eye blinks.

4. The proposed parameter-free feature set for monitoring the depth of anesthesia, while being efficient, offers the opportunity for easy experiment replication

and performance enhancement through the inclusion of additional features.

Approval of the results

The doctoral thesis relies on seven papers published in international scientific journals with the impact factor referred in the *Clarivate Analytics Web of Science* database, while, in total, the results have been published in ten scientific papers. The essential results have been presented in six international conferences.

In 2021 and 2022, promotional scholarships for academic research, granted by the Research Council of Lithuania, were received. In 2021, 2022, and 2023, the awards of the most active PhD student in the field of Electrical and Electronic Engineering, granted by Kaunas University of Technology, were received. In 2021 and 2022, three incentive scholarships for high quality publications, granted by Kaunas University of Technology, were received.

In 2023, one promotional scholarship for academic research in a global competition, granted by the IEEE Signal Processing Society, and three student travel grants for (i) a research visit to Tokyo University of Agriculture and Technology, granted by the Research Council of Lithuania, (ii) participation in the computational neuroscience academy summer school, granted by the Polish National Agency for Academic Exchange, and (iii) participation in the 18th IEEE International Symposium on Medical Measurements and Applications, granted by the IEEE Instrumentation and Measurement Society, were received.

In 2021 and 2022, two published papers from this thesis were recognized as Featured Articles by the editorial boards of the IEEE Transactions on Neural Systems and Rehabilitation Engineering and IEEE Journal of Biomedical Health and Informatics journals.

The statements presented for defense

1. The kurtosis and skewness serve as highly effective indicators for detecting electrical shifts and linear trends, and eye blink artifacts within a short segment of a single EEG channel.

2. Nonlinear features of a single frontal EEG channel outperform conventional relative band power analysis for discriminating between wakefulness and sleep Stage I, which have similar temporal and spectral characteristics.

3. Eye blinks in prefrontal EEG channels serve as a multifaceted component, acting both as a source of valuable information and as an artifact in the detection of driver fatigue.

4. The satisfactory performance of the proposed parameter-free feature set for monitoring the depth of anesthesia via a portable EEG confirms the possibility of an affordable alternative for such monitoring in developing countries.

Structure of the doctoral thesis

This doctoral thesis is organized as follows: Section 1 is dedicated to the elimination of common artifacts that appear in wearable EEG devices, namely, electrical shifts and linear trends, and eye blinks. This section provides a detailed explanation of the proposed algorithms, followed by the obtained results for both semi-simulated and real EEG data. Section 2 presents a nonlinear feature set for discriminating between wakefulness and sleep Stage I, validated on four databases with distinctive characteristics. In Section 3, two algorithms for detecting driver fatigue are proposed. These algorithms are based on the simultaneous analysis of EEG and eye blinks in prefrontal EEG signals. Sections 4 describes two algorithms for monitoring the depth of anesthesia using a single frontal EEG channel. The doctoral thesis wraps up with conclusions in Section 5.

Sections 1 to 4 of the thesis have been quoted verbatim from the previously published articles: [18–27]. The thesis consists of 160 pages, 40 figures, 17 tables, and 237 references.

1. EEG ARTIFACT REMOVAL

Analyzing EEG signals involves dealing with various artifacts, broadly categorized into physiological and non-physiological types. Physiological artifacts originate from the body's natural processes, such as muscle activity, eye movements, and cardiac activity, which can introduce unwanted signals into EEG recordings. On the other hand, non-physiological noise includes environmental interference, equipment artifacts, and other external factors that can distort EEG signals [28] (Fig. 1.1).

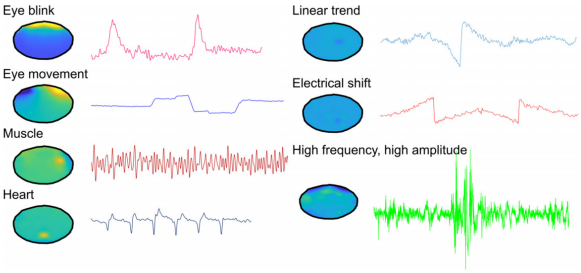

Fig. 1.1. Example on artifacts in EEG signals, adopted from [28].

Although the advent of portable single frontal channel EEG devices has transformed health monitoring and brain-computer interfacing, particularly in indoor and non-clinical environments, specific challenges regarding artifact handling arise when employing such devices due to continuous monitoring in real-world settings. Common artifacts in these devices include electrical shifts-linear trends (ESLT), and eye blinks. ESLT can result from electrode shifts or a temporary decline in the skin-electrode contact, leading to alterations in the baseline EEG signal. Eye blinks, typical physiological phenomena, pose a challenge due to their large amplitude compared to EEG signals.

1.1. Electrical Shift and Linear Trends

Recorded EEG signals with a portable system are more susceptible to non-physiological artifacts than those recorded in laboratory or clinical environments [29] due to the nature of data recording where the subject is free to move and perform their daily-based tasks. While a linear filter could remove the majority of these artifacts, some require more advanced techniques as they may appear in all EEG frequency bands [30]. Amongst them are ESLT, which may arise due to electrode shifts or a temporary decline of the skin-electrode contact, induced current transient drifts, and electrode pop [31–34].

Unfortunately, the elimination of ESLT artifacts from EEG signals has not been

widely regarded in the recent literature [30, 35–37]. Three independent component analysis (ICA) algorithms, named Infomax, SOBI, and FastICA, were firstly presented for EEG denoising with satisfactory ESLT removal [33]. Later, two fully automatic algorithms based on the discrete wavelet transform (DWT) and ICA, known as automatic wavelet independent component analysis (AWICA) [31] and enhanced AWICA (EAWICA) [34], were proposed for the filtering of several types of EEG artifacts including ESLTs. ICA-based algorithms cannot automatically reject the contaminated components and require several artifact markers to separate them from the clean ones. Artifact markers in such algorithms are usually pre-trained and are not adaptive to other databases [38]. In addition, the mentioned algorithm are computationally expensive, which is not favorable for ambulatory or semi-real time applications [30, 33, 37].

In [39], a multi-channel Wiener filter is proposed to eliminate ESLT artifacts from EEG signals [39]. Although it outperformed Infomax ICA, FastICA and canonical component analysis algorithms, the mentioned algorithm needs initial calibration; the user is required to mark some artifactual and non-artifactual segments manually to train the algorithm. Recently, artifact subspace reconstruction algorithm has been proposed for automatic elimination of artifacts in EEG signals, tackling the initial calibration and manual setting of the artifact markers [38]. Its performance, however, relies on a sufficient amount of EEG data and cannot be employed for the single EEG channel.

The proposed algorithms for ESLT removal, albeit with satisfactory performance, were designed for either offline or multi-channel EEG processing. Thus, efficient algorithms for automatic removal of ESLT in a short segment (i.e., $5s$) of single-to-few EEG channels, suitable for portable and low-cost devices are yet lacking. For this aim, wavelet-based (WT) algorithms can be suitable as they overcome the requirement of the initial calibration, several pre-trained artifact markers, and a large amount of EEG channels for filtering. While the effectiveness of WT-based approaches has been demonstrated for EEG signal denoising [37, 40–42], their use for the elimination of ESLT artifacts in EEG signals has not been explored or validated in literature.

Amongst WT algorithms, stationary wavelet transform (SWT) is more effective than DWT for EEG preprocessing since it is time invariant and provides a better time resolution for the artifact characterization. Thus, a smoother EEG is derived after thresholding in the wavelet domain [43, 44]. One of the main challenges in the SWT-based denoising algorithm is to select the optimal level of the decomposition, as EEG signals sampled at different rates may require a different number of decomposition levels [30, 35–37]. The most straightforward approach is to use the full tree decomposition of the contaminated signal and then filter the artifactual components. However, such an approach yields unnecessary computational burdens.

To avoid full decomposition, we introduce a kurtosis-based index for automatic adjustment of the optimal decomposition level of SWT, regardless of the sampling frequency. Using such an index can avoid unnecessary decomposition, make the algorithm automatic, and accelerate filtering. The feasibility of the proposed algorithm is validated on EEG signals recorded at different sampling rates and compared to the performance of AWICA and EAWICA algorithms.

1.1.1. The proposed SWT-kurtosis algorithm

The SWT uses high-pass and low-pass filters to decompose a signal into low and high-frequency bands, designated as the approximation $a(n)$ and detail $d(n)$ components, respectively. Two parameters must be specified before the SWT process: the wavelet basis function and the level of decomposition. The similarity between the wavelet basis function and the desired signal is the criterion for such a selection. Here, Daubechies 1 is selected as the basis wavelet function since it resembles the morphology of ESLT artifacts (Fig. 1.2).

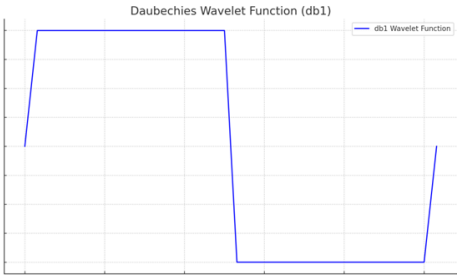

Fig. 1.2. The visual presentation of Daubechies 1 wavelet function.

Determining the decomposition level plays the principal role in designing an automatic SWT-based algorithm. To this end, the kurtosis is employed as the criterion to stop SWT decomposition automatically once it reaches the artifact components. In principle, kurtosis values below 3 can be attributed to either persisting or abruptly varying sample values in EEG recording. As EEG signals are quite dynamic, such behavior cannot be the representative of the brain activity [33]. Thus, it is expected that the prevalence of ESLT artifacts in EEG signals results in a platykurtic distribution (Fig. 1.3) [33, 45].

The ESLT artifacts consist of low and high-frequency components. Thus, these artifacts emerge in both detail and approximation components of SWT. During the SWT decomposition process, the kurtosis of approximation components is calculated at every two consecutive levels. The absolute difference λ of the computed kurtosis values is then used as the decisive factor whether to terminate or continue the SWT

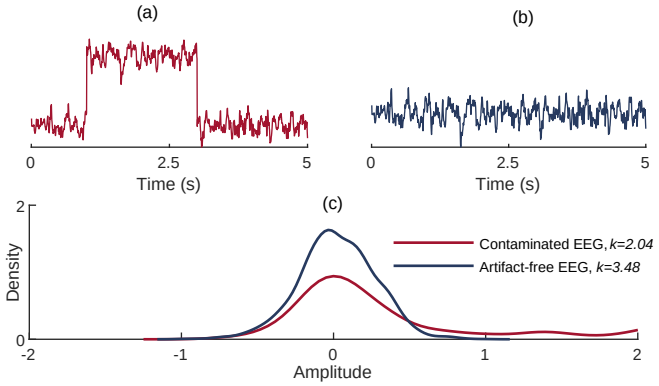

Fig. 1.3. EEG signals: contaminated (**a**), artifact-free (**b**) and the corresponding distributions (**c**). k is the kurtosis value.

decomposition process. λ is estimated as follows:

$$\lambda = |k_j - k_{j-1}|, \tag{1.1}$$

where k is the kurtosis of the approximation components and j is the decomposition level of SWT. If $\lambda > T$, it is assumed that SWT has reached the optimal decomposition level for the artifact component filtering, thereby stopping the decomposition process. The value of T is tuned based on the lowest error between the ESLT-free and filtered EEG signals (see Section 1.1.3). The last approximation component, $a_j(n)$, is removed to eliminate the low frequency components of the artifacts. Then, the obtained detail components are denoised to remove the artifact's high frequency components. Filtering of the detail components is performed based on the following thresholding function [37]:

$$d_\theta(n) = \begin{cases} d(n), & \text{if } |d(n)| \leq \theta \\ 0, & \text{otherwise} \end{cases}, \tag{1.2}$$

θ indicates the universal threshold estimated by:

$$\theta = \frac{\text{median}(|d(n)|)}{0.6745}\sqrt{2\log N}, \tag{1.3}$$

where $d(n)$ is the detail component and N is the signal length in samples. The processed EEG signal is then reconstructed by inverse SWT of the denoised detail components. Algorithm 1 displays the step of the proposed SWT-kurtosis for the elimination of ESLT artifacts.

Algorithm 1: SWT-kurtosis for ESLT removal

Input: Noisy EEG $z(n)$,
Output: Filtered EEG $\hat{x}(n)$
Initialisation $\lambda \leftarrow 0, j \leftarrow 2$
while true **do**
  $[d_{j-1}(n), a_{j-1}(n)] \leftarrow$SWT$(z(n), j-1)$
  $[d_j(n), a_j(n)] \leftarrow$SWT$(z(n), j)$
  $k_{j-1} \leftarrow$CalculateKurtosis$(a_{j-1}(n))$
  $k_j \leftarrow$CalculateKurtosis$(a_j(n))$
  $\lambda \leftarrow |k_j - k_{j-1}|$
  if $\lambda > T$ **then**
    Remove $a_j(n)$
    Denoise $d_1(n), ..., d_j(n)$ components with Eq. **1.2**
    $\hat{x}(n) \leftarrow$ Inverse SWT(*Denoised* $d_1(n), ..., d_j(n)$)
    break
  else
    $j \leftarrow j + 1$
  end if
end while
return $\hat{x}(n)$

Algorithms under comparison

The performance of the proposed algorithm is compared with the AWICA and EAWICA algorithms. These algorithms combine the DWT and ICA methods, in which DWT decomposes the EEG signal into its rhythms, followed by ICA for denoising. Both algorithms apply a two-step procedure by employing kurtosis and Renyi's entropy to detect and eliminate artifacts from EEG signals. For this purpose, three artifact markers must be set before processing. The finest parameters of the mentioned algorithms are shown in Table 1.1. For more details about AWICA and EAWICA algorithms, see [34].

Table 1.1. Finest artifact marker values for AWICA and EAWICA algorithms.

Algorithm	Parameters		
	Th1	Th2	Entropy order
AWICA	1	1.4	2
EAWICA	1.2	1	6

Performance metrics

To assess the filtering performance, the normalized root mean square error (NRMSE), the peak-signal-to-noise ratio (PSNR), and the correlation coefficient (CC) between the ESLT-free and filtered EEG signals are computed. NRMSE is expressed as follows:

$$\text{NRMSE} = \frac{\sqrt{\text{MSE}(x(n) - \hat{x}(n))}}{\max_{x(n)} - \min_{x(n)}} \times 100, \tag{1.4}$$

where MSE is the mean square error, $x(n)$ is the ESLT-free EEG signal and $\hat{x}(n)$ is the filtered EEG signal. NRMSE shows the average amplitude difference between the ESLT-free and filtered signal, where a smaller NRMSE corresponds to the better quality of the filtered signal. PSNR (dB) is defined as follows:

$$\text{PSNR} = 20\log_{10}\left(\frac{\max_{x(n)}}{\sqrt{\text{MSE}(x(n) - \hat{x}(n))}}\right), \tag{1.5}$$

PSNR is used to measure the peak error of the denoised signal. Essentially, PSNR evaluates the reconstruction loss quality, where a higher PSNR indicates the better quality of the reconstructed signal. CC is expressed as:

$$\text{CC} = \frac{\text{cov}(x(n), \hat{x}(n))}{\sigma_{x(n)}\sigma_{\hat{x}(n)}}, \tag{1.6}$$

where cov and σ stand for the covariance and standard deviation, respectively. CC evaluates the degree of linear dependence (phase distortion) between the ESLT-free and filtered signal.

1.1.2. Data

To develop and test the performance of algorithms, both semi-simulated and real data with different sampling frequencies have been employed. Table 1.2 describes the characteristics of the used databases.

Table 1.2. Data description for developing and testing the proposed SWT-kurtosis algorithm.

Database	Mendeley	CHB-MIT	EEGLAB
Sampling rate	200 Hz	256 Hz	128 Hz
Data type	Semi-simulated	Semi-simulated	Real
Usage	Development	Test	Test
Measurement type	Uni-polar	Bi-polar	Uni-polar

Semi-simulated data for the algorithm development

To develop our algorithm and select the T value, generated ESLT artifacts are added to artifact-free EEG signals collected from Mendeley semi-simulated EEG/EOG database [46]. The EEG signals were recorded from electrodes positioned according to the International System 10-20 and sampled at 200 Hz. These signals were carefully recorded to avoid the emergence of undesired biological and external interference. Ninety-five EEG epochs with a length of 5 seconds have been manually chosen from different channels. To produce semi-simulated data, triangular and rectangular waves with a different bandwidth and amplitudes have been added to the EEG signals as follows:

$$z(n) = x(n) + a \times r(n) + v(n), \tag{1.7}$$

where $z(n)$ is the contaminated EEG signal, $x(n)$ is the artifact-free EEG, $r(n)$ is the ESLT artifact, and $v(n)$ is a white noise (Fig. 1.4). The term a is used to indicate that the artifact's power may differ for all EEG channels. Therefore, the developing set for the algorithm includes a total of 95 contaminated EEG signals with different signal-to-noise ratios (SNR).

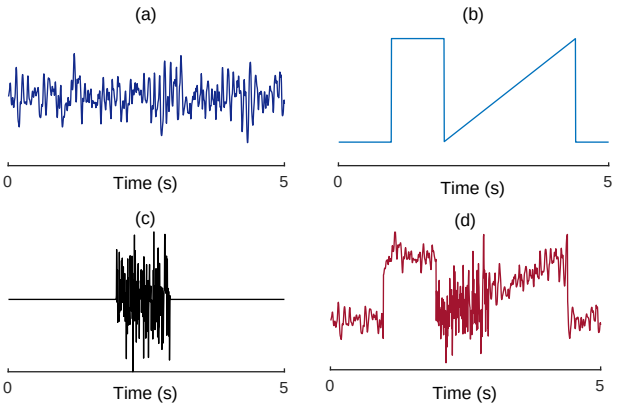

Fig. 1.4. Examples of artifact-free EEG (**a**), ESLT artifact (**b**), white noise (**c**), and contaminated EEG signal (**d**).

It should be noted that these data are used exclusively at the development stage, whereas, other databases are used for evaluating the algorithm's performance.

Semi-simulated data for the algorithm testing

To quantify the performance of the algorithms, another experiment is conducted with semi-simulated EEG signals sampled at 256 Hz with a length of 5 seconds collected from the CHB-MIT Scalp EEG database [47]. Selecting EEG segments from this database ensures a more realistic evaluation of the algorithm's performance as

these EEG signals contain other artifacts and waveform complexity. Considering four a values, the testing set of the algorithms includes a total of 48×4=192 contaminated EEG signals with different SNRs. It should be noted that the procedure to generate semi-simulated data for the algorithm testing is identical to that described in the previous section.

Real data

The EEG-LAB database [48] is comprised of EEG signals contaminated with several real artifacts, sampled at 128 Hz with a length of 238 seconds. Epochs that contain ESLT artifacts are manually selected to test the efficiency of the proposed algorithm.

1.1.3. Results

Threshold value tuning

In order to achieve an effective threshold value, T, four values ranging from 0.05 to 0.2 with a step of 0.05 are tested. T is adjusted with respect to the lowest mean NRSME and the highest mean CC values between 95 epochs of the ESLT-free and filtered EEG signals from the first semi-simulated data, which, in this study, is $T = 0.1$, as shown in Fig. 1.5. The semi-simulated CHB-MIT and real EEG-LAB data are filtered by $T = 0.1$.

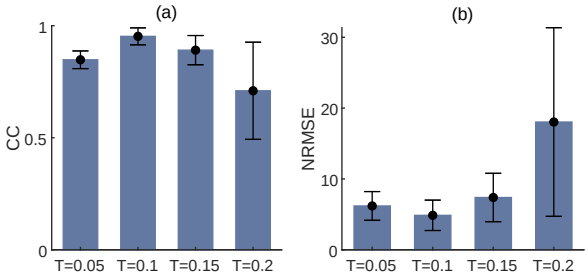

Fig. 1.5. Mean±standard deviation of CC **(a)** and NRMSE **(b)** between the ESLT-free and filtered EEG signals for different T values of the development data.

Filtering results for the testing data

Fig. 1.6 depicts examples of contaminated, and filtered EEG signals using all algorithms. In terms of visual inspection, the proposed algorithm shows enhanced performance than the AWICA and EAWICA in the removal of the prominent ESLT components.

Fig. 1.7 displays Beeswarm plot of the CC, NRMSE and PSNR values between

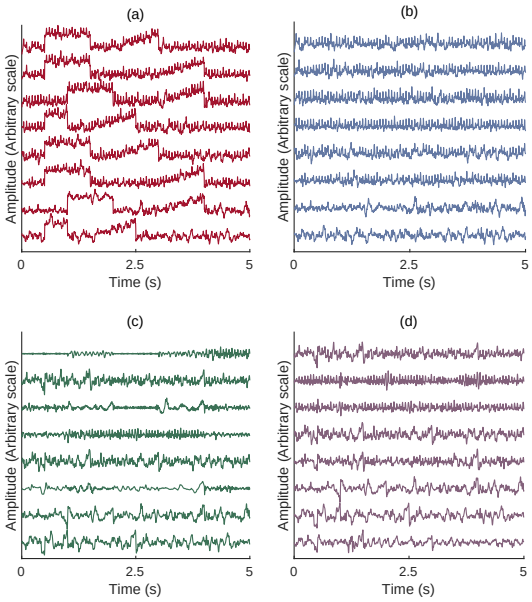

Fig. 1.6. Examples of contaminated (**a**), and EEG signals filtered by the SWT-kurtosis (**b**), AWICA (**c**), and EAWICA (**d**) algorithms.

the ESLT-free and the filtered EEG signals using all algorithms. Compared to AWICA and EAWICA, the SWT-kurtosis based algorithm displays higher mean of CC (0.92 vs. 0.58, 0.67) and PSNR (20.3 dB vs. 13.0, 13.6 dB), and lower mean of NRMSE (5.4 vs. 12.2, 11.5) values, suggesting that the EEG signals filtered by the proposed algorithm better approximate the original ESLT-free ones.

As for real data, Fig. 1.8 illustrates 5s long of 12 contaminated and filtered EEG signals. Due to the lack of real artifact-free EEG signals, the resultant filtered EEG signals from real EEG-LAB data are examined exclusively with the temporal inspection [34, 39, 40, 49]. According to the visual assessment of an EEG expert, the proposed algorithm successfully removed the artifact components. Surprisingly, AWICA and EAWICA were unable to remove the artifacts properly, having even modified the EEG components in some of the signals (#1 and #2).

1.1.4. Discussion

Here, an efficient SWT-based algorithm for ESLT removal in single-to-few EEG channels was introduced, which, compared to the conventional WT-based methods, does not require full tree decomposition of contaminated EEG signals for denoising. Instead, the proposed algorithm automatically terminates SWT decomposition when it reaches ESLT components. Automatic selection of the optimal decomposition level avoids unnecessary additional decomposition steps and speeds up the filtering

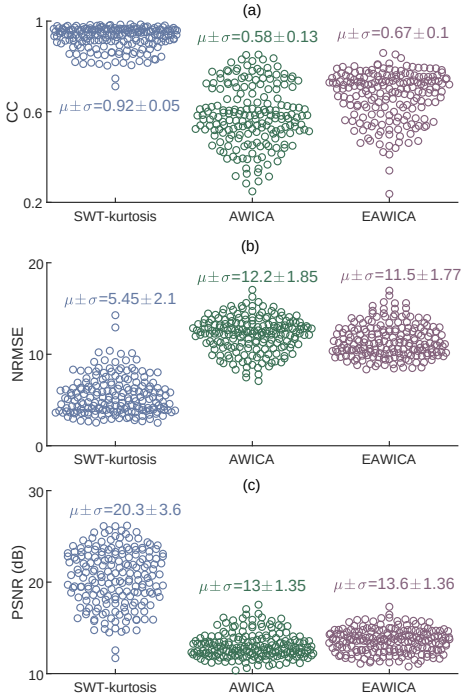

Fig. 1.7. Beeswarm plot of CC (**a**), NRMSE (**b**) and PSNR (**c**) between the ESLT-free and the filtered EEG signals for the SWT-kurtosis, AWICA, and EAWICA algorithms. μ and σ stand for mean and SD.

execution. In contrast to previously reported algorithms for ESLT removal, the proposed algorithm (i) mitigates the need for a large amount of EEG channels as it can adequately eliminate ESLT artifacts in a short segment of single-to-few EEG channels; (ii) is less dependent on human intervention since only one parameter is required to be set and such a parameter seems to be interchangeable between datasets; and (iii) dispenses initial calibration. With such characteristics, the proposed algorithm can be suitable for removing ESLT artifacts in portable single frontal channel EEG headbands.

The automatic SWT-based algorithm's success entails proper threshold selection criteria to stop the decomposition process and denoise the extracted components. Typically, the SWT decomposition level selection depends on the sampling frequency; consequently, EEG signals sampled at different rates require different decomposition levels for the denoising. The proposed algorithm mitigates this problem by combining SWT-based decomposition with kurtosis analysis to automate the selection of the final wavelet decomposition level, independently of the sampling frequency. This novelty was demonstrated by purposefully choosing databases with distinct sampling frequencies (128 Hz, 200 Hz and 256 Hz) to evaluate the proposed algorithm's performance. The AWICA and EAWICA algorithms, while automatic, are more computationally complex as they apply a two-step decision procedure based on the

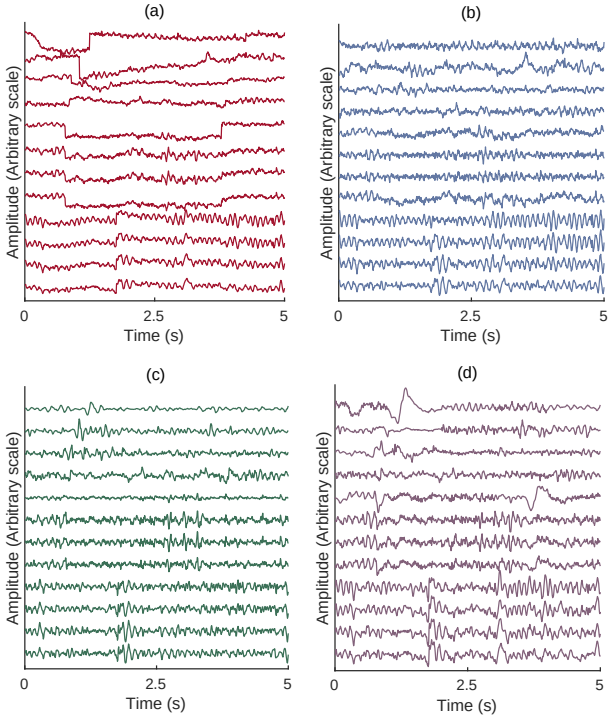

Fig. 1.8. Examples of real contaminated EEG signals (**a**) and the corresponding filtered EEG signals by the proposed SWT-kurtosis (**b**), AWICA (**c**), and EAWICA (**d**) algorithms.

kurtosis and Renyi's entropy to detect and eliminate artifacts, and rely on two signal decomposition-based methods (ICA and DWT). Moreover, the selection of artifactual components is only performed after the complete signal decomposition with DWT. Conversely, the proposed algorithm terminates SWT decomposition once the optimal level has been reached, thus decreasing the computational time.

In the semi-simulated EEG signals, the proposed algorithm demonstrated superior performance in comparison to these of AWICA AWICA and EAWICA with: (i) a higher mean of CC values, indicating more desirable phase preservation; (ii) a higher mean of PSNR values, suggesting better quality reconstructed signals; and (iii) a lower mean of NRMSE values, indicating more robust filtering. The same filtering behavior has been confirmed by the visual comparison of the filtered EEG signals contaminated with real ESLT artifacts. While the proposed algorithm effectively eliminated the artifacts and preserved the EEG components, the AWICA and EAWICA algorithms failed to remove artifact components completely, while even eliminating some desirable parts of the EEG signals. A plausible explanation for this could be that the AWICA and EAWICA algorithms erroneously set the artifacts markers, thereby eliminating desirable EEG parts instead of the artifacts. The selected artifact markers

are, however, according to the authors' guidelines. Nevertheless, the erroneous artifacts markers selection further emphasizes the disadvantage of the AWICA and EAWICA algorithms, while there is the need to set such markers accurately for each used database. The lack of interchangeability of set artifacts markers is a significant drawback in ambulatory EEG signals, as it is unrealistic to predict the most suitable markers for ESLT artifacts removal.

1.2. Eye Blinks

Among the physiological artifacts in EEG, eye blinks are prominent in frontal channels due to their amplitude, frequent occurrence (12 to 15 per minute), proximity to the electrodes, and the frequency range [50]. Eye blinks are involuntary and, thus, unavoidable in EEG recordings [51]. One possible solution is to record EEG with eyes-closed, however, such a recording can yield the undesirable alternation of EEG rhythms [52] and evidently is not applicable in experiments with visual stimulation. Specially for single frontal channel EEG devices, the filtering of eye blinks is crucial before further processing to avoid an erroneous brain activity analysis [51]. While numerous algorithms are available for multi-channel and offline eye blink filtering [38, 53, 54], unsupervised algorithms capable of removing eye blinks in a short segment of a single-channel EEG for real and semi-real time applications such as brain-computer interfacing are still lacking.

Subtraction, regression, and adaptive filters are amongst the most straightforward methods for eye blink removal in the single EEG channel. However, such filters require the artifact reference channel, thus increasing the hardware complexity, which is disadvantageous for portable single channel EEG headbands. Additionally, algorithms based on such filters presume that no bidirectional contamination exists between the recorded artifact reference and the desired EEG, which is not always correct [50].

Signal decomposition algorithms such as wavelet [40, 55, 56], empirical mode decomposition (EMD) [57], and variational mode decomposition (VMD) [58] require no artifact reference channel. Indeed, an automatic algorithm based on VMD and linear regression (AVMD) [59] was proposed for the removal of eye blinks in short segments of single-channel EEG, outperforming EMD, ensemble EMD, ICA, and wavelet-enhanced ICA algorithms. A common problem of signal decomposition-based algorithms is the inability to limit filtering to the actual artifactual eye blink interval, typically 200–400 ms long [60]. Instead, such algorithms filter the whole segment of the contaminated EEG signal, e.g., 3s, which can eliminate some of the non-artifactual components of EEG signals. Thus, algorithms capable of restricting filtering to the artifactual intervals without compromising the desired EEG components are needed.

Restricting filtering to the artifactual eye blink interval could be accomplished by using artifact detection strategies, such as amplitude thresholding, derivatives, or

template matching. Amplitude threshold-based algorithms show limitations when other high amplitude artifacts appear [61]. Moreover, eye blinks with an amplitude lower than the threshold cannot be detected [62]. Derivative-based algorithms detect sudden changes by presuming that a triangular-shape morphology represents an eye blink event [63], which is a controversial presumption [64]. Lastly, template matching algorithms employ a threshold to assess the similarity between EEG segments and a provided template. Thus, the success of template matching algorithms depends on correctly defining both the template and the threshold value. The iterative template matching and suppression algorithm [64] was proposed to detect and eliminate eye blinks from a single-channel EEG with an automatic threshold and template estimation. Despite the excellent performance, this algorithm is only applicable for offline processing since it requires a sufficient number of eye blink events for an accurate filtering. In specific portable-EEG applications, real-time removal of eye blinks is crucial, meaning that algorithms must filter the artifactual intervals in short segments.

Here, an efficient algorithm, VME-DWT, is presented for the unsupervised detection and filtering of eye blinks in a short segment (i.e., 3s) of a single-channel EEG without the mentioned limitations. The artifactual eye blink intervals are detected by using variational mode extraction (VME) [65], followed by an automatic DWT to filter the contaminated intervals. VME extracts an approximation of the eye blink signal from the contaminated EEG, facilitating the search for the eye blink peak to form the artifactual interval. DWT then only filters the selected interval, preserving the non-artifactual intervals of EEG signals, without requiring any prior calibration or artifact reference. The performance of VME-DWT is investigated on both semi-simulated and real contaminated EEG signals and then compared to the AVMD [59] and DWT [55] algorithms, which, as mentioned above, have been developed for the eye blink filtering in short segments of the single-channel EEG.

1.2.1. The proposed VME-DWT algorithm

The VME firstly extracts an approximation of the eye blink signal to localize the highest eye blink peaks, and detects the artifactual intervals containing eye blinks. Then the identified intervals are filtered by using DWT, maximizing the preservation of eye blink-free EEG. The block diagram of the proposed algorithm is shown in Fig. 1.9.

Eye blink detection using VME

The VME algorithm requires two parameters to be set: the compactness coefficient α and the approximate value of the center frequency ω_d of the desired mode. Although the authors in [65] recommend high α values to ensure that the

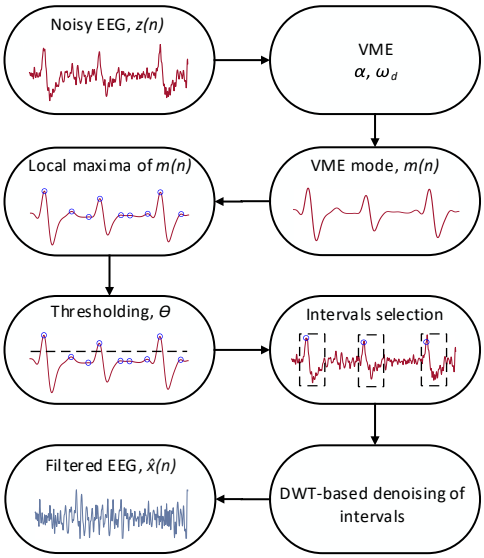

Fig. 1.9. The block diagram of the proposed algorithm.

detected center frequency is related to the desired mode, smaller α values are better suited to extract all eye blink-related components due to the eye blink frequency range (0.5–7.5 Hz) and its spectral overlapping in EEG signals. To find the best α fit, we initialize α at 7000, decreasing with a 1000-step until 2000. The approximate center frequency is selected based on the eye blink frequency to a value of 3 Hz.

After extracting the desired mode, $m(n)$, the eye blinks peaks are located by computing the local maxima of $m(n)$ that have values greater than the universal threshold defined in (Eq. 1.3) [40, 45, 54]. After localizing every eye blink's highest peak in $m(n)$, they will be projected to contaminated EEG to set intervals for the time-selective filtering of eye blink components. Since the eye blink duration varies from 200 to 400 ms [45,60,66,67], a 500 ms interval (125 ms pre- and 375 ms post the highest amplitude peak) is chosen to ensure that all eye blink components are included even if the algorithm does not precisely localize the highest eye blink peak.

Double eye blink

In some cases, two eye blink events might overlap. While the proposed algorithm can detect them, the filtering is performed twice, thus, increasing computational complexity and yielding extra data loss. To overcome this issue, a simple criterion that measures the distance between the identified eye blink peaks is employed. If the distance between two eye blink peaks is smaller than 500 ms, the artifactual window is updated to 125 ms pre-first highest eye blink peak and 375 ms post-second highest eye blink peak (Fig. 1.10).

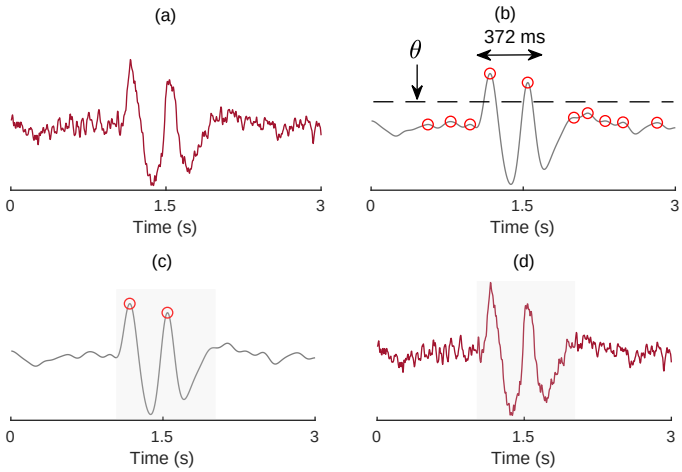

Fig. 1.10. Examples of a contaminated EEG with a double eye blink **(a)**, extracted VME mode with detected eye blink peaks **(b)**, formed the artifactual window on VME mode **(c)**, and EEG with projected artifactual interval **(d)**.

Eye blink filtering by using DWT

DWT decomposes an input signal $x(n)$ into low and high frequency components known as approximation $a(n)$ and detail components $d(n)$, respectively. The original input signal can be reconstructed entirely by $x(n) = \sum_{l=1}^{L} d_l(n) + a_L(n)$, where L is the number of the decomposition level.

DWT requires two parameters to be set: the mother wavelet and the decomposition level. Analogously to previous studies [34, 68], Daubechies 4 is selected as the mother wavelet as its morphology resembles that of eye blinks. The selection of the decomposition level is a more painstaking task as EEG signals from different databases might require a distinctive number of decomposition levels for denoising [34,37,40,42]. The most straightforward approach is to employ the full tree decomposition, however, such an approach may increase unnecessary computational requirements. To this end, we use a skewness-based index to control and find the best decomposition level. Since the eye blink amplitude is significantly higher than the EEG signal, its emergence can lead to an asymmetric distribution of the EEG signal [57, 69, 70]. Thus, large absolute skewness values in DWT components can indicate the eye blink existence (Fig. 1.11).

Compared to the EEG signal, the eye blink is a low-frequency phenomenon. Thus, its components are expected to emerge in the approximations $a(n)$ of the decomposed signal. The absolute difference of skewness values at two consecutive approximation components is, therefore, used as the decisive factor whether to terminate or continue the decomposition process:

$$\delta = ||S_j| - |S_{j-1}||, \tag{1.8}$$

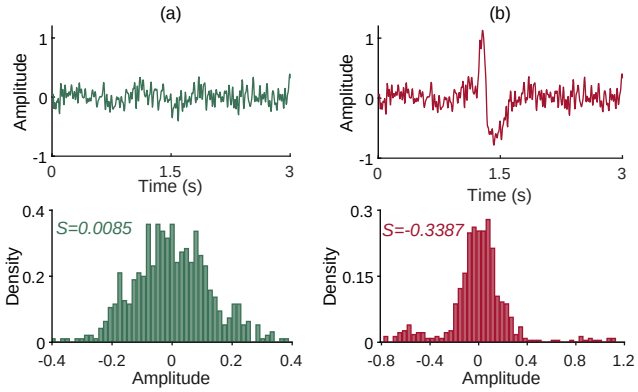

Fig. 1.11. Examples of eye blink-free **(a)** and contaminated **(b)** EEG signals with the corresponding distributions. S indicates the skewness value.

where S is the skewness and j is the level of decomposition. If $\delta > T$, it can be assumed that DWT has reached the blink components. The threshold value, T, is tuned based on the lowest error between the eye blink-free and filtered EEG signals. The main steps of the proposed VME-DWT are summarized in Algorithm 2.

Algorithms under comparison

To compare the performance of the proposed algorithm, AVMD and DWT algorithms, proposed for eye blink filtering in a short segment of single-channel EEG, were used.

AVMD

The key steps of AVMD are to (i) decompose the contaminated EEG signal into 12 modes by VMD, (ii) find the artifactual modes based on amplitude and frequency thresholds, (iii) employ the summation of the artifactual modes as the input of linear regression to estimate the eye blink in the contaminated EEG signals, and (iv) subtract the estimated eye blink from the contaminated EEG signal. The required parameters of AVMD have been set as described in [59].

DWT

The basis of the DWT denoising algorithm is to (i) decompose the input signal into l levels of coefficients by using a basis function, (ii) set the coefficients of each level with a higher value than the threshold to zero, and (iii) reconstruct the denoised signal with inverse DWT. In [55], four basis functions, *haar*, *coif*3, *sym*3, and *bior*4.4 with universal and statistical thresholding have been investigated. According to the authors, *bior*4.4 basis function with the statistical thresholding can be the finest choice for eye blink removal.

Algorithm 2: VME-DWT for eye blink removal

Input: Noisy EEG $z(n)$, α, ω_d, Fs, T
Output: Filtered EEG $\hat{x}(n)$

Initialisation $\theta, \delta \leftarrow 0, j \leftarrow 2$
{*Detect Artifactual Interval*}
$m(n) \leftarrow$VME$(z(n), \alpha, \omega_d)$
$\theta \leftarrow$ Eq. **2.6**
for $i = 2$ to $3 * Fs - 1$ **do**
  if $m(i) > m(i-1)$ && $m(i) > m(i+1)$ && $m(i) > \theta$ **then**
    $onset \leftarrow i - 0.125 \times Fs$
    $offset \leftarrow i + 0.375 \times Fs$
    $z_1(n) \leftarrow z(onset{:}offset)$
  end if
end for{*Filter Artifactual Interval*}
while true **do**
  $a_{j-1}(n) \leftarrow$DWT$(z_1(n), j-1)$
  $a_j(n) \leftarrow$DWT$(z_1(n), j)$
  $S_{j-1} \leftarrow$skewness$(a_{j-1}(n))$
  $S_j \leftarrow$skewness$(a_j(n))$
  $\delta \leftarrow ||S_j| - |S_{j-1}||$
  if $\delta > T$ **then**
    Remove $a_j(n)$
    $\hat{x}(n) \leftarrow$ Reconstruct filtered EEG by summation of $d_1(n), .., dj(n)$
    break
  else
    $j \leftarrow j + 1$
  end if
end while
return $\hat{x}(n)$

Evaluation criteria

Eye blink detection

To assess the accuracy of the eye blink detection, the true positive rate (TPR) and the false positive rate per interval (FPR) are computed as follows:

$$\text{TPR} = \frac{\text{TP}}{\text{TP} + \text{FN}}, \tag{1.9}$$

$$\text{FPR} = \frac{\text{FP}}{\text{FP} + \text{TN}}, \tag{1.10}$$

where TP (true positive), FN (false negative) and FP (false positive) stand for the correct, missed and false number of the detected eye blinks, respectively. It should be

noted that TN (true negative) concept does not exists in the continuous signal, therefore, FPR is assessed over the time intervals [64].

Filtering performance

The filtering performance of algorithms is evaluated in terms of the CC and relative root mean square error (RRMSE) computed between the eye blink-free and the filtered EEG signals. The RRMSE measures the amplitude distortion of the filtered EEG signals as follows:

$$\text{RRMSE} = \frac{\text{RMS}(x(n) - \hat{x}(n))}{\text{RMS}(x(n))}, \tag{1.11}$$

Lower RRMSE values indicate a better filtering quality.

1.2.2. Data

Semi-simulated and real eye blink-contaminated EEG signals have been used to develop and test the algorithm.

Semi-simulated data

To generate semi-simulated data, synthetic eye blink signals have been produced by repeating an eye blink template from [64] with different amplitudes at random time intervals. The generated eye blinks have been added to 1368 three-second long artifact-free EEG segments collected from [46]. The EEG signals were recorded according to the International System 10-20 with a sampling frequency of 200 Hz. EEG signals were carefully captured to minimize the appearance of the external and physiological artifacts. A white noise is also added to our semi-simulated data to resemble real world EEG data better:

$$z(n) = x(n) + r(n) + v(n), \tag{1.12}$$

where $z(n)$ is the noisy EEG, $x(n)$ is the artifact-free EEG, $r(n)$ is the eye blink artifact and $v(n)$ is the white noise that might emerge in EEG signals from other sources such as the environment or muscle contractions. Accordingly, we generated contaminated EEG signals with different SNR values.

Real data

The performance of all algorithms is tested on real data comprised of 3000 three-second long EEG segments from frontal channels, drawn from four brain computer interface public databases [71–74]. Table 1.3 displays the information about each database.

Table 1.3. A brief description of the employed databases for real EEG data analysis.

Database	[71]	[72]	[73]	[74]
Sampling rate (Hz)	512	200	256	250
Electrode montage	10-10	10-20	10-10	10-20
No. of used subjects	4	6	7	15
No. used signals	444	1036	724	796

The motivation behind using different databases is to investigate the adaptiveness of the proposed algorithm's parameters for EEG signals recorded in different conditions. These databases were purposely selected due to their realistic signal acquisition conditions as no artifact control or rejection was employed during recording. For more details about the data, see [71–74].

1.2.3. Results

Parameter tuning of the VME-DWT parameters

The parameter tuning of the proposed algorithm's required parameters is conducted by using 456 segments of the semi-simulated data. The α value, which plays the most important role for eye blink detection, is adjusted based on the highest mean of TPR and the lowest mean of FPR in the contaminated EEG signals with different SNR values. Fig. 1.12 confirms that the finest α value is 3000.

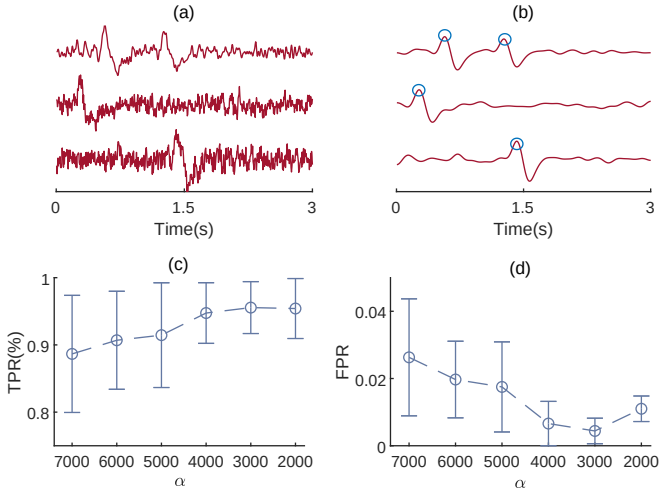

Fig. 1.12. Examples of contaminated EEG signals with different SNRs **(a)**, the corresponding desired mode extracted by VME **(b)**, the true positive rate **(c)**, and the false positive rate per interval **(d)**.

As for T, which controls the DWT decomposition level, it is tuned based on the

highest and lowest mean of CC and RRMSE, respectively, between the filtered and eye blink-free EEG signals. T values ranging from 0.05 to 0.25 with a step of 0.05 are employed. Fig. 1.13 shows that the finest T value is 0.1.

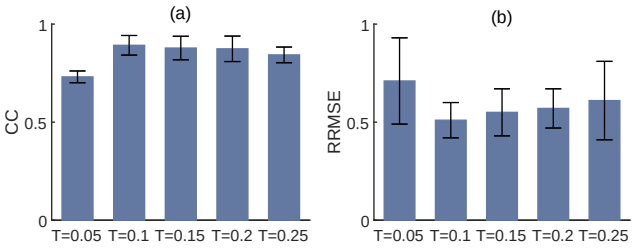

Fig. 1.13. The mean±standard deviation of CC **(a)** and RRMSE **(b)** between the eye blink-free and filtered EEG signals.

Note that these 456 signals were only used for the parameter tuning of the VME-DWT algorithm and are not included for the performance evaluation. The rest of the semi-simulated data and four real EEG databases are filtered with $\alpha = 3000$ and $T = 0.1$ values to investigate their adaptivness for different EEG databases.

Filtering results for semi-simulated data

Table 1.4 discloses the TPR and FPR values for eye blink detection in 912 three-second long segments of contaminated EEG signals with SNR ranging from -8 to +3 dB. The VME-DWT detected, on average, more than 95% of the eye blinks with an α value of 3000 for all SNRs. Fig. 1.14 shows examples of the contaminated and their

Table 1.4. Percentage of TPR and FPR of VME-DWT for eye blink detection.

SNR(dB)	TPR(%)	FPR
SNR≥0	99.54	0.0004
-6<SNR<0	96.45	0.0032
SNR≤-6	91.34	0.0136
Mean±SD	95.77±4.14	0.0057±0.007

corresponding eye blink-free and filtered EEG signals with different SNRs. In terms of the visual inspection, the VME-DWT eliminated eye blinks components better than AVMD and DWT.

The boxplots of the CC and RRMSE values between the eye blink-free and filtered EEG signals are shown in Fig. 1.15. Compared to AVMD and DWT, the VME-DWT displays a lower mean value of RRMSE (0.42 vs. 0.59, 0.87) and a higher CC mean value (0.92 vs. 0.83, 0.58), thus, indicating that the proposed VME-DWT

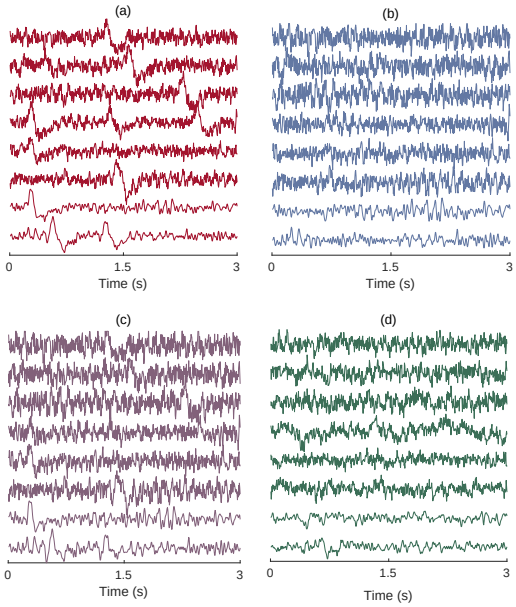

Fig. 1.14. Examples of contaminated **(a)**, and filtered EEG signals by the VME-DWT **(b)**, DWT **(c)**, and AVMD **(d)** algorithms.

can better preserve the original eye blink-free EEG signals.

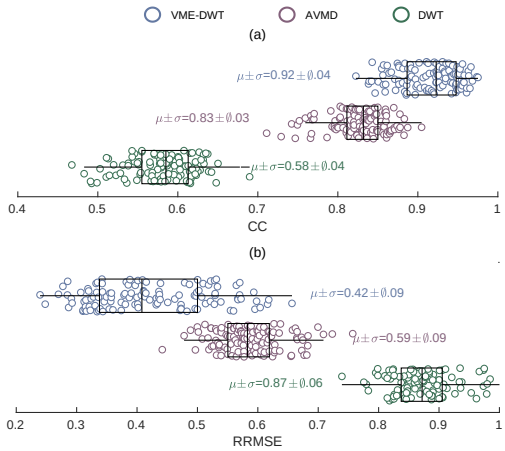

Fig. 1.15. Boxplots of CC **(a)** and RRMSE **(b)** between the eye blink-free and filtered EEG signals for all algorithms.

Filtering results for real data

Table 1.5 displays the TPR(%) and FPR for eye blink detection in all four real EEG databases. As it is shown, the proposed algorithm could detect the majority of

the eye blink artifacts in EEG signals captured with distinctive recording conditions. It should be noted that, due to unavailability of the artifact-free EEG, the computation of TPR and FPR for different SNRs is not possible.

Table 1.5. Percentage of TPR and FPR of VME-DWT for eye blink detection in four real EEG databases.

Database	[71]	[72]	[73]	[74]
TPR(%)	95.24	94.12	93.32	98.52
FPR	0.0042	0.0071	0.0098	0.0083

Fig. 1.16 depicts examples of real contaminated EEG signals from all four databases with their corresponding filtered EEG signals. As it can be observed, the proposed algorithm can better filter the intervals with eye blink artifacts.

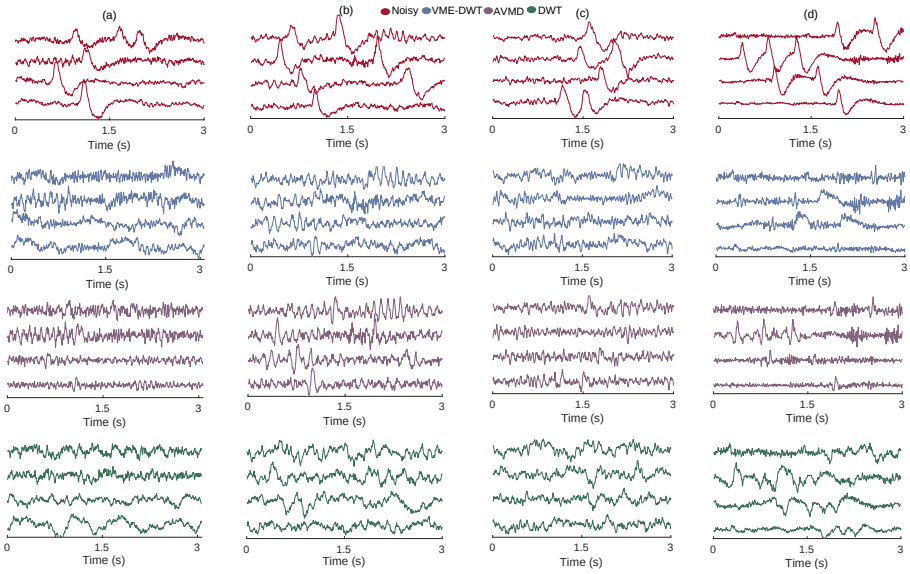

Fig. 1.16. Columns with examples of real contaminated EEG signal from [71] **(a)**, [72] **(b)**, [73] **(c)**, [74] **(d)**, and below the corresponding filtered EEG signals.

Because the real artifact-free EEG signals are unknown, the temporal criteria were only computed between the eye blink-free intervals of real and filtered EEG signals [39]. Table 1.6 suggests the superiority of VME-DWT to AVMD and DWT for the preservation of non-artifactual intervals.

Table 1.6. CC and RRMSE comparison (mean±standard deviation) between the eye blink-free intervals of contaminated and filtered EEG signals for real data.

Database	VME-DWT		AVMD		DWT	
	CC	RRMSE	CC	RRMSE	CC	RRMSE
[71]	0.94±0.03	0.16±0.04	0.89±0.08	0.18±0.10	0.68±0.11	0.84±0.18
[72]	0.97±0.02	0.14±0.02	0.93±0.04	0.21±0.12	0.73±0.03	0.96±0.03
[73]	0.93±0.04	0.15±0.05	0.88±0.07	0.19±0.06	0.64±0.14	0.76±0.23
[74]	0.98±0.01	0.09±0.04	0.84±0.06	0.19±0.09	0.62±0.14	0.94±0.34

1.2.4. Discussion

Here, the VME-DWT algorithm for the eye blink suppression in EEG signals was proposed. The obtained results suggest that the proposed VME-DWT: (a) can adequately detect and eliminate eye blinks in a short interval of a single EEG channel; (b) is automatic as no human involvement is required; (c) is less invasive compared to other decomposition-based algorithms since only contaminated intervals are filtered, and non-artifactual intervals remained unaltered; and (d) is needless to the artifact reference and initial calibration. The proposed VME-DWT also tackles the limitations of the classical artifact detection strategies such as the amplitude thresholding and template matching as it is robust to the other high amplitude artifacts and does not require any predefined template.

While the performance of VME is not highly sensitive to the value of the center frequency [65], regulation of the compactness coefficient, α, plays the key role for the accurate detection of eye blinks in EEG signals. Albeit a higher value of α can guarantee the extraction of the narrow-banded mode, in this application, however, smaller α values should be employed as the frequency range of the eye blink violates the VME presumption by overlapping in the delta, theta and alpha bands of EEG signals [68]. This is also the plausible explanation that the extracted desired mode by VME should not be directly subtracted from the contaminated EEG signals as it would either remove some low frequency components of non-artifactual EEG or preserve some high frequency components of eye blinks. Thus, the extracted mode is used for the more precise localization of the artifactual eye blink intervals. Our results suggest that α=3000 is the finest value for robust eye blink detection with the highest TPR and the lowest FPR (Fig. 1.12 (c), (d)).

The optimal DWT decomposition level for the eye blink filtering is achieved by a skewness-based index between two approximation components. Such an approach automatically terminates the decomposition procedure, evades unnecessary decomposition, and accelerates the filtering procedure. Furthermore, the skewness-based index, unlike other wavelet-based methods [34, 40], avoids the full tree decomposition of DWT or the manual selection of the decomposition level. The interchangeability and effectiveness of the proposed index have been proven by employing contaminated EEG signals with different recording conditions.

The performance is compared to the AVMD and DWT algorithms, proposed for the eye blink elimination in short intervals of a single EEG channel. In 912 semi-simulated EEG signals contaminated by eye blinks, the VME-DWT outperformed the AVMD and DWT, showing: (i) a higher mean of CC values, suggesting an enhanced EEG components' preservation, and (ii) a lower mean of RRMSE values, showing higher filtering robustness. As for real data, while the proposed VME-DWT showed a satisfactory performance, the AVMD and DWT algorithm failed to attenuate the eye blinks adequately (Fig. 1.16). Plausible explanations for such results are twofold. Firstly, the real EEG signals used in this research could require adjustment of the parameters set for the AVMD and DWT algorithms. However, having to adjust parameters for every new database would defeat the purpose of automatization, which is, evidently, unfavorable for the real-time EEG applications. Secondly, it is plausible that the number of the extracted modes or levels is insufficient, leading to the artifact markers failing to detect eye blinks.

While the proposed algorithm offers satisfactory performance, its limitations and potential solutions should be considered. Firstly, the presence of other low-frequency artifacts such as the electrode drift may hinder the accurate eye blink detection by the VME. Thus, high-pass filtering with a cut-off frequency of 0.5 Hz should be used before running the proposed algorithm. Secondly, the proposed algorithm only detects and eliminates artifacts associated with blinks, but no other artifacts such as eye saccades and muscle contractions. Nevertheless, it can be employed in conjunction with other filtering algorithms. Thirdly, this study presumes that contaminated EEG signals have only positive eye blink peaks. In bipolar EEG recordings (e.g., FT10-T8 channel), negative eye blinks might appear, and the proposed algorithm cannot detect them, unlike the AVMD and DWT. One potential solution could be to use the local minima of the extracted mode with the negative value of the threshold θ. Fourthly, while θ showed adequate performance for the detection of the highest eye blink peak from the VME mode, other strategies such as the algebraic approach [56] or the statistical threshold [55] may also improve the detection performance. Fifthly, the proposed approach for the double eye blink event has been developed experimentally and may require further investigation for more accurate performance. Nevertheless, these suggestions to mitigate the mentioned problems are just a hypothesis and require further investigation.

1.3. Conclusions of the Chapter

1. Skewness and kurtosis serve as effective indicators for detecting ELST and eye blink artifacts in short segments of EEG signals decomposed by using SWT and DWT methods.

2. The proposed algorithms demonstrate superior performance compared to

the current state-of-the-art methods for eliminating ESLT and eye blink artifacts, evidenced by a comprehensive evaluation on different EEG databases with diverse recording conditions.

3. The simplicity and adaptability of the proposed algorithms make them highly advantageous not only for addressing artifact removal in portable EEG headbands, but also in other applications where semi-real-time analysis is important.

2. SLEEP ASSESSMENT

Sleep, an essential state of altered consciousness, provides a profound framework for discerning and categorizing different levels of consciousness. It plays a critical role in the physical and mental recovery of individuals. However, it is estimated that 25% of the population in the European Union suffers from some form of sleep disorder. These disorders not only adversely affect the physical and mental health but also have significant economic impacts, including costly treatments, reduced efficiency, and increased risk of road accidents [5]. Therefore, there is a high demand for monitoring the quality and duration of sleep. The use of cost-effective portable EEG devices enables the reliable monitoring and evaluation of sleep patterns outside clinical and hospital settings. This capability is crucial for providing personalized and affordable sleep monitoring solutions.

Polysomnography (PSG) is considered the gold standard method for sleep monitoring. It simultaneously records several physiological signals such as, but not limited to, EEG, electrocardiogram (ECG), electrooculogram (EOG), and electromyogram (EMG). Despite its excellent appropriateness, it is an expensive procedure that requires to be conducted in clinical environments under the supervision of a sleep technician. Furthermore, subjects need to wear a large number of sensors that can affect their comfort and sleep behaviors [75]. To overcome the aforementioned issues, many researchers have developed algorithms for the automatic analysis of sleep using low-power wearable technologies that collect a single physiological signal from the human body, e.g., EEG [76], EOG [77], acceleration [78], respiration, [79], and photoplethysmography [80], also providing new possibilities for the home-based sleep monitoring [81]. Amongst the mentioned signals, the EEG has the richest information for the sleep analysis as the alternation in brain waves follows the awake and sleep stages [82–84]. Thus, a wide range of studies have employed a single EEG channel for the classification of awake and sleep stages.

2.1. Discrimination of Wakefulness from Sleep Stage I

Nonetheless, one of the major challenges reported in the EEG-based sleep monitoring studies is a low sensitivity to sleep Stage I when discriminating it from wakefulness [82, 85–90], which is due to the similar characteristics of the EEG signal in these two consecutive phases. The relevance of such discrimination lies in the estimation of the sleep onset latency, defined as the time interval needed to accomplish the transition from wakefulness to the first level of sleep, which is widely employed for assessing the quality of sleep [91]. One possible remedy is to use an auxiliary signal such as ECG [92], EMG and EOG [93], however, it increases the wearable complexity. On the other hand, selecting the location of the EEG channel is also of great importance

for the applicability, i.e., employing a frontal EEG channel, compared to an occipital one, is more convenient for the users.

Because of the complex and dynamic nature of EEG signals, and the resemblance of EEG characteristics between being awake and some sleep stages, extracting the appropriate EEG measures plays a vital role in the accurate monitoring of sleep. In general, EEG feature extraction strategies for sleep analysis are categorized into four classes: temporal [83], spectral [94], time-frequency [95], and nonlinear [96] analyses. Although the temporal analysis has the advantage of simplicity, intuition, and low computation, it is yet inefficient for interpreting the complex nonlinear variation of EEG in sleep. Alternatively, the feature extraction can be performed on EEG sub-bands with different frequency ranges [82,85,86]. Deep learning algorithms have also shown promising results for the classification of awake and sleep stages [87–90, 97–100], however, compared to the conventional methods, they require more computational and data resources [83].

Although there is still a controversy about the nonlinear nature of EEG, several studies showed the superiority of nonlinear measures over the linear ones in different EEG applications [101–103], in particular for the consciousness studies [104, 105]. Motivated by the fact that the differentiation between wakefulness and sleep Stage I might be related to the level of consciousness [106], and the efficiency of the feature extraction from EEG sub-bands for the sleep scoring [82, 85, 86], we propose a nonlinear feature set extracted from sub-bands of a single frontal EEG channel for the classification of wakefulness and sleep Stage I.

The efficiency of nonlinear measures usually relies on the manual setting of several parameters, thus, increasing human intervention. To this aim, we used EEG signals from four different sleep databases, where one of them is used for tuning the nonlinear features and the other three are used for investigating the effectiveness of the adjusted measures. The performance of the proposed feature set is also compared against the relative band power (RBP) analysis, considered as one of the most common techniques for the EEG-based sleep analysis [81–84]. The basis of the proposed algorithm is to (i) decompose the EEG signal into its sub-bands by using the DWT, (ii) compute two fractal dimensions and two entropy measures from each EEG sub-band, and (iii) discriminate wakefulness from sleep Stage I based on a support vector machine (SVM).

2.1.1. The proposed algorithm

The block diagram of the proposed algorithm is shown in Fig. 2.1. In the subsections below, the proposed algorithm is explained in detail.

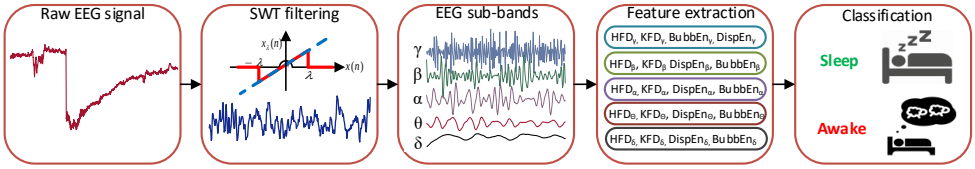

Fig. 2.1. Block diagram of the proposed algorithm for classification of awake and sleep Stage I cases using a single EEG channel.

Pre-processing

The recorded EEG signals are contaminated by artifacts that either are persisting or abruptly vary the amplitude in the EEG signal. As these artifacts contain both low and high frequency components, linear filters may not clean the signal satisfactorily. For this reason, we filtered the EEG signals by the kurtosis-based hard universal thresholding, (λ), of the stationary wavelet transform algorithm presented in [18].

DWT for EEG sub-bands decomposition

The DWT decomposes the input EEG signal $x(n)$ into several sets of high and low frequency components, i.e., detail $d(n)$ and approximation $a(n)$ components, characterizing the time evolution of the EEG signal in the corresponding frequency band. Based on multiresolution analysis, at the first level of DWT, the input EEG signal is decomposed into an approximation $a_1(n)$ and a detail $d_1(n)$. At the second level of DWT, $a_1(n)$ is decomposed into another approximation $a_2(n)$ and detail $d_2(n)$ components and so on, where the given EEG signal can be reconstructed by:

$$x(n) = \sum_{j=1}^{l} d_j(n) + a_l(n), \tag{2.1}$$

where l is the decomposition level. The frequency range of each approximation and detail component is computed as a function of the sampling frequency Fs and the decomposition level l, as follows:

$$a_l = \left[0, \frac{Fs}{2^{l+1}}\right], d_l = \left[\frac{Fs}{2^{l+1}}, \frac{Fs}{2^l}\right], \tag{2.2}$$

Another important issue for employing the DWT is to choose the basis function, generally selected based on the similarity of the desired signal and the basis function. Here, we use Daubechies 4 as proven to be suitable for the EEG sub-bands extraction [107]. As illustrated in Fig. 2.2, four levels of DWT are employed to extract the EEG sub-bands. It should be noted that the detail components of the first, second, third and fourth level correspond to gamma (γ), beta (β), alpha (α), and theta (θ), respectively, and the fourth level of the approximation component relates to the delta (δ) band.

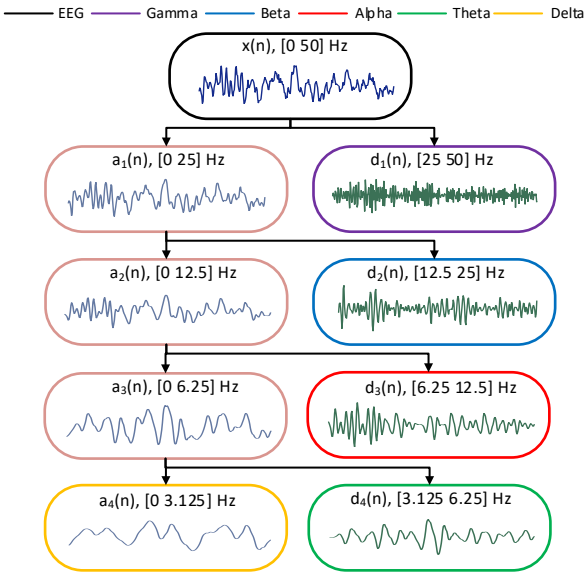

Fig. 2.2. An example of decomposed EEG signal into its sub-bands by DWT.

Feature extraction

After decomposing the EEG into sub-bands, four nonlinear measures called Higuchi's fractal dimension (HFD), Katz's fractal dimension (KFD), bubble entropy (BubbEn), and dispersion entropy (DispEn) are extracted to form the feature vector. Thus, the proposed feature vector contains 20 measures.

Fractal dimension (FD) is acknowledged as one of most effective measures for analyzing biomedical signals, extensively employed for EEG analysis in different applications [108]. HFD directly computes the FD value of a given signal $x(n)$ with $n = 1, 2, ...N$ in the time domain as follows [109]:

$$X_k^m = \{X(m + ik)\}_{i=0}^{[(N-m)/k]}, \tag{2.3}$$

where $m = 1, 2, ...k$ is the initial time and k is the interval time. The length of each X_k is expressed as:

$$L_m(k) = \frac{\sum_{i=1}^{(\frac{N-m}{k})} |X(m + ik) - X(m + (i-1)k)| * (n-1)}{k(\frac{N-m}{K})}, \tag{2.4}$$

Finally, the fractal dimension D is solved from

$$\langle L(k) \rangle \propto k^{-D}, \tag{2.5}$$

where $\langle L \rangle$ is the average of L_m.

KFD computes the fractal dimension according to the morphology, quantifying the crudity of the signal. For a given signal $x(n)$ with $n = 1, 2, ...N$, KFD is defined

as the ratio of the curve's length, divided by the maximum Euclidean distance of any point under consideration from the first point as follows [110]:

$$\text{KFD} = \frac{\ln \frac{L}{a}}{\ln \frac{d}{a}}, \tag{2.6}$$

where $L = \sum_{i=2}^{N} x_i - x_{i-1}$ is the length of $x(n)$, $d = Max(|x_1 - x_j|)$ for $j = 2, 3...N$ is the maximum distance from the initial point, and $a = \frac{L}{N-1}$ is the average distance between two successive points. While KFD shows more consistency for the FD computation due to its exponential transformation of FD values and the relative insensitivity to noise, HFD leads to a more accurate estimation of the signal's FD, yet more sensitive to noise.

BubbEn is originated from Renyi entropy that ranks the vectors in the embedding space of the signal [111]. Indeed, BubbEn uses bubble-sort algorithm to quantify the number of swaps, required by the permutation process. The main advantage of BubbEn is to be almost free of the parameters setting, i.e., the scaling factor has been removed, and the significance of embedding dimension has been highly reduced. BubbEn is computed based on the number of swaps needed to sort each vector and calculate the conditional Renyi entropy of the distribution H^m_{swaps} as follows:

$$\text{BubbEn} = \frac{H^{m+1}_{\text{swaps}} - H^m_{\text{swaps}}}{\log(\frac{m+1}{m-1})}, \tag{2.7}$$

where m is the embedding dimension.

DispEn quantifies the randomness of a signal by using the symbolic dynamics and the Shannon entropy [112]. Unlike BubbEn, it requires three parameters to be set before the analysis; the embedding dimension, the number of classes, and the time lag. The basis of DispEn computation is to (i) map N elements of the given signal into c classes, (ii) generate embedding vectors as $K = N - (m-1) \times d$, where m is the number of embedding dimensions and d is the time delay, and (iii) compute the probabilities p_i of each of the c^m dispersion patterns. DispEn is formulated as follows:

$$\text{DispEn} = -\sum_{i=1}^{K} p_i \times \log(p_i), \tag{2.8}$$

Classification

Here, we use the SVM with the radial basis function kernel to classify the wakefulness and sleep Stage I cases. The extracted features are firstly normalized based on the z-score approach and then randomly split into the training-validation (70%) and test (30%) sets. To obtain solid results, the training-validation procedure is executed based on 10-fold cross-validation (CV), and the testing procedure is conducted only on the unseen data set. It should be noted that the model's hyperparamters are optimized

during the training-validation procedure based on the Bayesian optimization method using the MATLAB function *'OptimizeHyperparameters'*. To assess the performance, sensitivity (Sen), specificity (Spe), accuracy (Acc), and area under the curve (AUC) are computed as follows:

$$\text{Sen} = \frac{\text{TP}}{\text{TP} + \text{FN}} \times 100, \tag{2.9}$$

$$\text{Spe} = \frac{\text{TN}}{\text{TN} + \text{FP}} \times 100, \tag{2.10}$$

$$\text{Acc} = \frac{\text{TP} + \text{TN}}{\text{TP} + \text{TN} + \text{FN} + \text{FP}} \times 100, \tag{2.11}$$

$$\text{AUC} = \int \text{Sen}(T)(\text{1-Spe})'(T)dT, \tag{2.12}$$

where TP and FN represent the number of correctly and wrongly classified sleep cases, TN and FP stand for the number of correctly and wrongly classified awake cases, and T is the binary threshold of the classifier.

Method under comparison

To compare the performance of the proposed feature set, the RBP analysis, which has been widely used for the classification of the sleep stages [81–84], is investigated. After filtering and DWT analysis for splitting the EEG into its sub-bands, the RBP of δ, θ, α, β, and γ are computed as follows:

$$\text{RBP} = \frac{P_{\text{Band}}}{P_{\text{EEG}}}, \tag{2.13}$$

where P represents the power and is computed by the root mean square of each sub-band. In addition to the conventional RBP measures, five ratios of powers in the different frequency bands, i.e., alpha to delta, alpha to theta, beta to delta, beta to theta, and theta to delta have been computed, as suggested in [82]. Hence, the RBP feature set includes ten measures.

2.1.2. Data

Here, 20s-long single frontal channel EEG signals, representing awake and sleep Stage I states from four different databases, namely, Sleep Telemetry [113], DREAMS [114], DCSM [115], and MESA [116] are used. Table 2.1 displays the scoring method, the sampling rate, the employed channel, the sleep disorder status, the number of subjects, awake (W) and sleep Stage I (S) states of each database.

Table 2.1. Description of the used databases in summary.

Database	Sleep Telemetry	DREAMS	DCSM	MESA
Scoring	R&K	R&K	AASM	AASM
Fs (Hz)	100	200	256	256
Sleep disorders	Yes	No	Yes	Yes
Channel	Fpz-Cz	Fp1-A1	F3-A1	Fz-Cz
No. Subjects	22	20	20	27
No. W	4920	4576	3921	7000
No. S	4604	1788	2142	4122

Sleep Telemetry

This database [113] includes the recorded PSG data to investigate the influence of Temazepam on 22 Caucasian men and women who were healthy or had mild difficulty falling asleep. During two nights, 9 hours of PSG data were collected by using a wearable miniature telemetry system in hospital settings. Then, two experts manually scored the sleep patterns based on the Rechtschaffen and Kales manual (R&K) [117]. In this research, 9524 20s-long EEG epochs from the Fpz-Cz channel with a sampling rate of 100 Hz are used, of which 4920 correspond to the awake stage.

DREAMS

This database [114] includes the whole night PSG recording from 20 healthy subjects (16 females), collected in a sleep laboratory of a Belgian hospital. Each record contains three mono-polar EEG channels, namely, Fp1, O1, and CZ or C3, referred to A1 and sampled at 200 Hz. A laboratory sleep expert visually annotated the sleep stages according to the R&K on the basis of 20s epochs. Here, we used 6364 20s-long EEG epochs from the Fp1 channel, of which 4576 correspond to awake cases. It should be noted that EEG signals were down-sampled to 100 Hz for reducing the computation.

DCSM

This database [115] includes whole-night lab-based PSG recordings collected from subjects who visited the Danish center for sleep medicine for the diagnosis of non-specific sleep disorders. Sleep stage scoring was performed by five experts according to the American Academy of Sleep Medicine (AASM) criteria [118]. Each record contains three EEG channels, sampled at 256 Hz and band-pass filtered at 0.3 Hz to 70 Hz. In this work, we used 6063 20s-long EEG epochs of the F3-A1 channel from 20 adult subjects (10 male) with different sleep disorders, of which 3921 correspond to wakefulness. Before the processing, the sampling rate was changed to 100 Hz.

MESA

The multi-ethnic study of the atherosclerosis (MESA) database comprises of at least 8 hours of overnight PSG recordings collected from subjects with different sleep disorders by the National Sleep Research Resource (NSRR) [116]. Each record includes three EEG channels, namely, Fz-Cz, Cz-Oz, and C4-A1, sampled at 256 Hz. To specify the sleep stages, 30s-long EEG epochs were scored according to the AASM criteria. Here, we used the first 20s long of 11122 EEG epochs of the Fz-Cz channel collected from 27 subjects, of which 7000 relate to awake cases. Before the processing, the sampling rate was reduced to 100 Hz.

2.1.3. Results

Tuning of nonlinear features

As it was already mentioned, the efficiency of a nonlinear measure depends on the setting of its parameters. To this aim, the Sleep Telemetry database is used to tune the values of the required parameters based on the p value of the conducted Wilcoxon Rank-Sum Test between awake and sleep Stage I cases. Then, each tuned measure is employed for the analysis of the other three databases. The motivation behind using the Sleep Telemetry database for parameter tuning of the proposed feature set is its diverse cohorts as it includes both genders with and without sleep disorders. The most important parameter of HFD that should be tuned before the processing is the the maximum interval, K_{max}, that HFD values are computed in. To find the best fit, we varied it from 4 to 16, and found K_{max}=12 as the finest value. As more stability of the BubbEn value is achieved by a higher embedding dimension [111], we investigated values from 10 to 30 and found the embedding dimension of 22 as the finest value. The guideline for the parameters setting of DispEn has been provided in [112]. Accordingly, we found the embedding dimension of 2, 6 number of classes, and the time lag of 1 as the finest values, also suggested in [107]. Fig. 2.3 shows the boxplots of the proposed features for awake and sleep Stage I after the parameter tuning[1].

Classification results

Table 2.2 displays the training and validation results of the proposed and RBP features sets for all databases. As observable, the proposed feature set obtained better results than the RBP for both training and validation. Fig. 2.4 demonstrates the classification results of the unseen testing data in terms of Acc, Sen, and Spe for all four databases. The comparison confirms the superiority of the proposed feature set over the RBP analysis.

[1]It should be noted that the outliers have been removed for the better visual comparison, and features were normalized based on z-score method

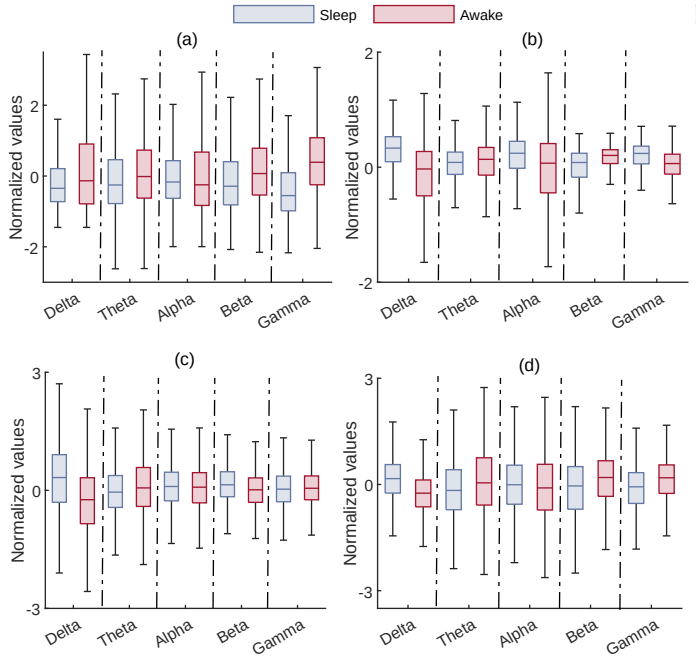

Fig. 2.3. Boxplots of the proposed features in different EEG bands: HFD **(a)**, KFD **(b)**, BubbEn **(c)** , and DispEn **(d)**.

Table 2.2. The average training-validation results of the SVM classifier for all databases using both feature sets.

		Training			Validation		
	Database	Acc (%)	Sen (%)	Spe (%)	Acc (%)	Sen (%)	Spe (%)
Proposed	Sleep Telemetry	98.7	99.2	96.2	87.6	85.2	90.8
	DREAMS	98.9	97.9	99.1	95.7	90.6	97.8
	DCSM	99.4	99.1	100	96.2	94.6	98.3
	MESA	98.1	95.9	99.2	89.2	85.8	90.8
RBP	Sleep Telemetry	91.5	89.1	92.9	75.6	73.8	78.9
	DREAMS	94.4	89.9	97.8	89.8	82.7	95.8
	DCSM	95.4	89.2	98.9	89.7	95.8	80.3
	MESA	93.1	84.6	97.3	89.6	82.1	94.6

When applied to the Sleep Telemetry database (Fig. 2.4a), the proposed feature set outperformed the RBP by showing 10.71%, 10.93%, and 10.76% higher mean values for Sen, Spe, and Acc, respectively. Regarding the DREAMS database (Fig. 2.4b), while both feature sets showed similar Spe values, the proposed feature set surpassed the RBP in terms of Sen (87% vs. 71%) and Acc (92% vs. 88%). As for the DCSM database (Fig. 2.4c), the proposed feature set gained 16.79%, 2.53%, and 7.86% higher mean values for Sen, Spe, and Acc, respectively. Regarding the

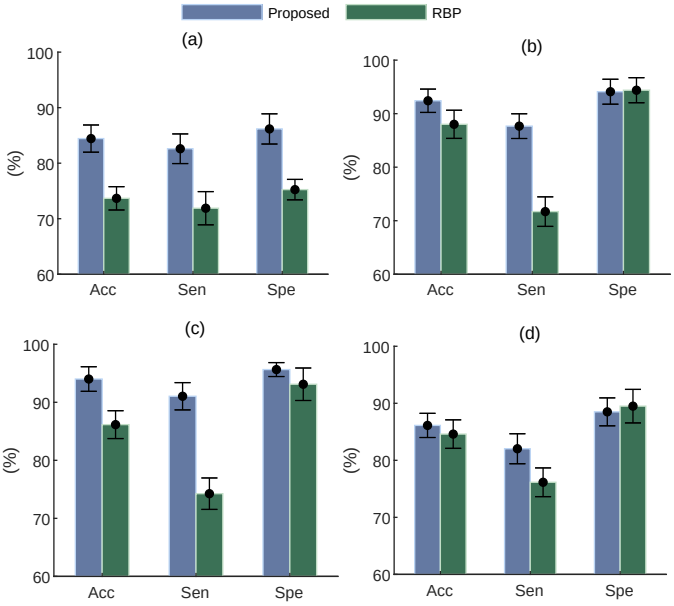

Fig. 2.4. The comparison between Acc, Sen, and Spe values (mean±standard deviation) for both feature sets using Sleep Telemetry **(a)**, DREAMS **(b)**, DCSM **(c)**, and MESA **(d)** databases.

MESA database (Fig. 2.4d), while both feature sets showed comparable Spe and Acc values, the proposed feature set showed 5.88% higher mean of Sen. According to the conducted independent two-sample t-test, there is a statistically significant difference between the Sen values obtained by the proposed and the RBP feature sets (p<0.05).

Fig. 2.5 shows the receiver operating characteristic (ROC) curves and the corresponding area under the curve (AUC) values of the unseen testing data for all four databases obtained by both feature sets. As it is displayed, higher AUC values were achieved by the proposed nonlinear feature set for Sleep Telemetry (0.91 vs. 0.79), DREAMS (0.97 vs. 0.89), DCSM (0.98 vs. 0.92), and MESA (0.92 vs. 0.89) databases.

2.1.4. Discussion

The aim of this study was to discriminate the wakefulness from sleep Stage I by using a single frontal EEG channel. Thus, we proposed a nonlinear feature set extracted from the EEG sub-bands, and verified its effectiveness by using four different databases. The importance of this research lies in the analysis of the sleep onset latency, reflecting the overall sleepiness and the sleep quality, which can also be employed for the prognosis of coma recovery. Another important application of such discrimination is the detection of drowsiness, which is responsible for almost 25% of

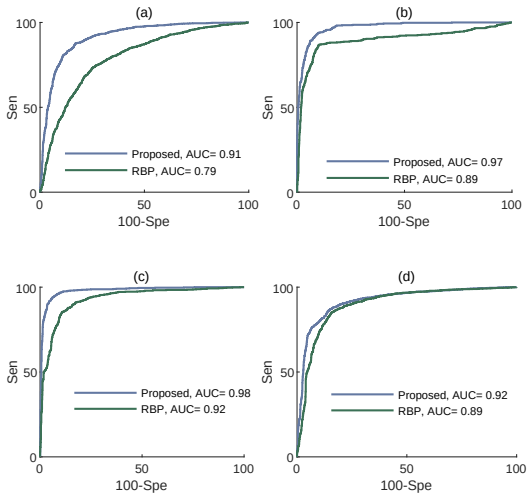

Fig. 2.5. The ROC curves and the corresponding AUC values using both feature sets for Sleep Telemetry **(a)**, DREAMS **(b)**, DCSM **(c)** , and MESA **(d)** databases.

the road accidents in the European Union [119].

To this purpose, HFD, KFD, BubbEn, and DispEn extracted from EEG sub-bands were investigated. The FD measures the degree of complexity and self-similarity by assessing how rapidly the signal increases or decreases with changing the scale. As EEG is expected to show more complexity through wakefulness, FD values are assumed to show higher values. On the other hand, entropy quantifies the uncertainty of the signal, thus, it is presumed to observe more uncertainty during wakefulness [106].

Compared to state-of-the-art algorithms, the advantage of our algorithm can be discussed in twofold. Firstly, while the majority of studies only considered one or two databases for reporting the results [76, 83, 84, 86, 88–90, 95, 97–99], we evaluated the performance of the proposed algorithm by using four databases. Hence, the reported results here are more solid as different databases with distinguishing characteristics were employed. Secondly, compared to deep learning methods [49, 98, 99], our algorithm requires less computational power and resources. In addition, deep learning based-methods require a lot of background knowledge and experience to be designed and implemented.

The main burden for employing a nonlinear measure is the adjustment of its parameters, playing an important role for the efficiency. On the other hand, the interchangeability of a tuned feature for other databases is also another concern that must be noted. To this purpose, we found the appropriate parameter values of each feature by using Sleep Telemetry database and tested their effectiveness on three different databases. The obtained results attested the effectiveness of the proposed feature set and their tuned parameters.

As shown in the results, the obtained Sen values by the proposed feature set

outperformed the RBP for all four databases. Indeed, EEG signals show strong nonlinearity [101], thus, it is expected to achieve a better performance when using nonlinear features. While the obtained results of the proposed feature set show no noticeable difference between the Sen and Spe values for each database, the obtained Sen and Spe values by the RBP of DREAMS and DSCM databases confirm a high rate of misclassified sleep Stage I cases. The plausible explanation can lie in the fact that the theta activity and higher frequency sleep spindles can be better captured in occipital channels [82].

Regardless the accuracy, another important criterion for selecting the channel in portable EEG devices should be the comfort of the subjects. For example, the use of EEG channels from the occipital region of the scalp can lead to inconvenience as it is usually covered by hair and is found intrusive for falling asleep. Alternatively, the frontal region of the scalp, in particular a prefrontal channel, is more suitable for the long-term recordings as it is a hairless region, i.e., it is less subjected to noise, thus, allowing the subject to have more comfortable sleep positions.

Although the proposed feature set shows promising results, there are a few concerns that must be investigated further. Firstly, subject-independent analysis has not been performed here as only a small fraction of subjects of each database were used. Considering the inter-subject variability [120–122], the performance of feature sets may show different results. Secondly, several studies showed that sleep Stage I and awake cases may also be misclassified as the REM stage, which was not addressed here. Thirdly, we have only investigated 20s-long EEG epochs. The effectiveness of the proposed feature set should be evaluated in different time window lengths. In particular, for the real-time monitoring of driver drowsiness [123], the performance of the proposed feature set should be assessed by using shorter signals. Yet, for the semi-real time detection of driver drowsiness, i.e., 20s-long epochs [20, 124], the proposed feature set is still a good option. Fourthly, the investigation of other sub-bands like sigma (σ) also may improve the classification results. Fifthly, it might be beneficial to combine linear and non-linear measures to form the feature set.

2.2. Conclusions of the Chapter

1. The study showcases the effectiveness and versatility of a novel nonlinear feature set, consisting of fractal and entropy metrics, extracted from a sole frontal EEG channel for distinguishing between wakefulness and sleep Stage I.

2. The proposed feature set outperformed the RBP with the higher mean of the Sen to sleep Stage I for the Sleep Telemetry (82.6% vs. 71.8%), DREAMS (87.6% vs. 71.8%), DCSM (91.0% vs.74.2%), and MESA (82.0% vs. 76.1%) databases.

3. DRIVER FATIGUE DETECTION

Driver fatigue detection is a critical application in monitoring altered states of consciousness and is central to this research's objective of utilizing low-cost portable EEG systems. Fatigue represents a transition from full alertness to drowsiness – a subtle yet significant shift in consciousness that impairs the cognitive functions and reaction times, thereby increasing the risk of accidents.

It is estimated that fatigue driving is responsible for 25% of road accidents in the European Union [119]. In the United States alone, a study by the AAA Foundation for Traffic Safety estimated that over 328,000 crashes annually are caused by driver fatigue, resulting in 109,000 injuries and approximately 6,400 fatalities [125]. Therefore, detecting fatigue and alerting the driver is crucial for reducing road accidents and saving lives [126]. The employment of portable EEG devices offers a practical solution for monitoring and assessing driver fatigue. Their lightweight design and ease of wear make them ideal for real-life applications, providing a valuable tool to enhance road safety and prevent fatigue-related incidents.

In general, two main modalities have been widely investigated for the detection of the driver fatigue in literature; subjective and physiological approaches [127]. The subjective strategies such as self-reported fatigue [128] and video measurement of facial expressions [129] or head postures [130] are prone to the biased individualistic feedback and privacy violation [131], respectively. The latter is the analysis of physiological signals such as ECG [132], photoplethysmogram [133], EOG [134], and EEG [135], whose robustness and effectiveness have been widely demonstrated through various algorithms and the subsequent conclusions. Amongst the physiological signals, EEG is recognized as the most effective one as the electrical activity of brain contains inherent information associated with the underlying processes of fatigue [136]. Consequently, the discrimination between the fatigue and alert driving by using EEG has been widely addressed in literature [137, 138].

3.1. The Influence of Eye Blink Artifacts on Prefrontal EEG Signals for Detection of Driver Fatigue

Following the advent of consumer EEG headbands with few channels, researchers have designed various portable systems to monitor the driver state in the real-world application. A comprehensive review of such systems can be found in [138]. According to this review, the alteration of EEG band powers is the most straightforward indicator of the alert and fatigue states. Indeed, in the fatigue state, the power of alpha and beta bands decreases while the power of the theta band increases [139, 140].

One of the greatest challenges leading to the fallacious band power analysis of EEG is its vulnerability to the eye blink artifact that frequently manifests itself with a

prodigious spike [50], distorting up to the alpha band of the EEG signals [68,141,142].

On the other hand, although the existence of eye blinks jeopardizes the punctilious decoding of EEG signals, its related analysis has been recognized as a valuable guidance on the detection of fatigue [143–145]. The mentioned investigations recorded eye blinks by placing two electrodes below and above one eye, which can yield the inconvenience for subjects on daily basis and reduces the visual field [146]. The alternative solution, which reduces the wearable complexity, is to extract eye blink features from frontal EEG channels, where the power of the eye blink is strong [134, 146, 147]. Indeed, combined with the spectral analysis of low-channel EEG signals, blink-related features derived from EEG can improve the driver fatigue detection [148, 149].

To the best of our knowledge, researchers either filtered eye blinks to improve the quality of EEG analysis [139, 140, 150–153], or extracted blink-related measures as additional features besides the analysis of contaminated EEG [134, 146, 148, 149]. Here, therefore, we present an algorithm for simultaneous eye blink feature extraction and the elimination from low-channel prefrontal EEG signals to enhance the detection of driver fatigue without requiring any artifact reference, synthetic data generation or initial calibration. The main steps of the proposed algorithm are to (i) find the eye blink intervals (EBIs) by VME [65] from the Fp1 channel and extract blink-related features, (ii) project the identified EBIs to the rest of EEG channels and employ the principal component analysis (PCA)-DWT based algorithm to remove eye blink components, and (iii) combine the derived blink-related measures with the band power features of the filtered EEG signals for the classification of the driver state.

To evaluate the impact of eye blinks on EEG-based driver fatigue detection, we consider two scenarios. In the first scenario, we compare the accuracy of driver fatigue detection by using solely band power analysis of EEG signals before and after filtering out eye blinks. In the second scenario, we complement this analysis by incorporating derived blink features to examine if these features enhance the accuracy of fatigue detection.

3.1.1. The proposed algorithm for simultaneous eye blink characterization and elimination

The block diagram of the proposed algorithm is shown in Fig. 3.1. As observable, the proposed algorithm identifies the EBIs from EEG by VME, extracts blink-related features, filters EBIs from EEG by the PCA-DWT, and employs the blink and the band power features of the filtered EEG signals to investigate the accuracy improvement of the driver state monitoring.

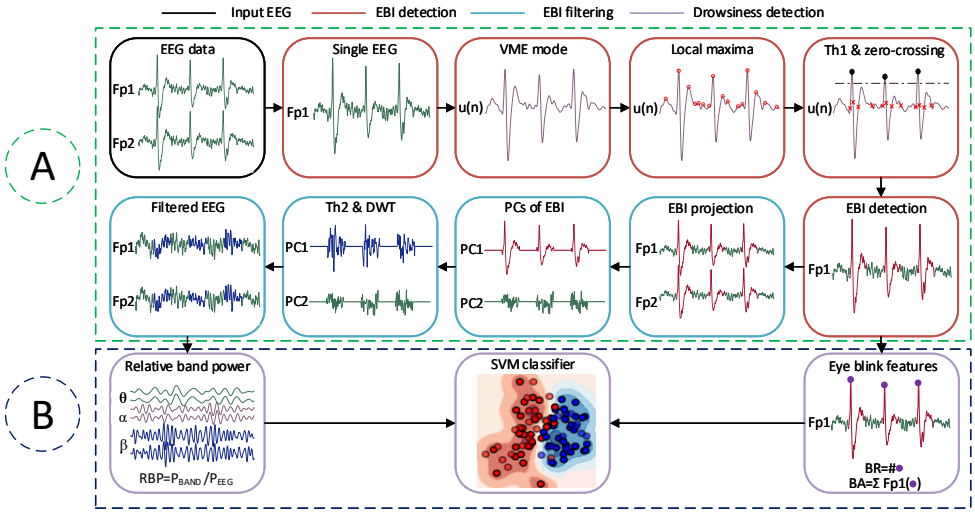

Fig. 3.1. Block diagram of the proposed algorithm for simultaneous eye blink feature extraction and elimination to improve the quality of driver's status monitoring. Blocks in the green dashed line (circle A) show the steps of the proposed algorithm for eye blink detection (red-colored) and filtering (light blue-colored) from EEG, and blocks in dark blue dashed lines (circle B) demonstrate the procedure of driver fatigue detection by using blink and filtered EEG band power features by SVM (purple-colored).

EBI detection

The VME requires two parameters to be set before the processing; compactness coefficient α, which regulates the bandwidth of the desired mode, and the center frequency ω_d, which is set based on the nature of the desired mode. In our previous research [19], we showed that the best α and ω_d values to get an appropriate estimation of the eye blink signal for different SNR values are 3000 and 3 Hz. In order to detect the EBIs, we firstly extract the local maxima of the desired mode to localize the highest eye blink peaks by selecting the candidates which have greater values than the modified universal threshold [154] as follows:

$$Th_1 = K\sigma\sqrt{2\ln N}, \tag{3.1}$$

$$\sigma = \frac{\text{median}(|u(n)|)}{0.6745}, \tag{3.2}$$

where $u(n)$, N, and K represent the extracted desired mode, the number of samples, and an empirical value, respectively. In this experiment, K is set to 0.5.

The main challenge for identifying an EBI is its duration as it can last from 200 to 2000 ms [45, 64, 68]. To this end, zero-crossing analysis is employed in such a way that one zero-crossing before and three zero-crossings after the eye blink highest peak [68] are involved (Fig. 3.2a). In some particular cases, e.g., the fatigue state,

two or more eye blink events might merge. Although the proposed algorithm may detect them correctly, but the filtering is performed multiple times that can lead to extra data loss. To overcome this problem, a distance criterion is used in such a way that if the interval between two or more identified blink events is less than 500 ms, one zero-crossing before the first highest eye blink peak and three zero-crossings after the last highest eye blink peak are included (Fig. 3.2b). After EBIs detection from the single-EEG channel, they will be projected to the rest of the channels.

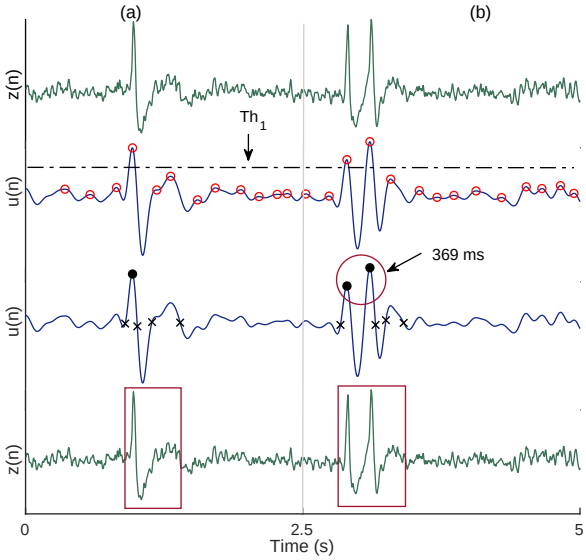

Fig. 3.2. Eye blink interval detection from Fp1 channel with one **(a)** and two **(b)** blink events.

Derived blink features

As stated in literature, the alternation of eye blink behavior is a recognized tool in the evaluation of different cognitive states [155–160]. Indeed, the fatigue state can influence the eye blink conditioning by increasing the blink rate (BR) [155] and decreasing the average blink amplitude (ABA) [148] (Fig. 3.3). As the proposed algorithm firstly identifies the highest eye blink peaks, BR and ABA can be directly computed as the number and the mean magnitude of such peaks, respectively.

Filtering of EBIs

PCA employs the second-order statistical heuristic to decompose m channel EEG signals into M principal components (PCs), ordered from high to low variations. As the eye blink's amplitude is significantly higher than the EEG, it is expected to have the higher variance value [57,70], i.e., eye blink components are expected to lie in first few

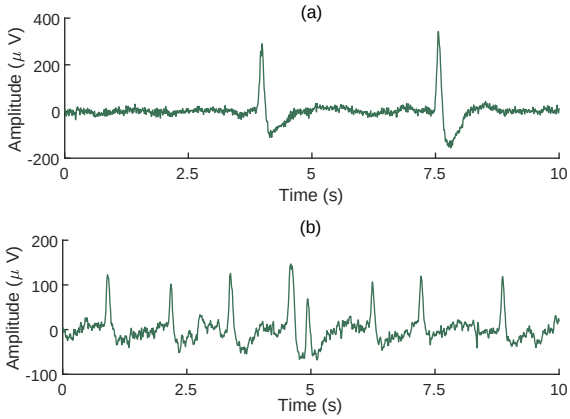

Fig. 3.3. Examples of EEG signals in alert **(a)** and fatigue **(b)** states.

PCs. To find the artifactual PCs, we define the following modified empirical threshold, inspired by [45]:

$$Th_2 = \overline{P} + \frac{d}{\sqrt{N_0}}, \tag{3.3}$$

where $\overline{P}$ and d are the mean and the standard deviation of PCs variances, and N_0 is the number of EBI samples. Each PC with a variance value greater than the threshold is considered as an artifactual component. Traditionally, PCA denoising algorithms reject the artifactual PCs and reconstruct the filtered signal without the rejected ones [38, 161–163], however, complete rejection of the artifactual PCs in low-channel EEG signals leads to the elimination of the neural activity, as the number of PCs is equal to the number of available channels. To overcome this issue, we employ the DWT to filter the artifactual PCs. The DWT denoising-based algorithm requires two parameters to be set; the mother wavelet and the number of decomposition levels. As for the mother wavelet, Daubechies 4 has been shown as one of the most effective basis functions for the eye blink filtering [34, 68]. The number of decomposition level is set according to the sampling frequency. As the sampling rate of both databases is 256 Hz, five levels of decomposition are selected. The DWT coefficients of each level that exceed the universal threshold are set to zero. Then, the filtered component is reconstructed by inverse DWT of the thresholded coefficients. To reconstruct the filtered EEG signals, inverse PCA is performed on the PCs after denoising.

EEG band power features

As already stated, EEG band power analysis is still recognized as the first-line technique to discriminate alert and fatigue states in consumer EEG systems [138]. After the eye blink removal, RBP of theta, alpha, and beta are computed. It should be noted that delta band analysis was excluded as it is mostly related to the deeper

level of sleep (Stages III and IV). Thus, the EEG feature set consists of six measures from two prefrontal channels.

Classification of the alert and fatigue states

To classify alert and fatigue states, SVM, which is one of the most commonly used classifiers for EEG studies, is employed [139,152]. The basis of SVM is to project the data upon a hyperplane that maximizes the margin between different classes. Here, SVM with the Gaussian kernel is employed. The SVM's hyperparameters have been optimized according to grid-search on 10-fold CV.

MAICA

To evaluate the performance of eye blink removal, we compare the proposed algorithm with the moving average ICA (MAICA), which was originally designed to eliminate artifacts from low-channel EEG signals. This comparison focuses on the effectiveness of detecting driver fatigue after the removal of eye blinks.

Evaluation criteria

Eye blink detection

As the first step of proposed algorithm is to identify eye blinks, TPR and false detection rate (FDR), revealing the percentage of correctly and falsely detected blinks, are computed as follows:

$$\text{TPR} = \frac{\text{Number of correctly detected blinks}}{\text{Actual number of blinks}} \times 100, \tag{3.4}$$

$$\text{FDR} = \frac{\text{Number of falsely detected blinks}}{\text{Number of all detected blinks}} \times 100, \tag{3.5}$$

Driver state classification

To investigate the performance of driver fatigue detection, Sen, Spe, Acc, and AUC are computed as follows:

$$\text{Sen} = \frac{\text{TP}}{\text{TP} + \text{FN}} \times 100, \tag{3.6}$$

$$\text{Spe} = \frac{\text{TN}}{\text{TN} + \text{FP}} \times 100, \tag{3.7}$$

$$\text{Acc} = \frac{\text{TP} + \text{TN}}{\text{TP} + \text{TN} + \text{FN} + \text{FP}} \times 100, \tag{3.8}$$

$$\text{AUC} = \int \text{Sen(T)}\ (1\text{-Spe})'(\text{T})\ d\text{T}, \tag{3.9}$$

where TP and FN represent the number of correctly and missed detected fatigue subjects, TN and FP stand for the number of correctly and missed detected alert subjects, and T is the binary threshold of the classifier.

3.1.2. Data

The EEG data were collected from 12 healthy young male subjects aged between 19–24 in a highway driving simulation experiment with a low traffic density [152]. The subjects were asked to avoid using any kind of medication, alcohol, or coffee, and have normal hours of sleep before the experiment, which started at 9 AM. To acquaint the participants with the experimental environment, they practiced the driving task 5 minutes prior to the final experiment. After the training session, each participant was asked to be away from the simulator for 10 minutes to engage in unconstrained movement within the laboratory. This study was approved by the Academic Ethics Committee of Jiangxi University of Technology. The experiment consisted of two phases. In the first, the subjects performed the experiment for 20 minutes, and the last 5 minutes were considered as the alert state. In the second, the subjects kept performing the experiment for 40 ± 100 minutes until the results of self-report fatigue survey suggested that the subject was in a driving fatigue state, and the last 5 minutes were labeled as the fatigue state.

The data comprised of 30 EEG channels (Fp1, Fp2, Fz, F3, F4, F7, F8, Fz, FC3, FC4, FT7, FT8, T3, C3, Cz, C4, T4, TP7, CP3, CPz, CP4, TP8, T5, P3, Pz, P4, T6, O1, Oz, O2), referenced to two electrically linked mastoids at A1 and A2, and sampled at 1000 Hz. Additionally, horizontal and vertical EOG signals were recorded to monitor eye movements and blinks. As the pre-processing step, EEG signals were band-pass filtered with a frequency range of 1–30 Hz and down-sampled to 256 Hz for reducing the computational load. Then, EEG data were segmented into 20s-long epochs [124, 148] to generate 14 segments. With 12 participants, a total of 168 segments were formed for the alert state, and 168 segments were formed for the fatigue state. To increment the resemblance of data analysis with a consumer prefrontal EEG headset [164], only Fp1 and Fp2 channels are used to detect the driver fatigue.

3.1.3. Results

Eye blink detection and filtering

According to the manual inspection of simultaneously recorded eye blinks channels, the proposed algorithm could detect 92% and 89% of eye blink with FDR of 5% and 4% in alert and fatigue states, respectively. Fig. 3.4 shows examples of the filtered driver EEG signals in fatigue and alert states. While both algorithms suppressed eye blink components adequately in the alert state, it seems that the

proposed algorithm surpassed the MAICA in the fatigue state.

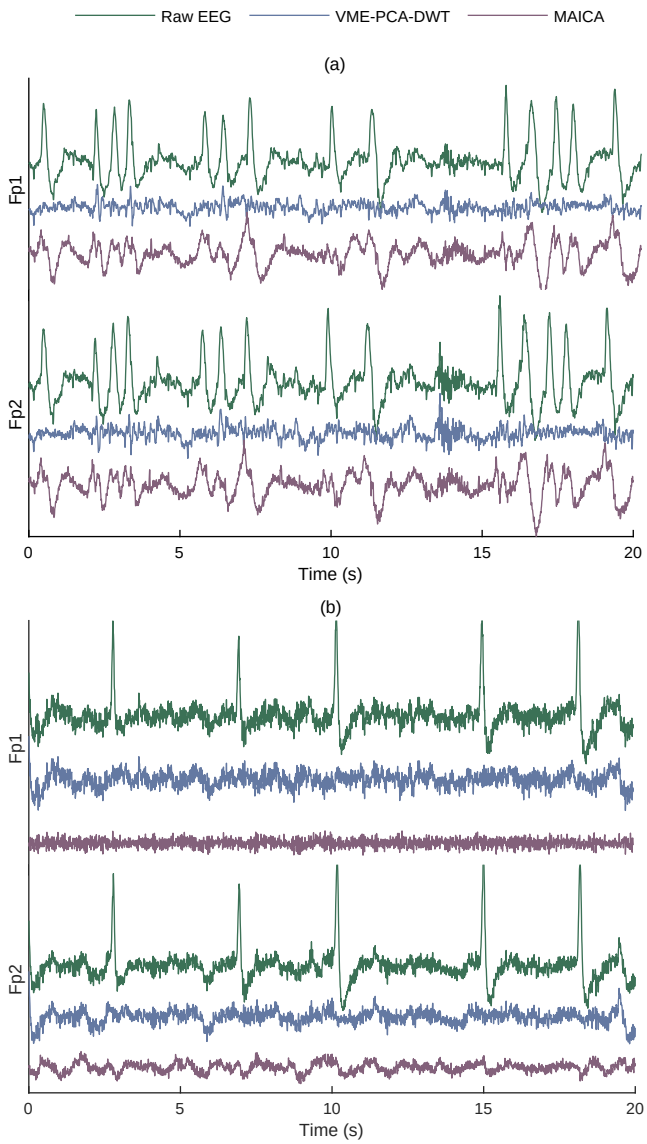

Fig. 3.4. Examples of two-channel EEG configuration (Fp1 and Fp2) with the corresponding filtered signals in fatigue **(a)** and alert **(b)** states.

Driver fatigue detection

To assess the improvement of driver fatigue detection after eye blink detection and removal, firstly, the classification results are shown in terms of band power features

of the raw and filtered EEG signal by both algorithms, and solely blink features (Table 3.1). The comparison between blink and unfiltered band power EEG features confirms the superiority of EEG over the blink analysis with a higher mean of Sen (64% vs. 61.4%), Spe (65.8% vs. 58.6%), and Acc (64.3% vs. 60.1%). For the filtering scenario, as observable, the proposed algorithm outperformed the MAICA by a higher mean of Sen (72.4% vs. 68.1%), Spe (70.7% vs. 67.6%), and Acc (71.1% vs. 67.7%), confirming the better quality of eye blink filtering.

Table 3.1. Mean±standard deviation of Sen, Spe, and Acc for the blink and EEG band power features of raw and filtered EEG signals.

Scenario	Sen (%)	Spe (%)	Acc (%)
Raw EEG	64.0±1.7	65.8±2.1	64.3±1.3
Blink	61.4±1.8	58.6±1.5	60.1±1.4
MAICA	68.1±1.8	67.6±1.9	67.7±1.5
VME-PCA-DWT	72.4±1.2	70.7±1.4	71.1±1.1

Fig. 3.5 shows the improvement of driver fatigue detection with employing BR and ABA as complementary features besides the band power features of EEG signals before and after eye blink removal by the proposed algorithm. As it is shown, a higher mean of Sen (80.7% vs. 72.1%), Spe (75.2% vs. 70.1%), and Acc (78.1% vs. 71.2%) were achieved by simultaneous eye blink feature extraction and elimination.

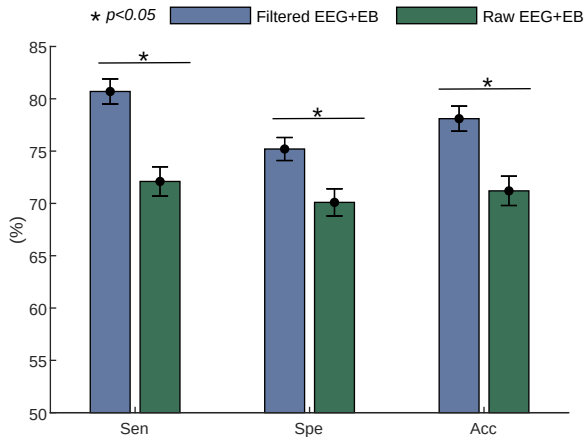

Fig. 3.5. The quality improvement of driver fatigue detection when using BR and BA before and after eye blink removal by the proposed algorithm. EB indicates eye blink.

3.1.4. Discussion

Here, an algorithm that entails both extraction of blink-related features and the elimination of eye blinks from low-channel prefrontal EEG signals to improve the quality of driver fatigue detection was presented. The current state-of-the-art research either considers eye blinks as a source of information [148, 149] or artifacts [139, 140], while undermining the possibility that eye blinks can be a source of both. Indeed, we have shown that blink feature extraction followed by its removal from low-channel prefrontal EEG signals could further increase the accuracy of driver fatigue detection, when compared to those that consider it either as solely a source of artifact or information.

There are four motivations behind the selection of such a channel configuration (Fp1 and Fp2). Firstly, we could investigate the quality of eye blink removal in real-world EEG signals by the classification results of the driver states. Indeed, the eye blink has its strongest power in prefrontal channels, therefore, it is expected to affect the classification results [140]. Secondly, extracting BR and ABA from one prefrontal channel can be more effective than other EEG channels as eye blink strongly influences the forehead EEG channels [147]. Thirdly, by using such a configuration, we can claim that the proposed algorithm can be integrated into low-cost EEG headbands such as the brainmachine system [164]. Fourthly, collecting EEG signals from the hairless region is less challenging for daily basis and long-term monitoring. Indeed, placing the EEG headset at the back of the head for monitoring posterior EEG signals can yield the inconvenience for drivers by not allowing them to use the headrest [148]. Yet, some researches showed that analysis of posterior EEG signals may achieve a better accuracy for the detection of the driver fatigue [149, 152].

In the first experiment, the proposed algorithm outperformed the MAICA for eye blink removal by showing 4.3%, 3.1%, and 3.4% higher mean values for Sen, Spe, and Acc, respectively (Table 3.1). The plausible explanations of such superiority can be twofold. Firstly, the proposed algorithm identifies the EBIs (e.g., 1.5s) and only filters such segments, thus, it is less invasive to the non-artifactual segments of EEG signals. On the other hand, the MAICA filters the whole length of EEG signals (i.e., 20 s), therefore, some non-artifactual components can be removed. Secondly, despite the fact that MAICA rejects the artifactual ICs and reconstructs the filtered signal with the remaining ones, the proposed algorithm uses the DWT to filter eye blink components from the artifactual PCs. This property can significantly improve the quality of filtering in low-channel EEG systems where the number of the extracted components is equal to the number of available EEG channels [45, 68]. One may argue that the MAICA may generate more ICs if a different configuration of parameters is set, therefore, ICs rejection should not highly affect the filtering performance. It should be noted that generating more artificial data increases the computational complexity.

In addition, adjustment of the parameters for every new data makes the algorithm subject-dependent.

The second experiment aimed at investigating the quality enhancement of driver fatigue detection by using the derived BR and ABA besides the band power features of EEG signals before and after eye blink removal by the proposed algorithm. The comparison between Table 3.1 and Fig. 3.5 shows the employment of BR and ABA could enhance the Acc of the driver state in both raw (71.2% vs. 64.0%) and filtered (78.1% vs. 71.1%) EEG signals. On the other hand, adding BR and ABA to the band power features of filtered EEG signals showed a noticeable improvement in the mean value of Sen, Spe, and Acc by 8.6%, 5.1%, and 6.9%, compared to the band power features of the raw EEG. Basically, the obtained results confirm the usefulness of employing BR and ABA as complementary features for analyzing the EEG driver monitoring in low-channel EEG signals.

While the proposed algorithm could properly extract blink-related features and remove eye blinks from low-channel prefrontal EEG signals to improve the accuracy of driver fatigue detection, there are some conditions that should be considered. Firstly, the EBI detection is highly sensitive to the existence of DC components and low frequency artifacts such as electrode drifts, therefore, the EEG signals must be passed through a high-pass filter with a cut-off frequency of 1 Hz. Secondly, the proposed algorithm only filters eye blink artifacts, but not other artifacts such as muscle contractions. Elimination of other artifacts may also improve the detection of driver fatigue [140, 153]. Yet, the proposed algorithm can be used in conjunction with other EEG denoising algorithms such as [165, 166]. Thirdly, we have only considered EEG band power features, BR, and ABA to form the feature vector. It should be possible to improve the quality of the driver fatigue detection by employing more features and advanced classifiers, as described in [134,146]. Nevertheless, here, we primarily aimed to show the importance of simultaneous eye blink feature extraction and elimination for the EEG-based monitoring of the driver state. The major limitation of this work is to use one public driver EEG database which contains only young healthy male subjects. Some studies showed that age and gender characteristics of subjects may also be important factors yielding the fatigue driving [167–170]. Thus, the future work direction will be validating the robustness of the proposed algorithm on a larger database with more diverse cohorts (e.g., female and elderly subjects).

3.2. Fusion of EEG and Eye Blink Analysis using a Single Fp1 Channel

Although several EEG-based studies reported the accuracy above 90% for the detection of driver fatigue, a majority of them have considered multi-channel EEG recordings, e.g., [131, 135, 171–173], which increases the complexity of wearable instrumentation [174] and is cumbersome for the long-term driving. Yet, the advent

of low-cost portable single channel EEG headbands has provided a new possibility for the driver fatigue detection in the real-world scenario [140, 175]. On the other hand, recording EEG from the prefrontal cortex can be more convenient since it is a non-hair bearing area, i.e., it is less suspicious to noise [139], and can provide the user with more comfort by allowing them to use the headrest during driving [148]. Moreover, the emergence of eye blinks in prefrontal EEG signals can also be used to characterize the fatigue driving [147]. Hence, algorithms capable of detecting the driver fatigue by using a single prefrontal EEG channel should be prioritized.

According to the best of author knowledge, only a few studies have investigated the effectiveness of prefrontal EEG signals for the detection of driver fatigue. Ogino *et al.* [176] employed the PSD of an Fp1 EEG channel and reported the accuracy of 64.9% by a SVM classifier. Qiu *et al.* [153] investigated the performance of three entropy features, i.e., permutation, sample, and fuzzy, for detection of the driver fatigue using Fp1 and Fp2 EEG channels and reported the accuracy of 95%. In another study, Cai *et al.* [177] derived 9 entropy measures from Fp1 and Fp2 channels and reported the accuracy of 94% by the light gradient boosting machine classifier. More interestingly, Ko *et al.* [148] showed that extracting blink-related features from a prefrontal EEG channel enhanced the accuracy of driver fatigue detection when employed alongside the EEG. Indeed, despite the aforementioned studies that considered eye blinks as a source of artifact in prefrontal EEG channels that should be removed before the EEG analysis, it was shown that extracting blink features combined with band power analysis of EEG can help improve the accuracy of monitoring a driver's cognitive state. Followed by [147, 148], in our previous study [20], we showed that the eye blinks have both beneficial and detrimental influence on the prefrontal EEG signals for the driver fatigue detection. After extracting the blink-related measures and removing eye blinks from the Fp1 and Fp2 channels, the RBP of the filtered EEG signals and the blink features were fed to a SVM, and the mean accuracy of 78.2% was achieved.

In spite of the promising results reported by the mentioned studies, employing only one database for the detection of driver fatigue is a potential limitation. In particular, when using nonlinear measures such as entropy, the interchangeability of tuned features for other databases is of great importance. Here, we present an algorithm for the detection of driver fatigue while using a single Fp1 EEG channel, where its performance is evaluated by two different databases; the first one is used for the adjustment of the proposed method's parameters, whereas the second one is used to evaluate the effectiveness of the tuned parameters.

Generally, the onset of fatigue in EEG might be better revealed by its sub-bands analysis [126, 148, 176, 178]. On the other hand, as shown in the context of consciousness studies that EEG may show more complexity when the subject is in an alert state [104, 137, 179], it can be expected that complexity measures will be

good indicators for the detection of driver fatigue. Furthermore, it has been shown that blinks have both beneficial and detrimental influence on EEG for the detection of driver fatigue [20]. Supported by the above-mentioned presumptions, our proposed algorithm firstly identifies EBIs in EEG by the moving standard deviation (MSD) algorithm to extract blink-related features. Secondly, EBIs are filtered from the EEG by the DWT. Thirdly, the filtered EEG is split into its sub-bands for the extraction of RBP and nonlinear measures. Finally, the prominent features are selected by the neighborhood component analysis (NCA) algorithm and fed to different classifiers for discrimination of the fatigue and alert driving.

3.2.1. The proposed algorithm

The block diagram of the proposed algorithm is illustrated in Fig. 3.6. As shown, firstly, the raw EEG signal is band-pass filtered for the noise reduction and re-sampled for reducing the computational burden. Secondly, EBIs are identified by using the MSD algorithm, and three blink-related measures are derived. Thirdly, the identified EBIs are filtered from the EEG signal based on the DWT algorithm, and then linear and nonlinear features are extracted from the filtered EEG sub-bands. Finally, a subset of prominent features is selected and fed to different classifiers to discriminate between the fatigue from alert driving states. The detailed explanation of the proposed algorithm is described in subsections below.

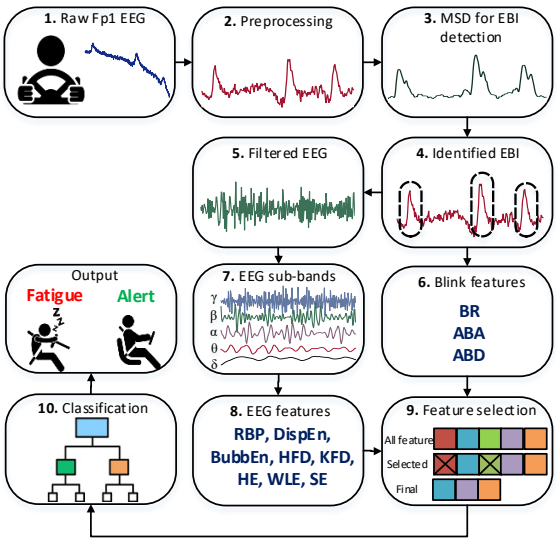

Fig. 3.6. Block diagram of the proposed method for classifying the fatigue and alert driving by using a single Fp1 EEG channel.

Pre-processing

In order to remove high and low frequency artifacts from the EEG signal, a zero-phase fourth order Butterworth band-pass filter with the cut-off frequencies at 1 and 40 Hz is applied to the raw EEG signal. Then, the filtered signal is re-sampled to 100 Hz to reduce the computational burden.

Detection of eye blink intervals

The basis of MSD is to perform window sliding on the whole sequence of a signal to compute the standard deviation values of the local k data points, where k is the width of the window. Due to the substantial differences in the inherent characteristics of eye blink and EEG signal, it is expected that EBIs be reflected in the amplitude of the MSD sequence obtained from the contaminated EEG signal. In order to detect EBIs, firstly, the local maxima of the MSD sequence obtained from the EEG are identified. Then, those with a value greater than the modified universal threshold (Th_1) [20] are selected as the potential eye blink highest peaks (Fig. 3.7b)

$$Th_1 = A\left(\frac{\text{median}(|s(n)|)}{0.6745}\right)\sqrt{2\ln N}, \tag{3.10}$$

where $s(n)$ is the MSD of EEG, N is the signal length, and A is the scaling factor. Secondly, if the distance between two potential eye blink highest peaks is less than 0.2s, the higher peak is selected as the final candidate (Fig. 3.7c). Thirdly, the identified eye blink highest peaks are projected to the EEG signal. As shown in Fig. 3.7d, the locations of the eye blink highest peaks in the EEG are not accurate. To overcome this problem, a window is formed around each identified peak with a 0.2s length before and after the peak. Then, the maximum signal value within this window is considered as the highest eye blink point (Fig. 3.7e). After finding the highest peak of EBIs, given the fact that an EBI duration usually varies from 200 to 500ms [67], 500ms intervals (125ms pre- and 375ms post the highest amplitude peaks) are chosen as the identified EBIs (Fig. 3.7f). The main steps of the MSD-based method for the identification of EBIs are summarized in Algorithm 3.

Blink-related features

As stated above, blink measures extracted from the EEG have been shown promising for the detection of driver fatigue. It is common knowledge that when subjects are performing tasks requiring visual attention, e.g., driving, they blink less to stay more focused [180, 181]. Consequently, given the fact that the concentration level decreases in the fatigue state, blink-related measures can be of discriminative power in the classification between alertness and fatigue states. In particular, it was demonstrated that while the eye blink rate increases in the fatigue state, its amplitude

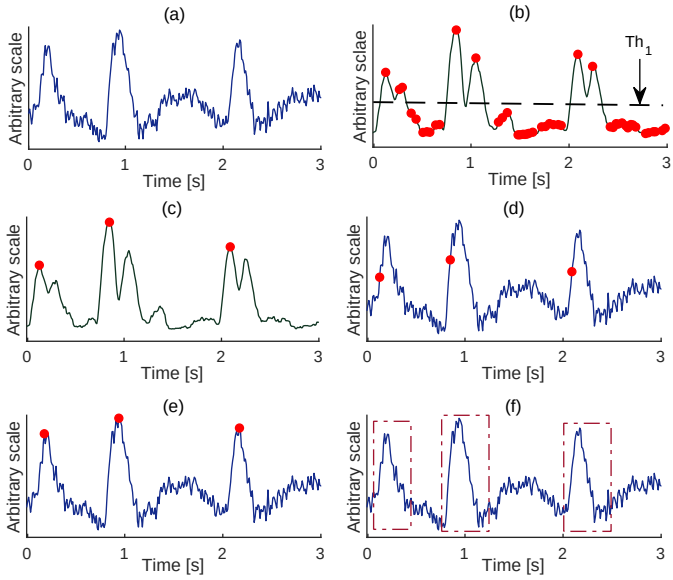

Fig. 3.7. An example for EBIs detection from an Fp1 EEG channel. EEG signal **(a)**, the MSD of EEG signal with the local maxima that exceeds Th_1 **(b)**, the MSD with the potential eye blink highest peaks **(c)**, the potential eye blink highest peaks of MSD projected to the EEG **(d)**, the corrected location of the highest eye blink peaks in EEG **(e)**, and the identified EBIs in EEG **(f)**.

decreases [148]. Justified similarly, three blink measures called BR, ABA, and the average distance between the blinks (ABD) are computed. Let $z[n]$, $n = 1, 2, ...N$ be the 20s contaminated EEG signal, $M = M_1, M_2, ...M_i$ where $M \in n$ be the location of the detected eye blinks, and i be the number of the detected blinks (Fig. 3.8). The BR, ABA, and ABD are expressed as follows:

$$\text{BR} = \frac{i}{20}, \tag{3.11}$$

$$\text{ABA} = \frac{\sum(z(M_i))}{i}, \tag{3.12}$$

$$\text{ABD} = \frac{\sum(M_i - M_{i-1})}{i-1}, \tag{3.13}$$

Filtering of eye blink intervals from EEG

Although blink-related features extracted from EEG are promising for the detection of fatigue driving [147, 148], eye blinks have been shown to have an adverse influence on the analysis of EEG due to their amplitude [20]. To minimize such a negative influence, given the sampling rate and the frequency range of eye blinks in

Algorithm 3: The MSD for localization of one EBI

Input: EEG $z(n)$, Fs, k

Output: EBI highest peak n_1, EBI $z_2(n)$

Initialisation $Th1 \leftarrow 0$, $q \leftarrow []$, $r \leftarrow []$, $m \leftarrow 1$

$s(n) \leftarrow$MSD$(z(n), k)$
$Th1 \leftarrow$ see equation (4)
for $i = 2$ to length$(z(n)) - 1$ **do**
  if $s(i) > s(i-1)$ && $s(i) > s(i+1)$ && $s(i) > Th1$ **then**
    $q \leftarrow [q \;\; i]$
  end if
end for
for $i = 1$ to length$(q) - 1$ **do**
  $d \leftarrow \text{abs}(q_i - q_{i+1})$
  $r \leftarrow q_i$
  while $d < 0.2 \times Fs$ **do**
    $r \leftarrow \text{find}(s = \max(s(q_i), s(q_{i+1})))$
    $m \leftarrow m + 1$
  end while
  $i \leftarrow i + m$
  $\text{onset}_1 \leftarrow r - 0.2 \times Fs$
  $\text{offset}_1 \leftarrow r + 0.2 \times Fs$
  $z_1(n) \leftarrow z(onset_1 : offset_1)$
  $n_1 \leftarrow \text{find}(z_1(n) = \max(z_1(n)))$
  $\text{onset}_2 \leftarrow n_1 - 0.125 \times Fs$
  $\text{offset}_2 \leftarrow n_1 + 0.375 \times Fs$
  $z_2(n) \leftarrow z(\text{onset}_2 : \text{offset}_2)$
end for
return $n_1, z_2(n)$

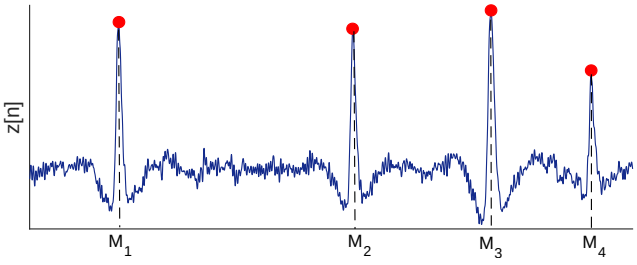

Fig. 3.8. An example for extraction of the blink-related features from an Fp1 EEG channel. M stands for the locations of four (i=4) blinks.

EEG, i.e., 0.5 to 7.5 Hz, the identified EBIs are filtered by hard-thresholding DWT with three decomposition levels, where those values of the component at each level

that transcend the universal threshold are settled to zero. Then, the filtered EEG signal is restored by inverse DWT of the thresholded components.

EEG sub-bands extraction

One of the main applications of DWT in EEG studies is to extract its sub-bands [34, 182]. Given the reduced sampling rate of EEG, four-level DWT can extract EEG sub-bands, where detail components of the first, second, third and fourth level associate with gamma (γ, >25 Hz), beta (β, 12.5-25 Hz), alpha (α, 6.25-12.5 Hz), and theta (θ, 3.125-6.25 Hz), respectively, and the fourth level of approximation component corresponds to the delta (δ, <3.25 Hz) band.

EEG features

After eye blink removal and splitting the EEG into its sub-bands, eight features, namely, RBP, log energy entropy (LeEn), Shannon entropy (SE), DispEn, BubbEn, HFD, KFD, and Hurst exponent (HE), are extracted from each sub-band as follows:

$$\text{LeEn} = -\sum_{i=1}^{N} \left(\log_2(p(B_i))\right)^2, \tag{3.14}$$

$$\text{ShEn} = -\sum_{i=1}^{N} p(B_i) \times \log_2(p(B_i)), \tag{3.15}$$

$$\text{HE} = \frac{\log_2(R/S)}{\log_2(L)}, \tag{3.16}$$

where B stands for the sub-band, p represents the probability of obtaining B_i, and R, S, and L represents the range, standard deviation, and the length of the sub-band.

Following the presumption that altering the power ratio of EEG sub-bands is correlated with the fatigue state [126, 148, 176], i.e., the power ratio of EEG higher frequency bands decrease while the opposite for the lower bands happens, it can also be expected that the extraction of nonlinear measures from EEG sub-bands is more effective than the signal itself. Therefore, in addition to the RBP, FD and entropy measures are also extracted. The FD features measure the degree of the signal's complexity and self-similarity by evaluating how quickly the signal increases or decreases with altering the scale. On the other hand, entropy features assess the signal's uncertainty. As EEG is assumed to show more complexity and uncertainty in the alert state [104, 183], such measures can be good markers for the fatigue detection. The tuning of the nonlinear features is described in Section 3.2.3.

Feature selection

In total, 43 features (3 blink-related) are extracted from the EEG signal. To reduce the dimension of the feature vector, we employ the NCA [184], which selects the best feature subset by maximizing an object function, assessing the mean leave-one-out classification accuracy over the training data. Indeed, NCA outputs a weighting vector related to the feature vector by optimizing the nearest neighbour learning classifier. The reason for using the NCA over the other feature selection methods is that it is a non-parametric algorithm, therefore, no specific regulations are required.

Classification

After selecting the prominent features, they are normalized by using the z-score approach and randomly divided into the training-validation (70%) and test (30%) subsets. To secure the robustness of results, the training-validation process is conducted according to the 10-fold CV, and the testing is only established on the unseen subset. Here, we used SVM, linear discriminant analysis (LDA), k-nearest neighbor (kNN), and AdaBoost, artificial neural network (ANN), and random forest (RF) models to classify between the fatigue and alert driving states. The motivation behind using these models is their proven feasibility for the EEG-based studies, in particular, driver fatigue detection [139, 173, 174, 185]. The fine-tuning of the model's hyperparameters is conducted during the training-validation step by the Bayesian optimization method [186].

Evaluation criteria

Eye blink detection and filtering

To investigate the performance of eye blink detection, the critical success index (CSI) is used as follows:

$$\text{CSI} = \frac{\text{TP}}{\text{TP+FN+FP}}, \tag{3.17}$$

where TP, FN, and FP represent the number of correctly, missed, and falsely detected eye blinks. Regarding the eye blink filtering, given that both databases contain the concurrent recorded EOG signals, the SNR is utilized as follows:

$$\text{SNR} = 10 \times \log_{10}\left(\frac{\frac{1}{N}\sum_{i=1}^{N} PSD_{EEG}}{\frac{1}{N}\sum_{i=1}^{N} PSD_{EOG}}\right), \tag{3.18}$$

where *PSD* stands for the power spectral density [187]. It should be noted that the SNR of the raw EEG is computed before applying any filtering, and the SNR of filtered EEG signal is computed based on filtered EEG and estimated EOG signal by the proposed algorithm.

Model assessment

The performance of the models is assessed according to the Sen, Spe, Acc, and AUC, as explained in the previous chapter.

3.2.2. Data

Here, we used two different databases to validate the performance of the proposed algorithm. The first one was used for tuning the parameters of the proposed algorithm, whereas the second one was only employed for assessing the robustness of the tuned parameters. To increase the analogy of data analysis with a consumer prefrontal EEG headset (NeuroSky) [16], only the Fp1 channel was used.

Database A

Database A, used in this section, is the same database detailed in the previous section. For more information, refer to Section 3.1.2.

Database B

This database comprises of EEG signals collected from 16 subjects (8 male) aged from 17 to 25 in a platform environment with a static simulator [153]. To collect the EEG, a 32-channels EEG cap system, referenced to the A2 mastoid with a sampling rate of 1000 Hz was used. Additionally, vertical EOG signals were recorded concurrently. All subjects were healthy during the experiment week, and had a proper sleep the night before the experiment. They were also prohibited to consume beverages that contain caffeine or alcohol. Before performing the experiment, the subjects were familiarized with the experimental environment and the operation process. After ensuring the subjects' preparation and calmness during the experiment, laboratory assistants commenced to record 5 minutes of EEG data, which were labeled as the alert state. After that, the subjects were asked to keep driving till the Li's subjective fatigue scale and Borg's CR-10 scale indicated that the subject was in the fatigue state. Then, the last 5 minutes of the EEG data were labeled as the fatigue state. Accordingly, 480 20s-long EEG epochs in the fatigue and alert states are formed, of which 240 belong to the fatigue state.

3.2.3. Results

In this section, the experimental results obtained from both databases are described. It should be noted that the regulation of the required parameters for eye blink detection and nonlinear measures, as well as the feature selection, have been conducted on the EEG signals from Database A. Then, the tuned parameters and the selected features were used for the analysis of Database B.

Eye blink detection, filtering, and feature extraction

The MSD algorithm requires two parameters to be tuned for EBIs detection; the window length k and the scaling coefficient of the universal threshold A. Regarding the window length, we have considered values from 0.1s to 0.3s with a step size of 0.05s. Although no noticeable difference was found in the morphology of EBIs, we selected $k = 0.2s$ (Fig. 3.9).

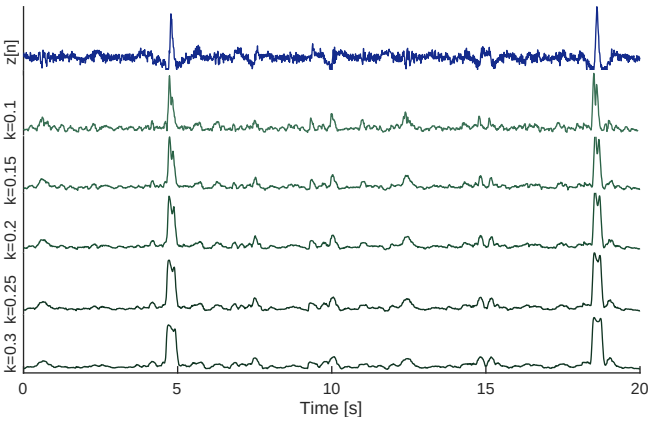

Fig. 3.9. The contaminated EEG (dark below) and its corresponding MSDs with different window sizes (green).

Regarding the scaling factor of the universal threshold, values from 0.25 to 1 with a step size of 0.25 were investigated. The best fit, $A = 0.5$, was selected based on the highest mean of CSI (Fig. 3.10a). Afterwards, the identified EBIs were filtered based on the DWT. Given having the simultaneous recorded vertical EOG, the SNR values were compared before and after the filtering (Fig. 3.10b). The adequacy of the tuned parameters for the detection and filtering of EBIs for Database B was also confirmed in Fig. 3.10(c–d).

In order to compare the performance of eye blink detection of the proposed method with our previous study [20], the CSI in terms of mean $\pm$ standard deviation is displayed in Table 3.2. Although the MSD outperformed the VME, according to the conducted independent two-sample t-test, no statistical difference was observed between the obtained results (p>0.05). Yet, the MSD performed faster than the VME as less computations are required.

Tuning EEG nonlinear features

In order to tune the parameters of the employed nonlinear measures that required optimization, i.e., DispEn, BubbEn, and HFD, we considered the lowest p value of conducted Wilcoxon Rank-Sum Test between the alert and fatigue driving cases [34].

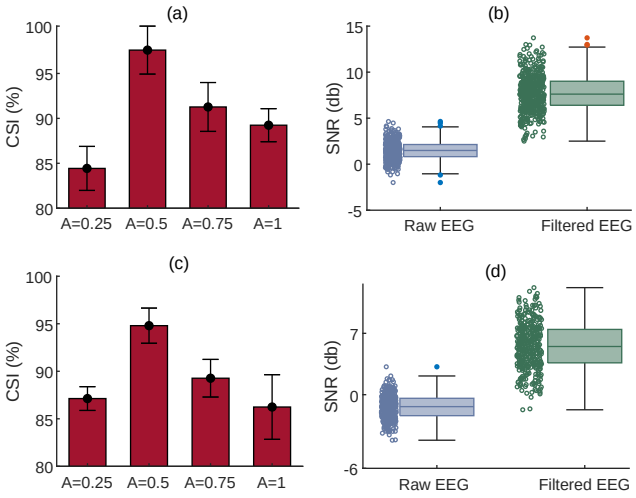

Fig. 3.10. Results for EBIs detection and filtering. Database A **(a)-(b)**, and Database B **(c)-(d)**.

Table 3.2. The comparison between eye blink detection methods in terms of mean ± standard deviation of CSI values.

Database	MSD	VME
Database A	96.8 ± 3.2	94.4 ± 4.3
Database B	94.6 ± 3.7	92.2 ± 5.3

Regarding the HFD, the maximum interval time, K_{max}, that FD values are computed in, values from 2 to 10 were varied, and K_{max}=4 was found as the finest value. Regarding the embedding dimension of BubbEn, values from 4 to 16 were tested. We selected the embedding dimension of 8 as a good fit. Regarding the DispEn, we tested several configurations, and found the embedding dimension of 4, 2 number of classes, and the time lag of 1 as a good fit.

Classification results

Table 3.3 displays the weighted features using NCA, optimized by the stochastic gradient descent algorithm. The features with a weight value greater than 0.5 (18 features) are selected for the classification. Fig. 3.11 demonstrates the classification results of the unseen testing data in terms of Acc, Sen, Spe, and AUC for all four models. The comparison confirms the superiority of the AdaBoost over the other models. When fed the selected feature set of Database A to the models, the AdaBoost classifier outperformed the others by showing the mean Acc, Sen, Spe, and AUC of 88.4%, 90.2%, 87.7%, and 0.94, respectively. Followed by that, SVM with the mean Acc of 83.7% was the second best model (Fig. 3.11a–b).

Table 3.3. The weighted features by using NCA, (selected features are in bold).

Features	Weights				
	EEG bands				
	Delta	Theta	Alpha	Beta	Gamma
RBP	**0.59**	0.13	0.21	**1.84**	0.31
DispEn	**0.74**	0.12	0.05	0.31	**0.56**
BubbEn	0.07	0.08	0.14	0.01	**0.74**
HFD	0.11	0.34	**0.86**	**1.42**	**0.85**
KFD	0.09	**1.26**	**1.71**	0.33	**1.16**
HE	0.02	0.36	0.01	0.01	**1.14**
WLE	**1.38**	**1.73**	0.35	0.13	**1.98**
SE	0.08	**0.88**	0.04	0.24	0.37
	blink				
BR	**1.12**				
ABA	**0.79**				
ABD	0.05				

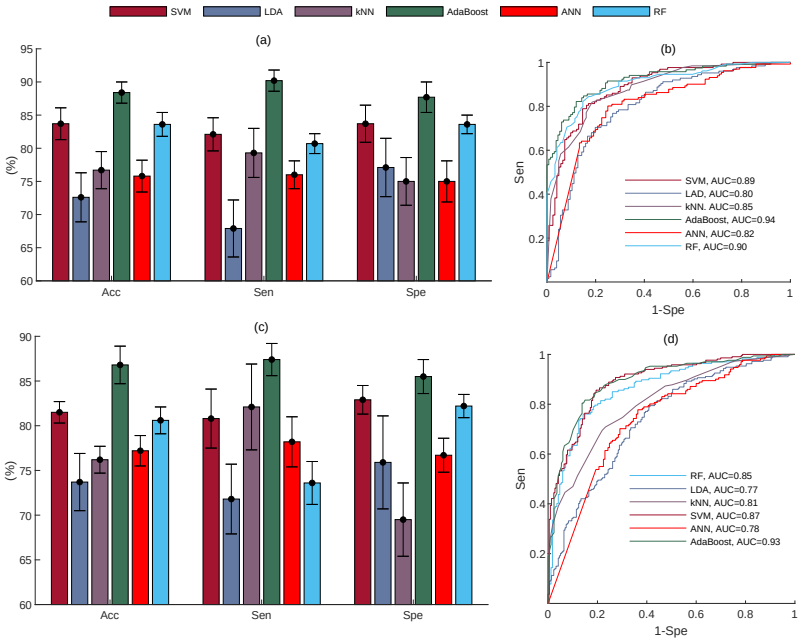

Fig. 3.11. Classification results for the detection of driver fatigue by all models. Database A **(a)-(b)**, Database B **(c)-(d)**.

Based on the performed independent two-sample t-test, there is a statistically significant difference between the Acc, Sen, and Spc values of AdaBoost and other classifiers (p<0.05). Regarding Database B, (Fig. 3.11c–d), similar to Database A, the AdaBoost model achieved the highest mean Acc, Sen, Spe, and AUC values of 87.4%, 85.5%, 86.8, and 0.93, respectively. Except for the Spe values of AdaBoost, SVM,

and RF, there is a statistically significant difference between the obtained results by AdaBoost and other classifiers (p<0.05).

Comparison with state-of-the-art methods

Table 3.4 displays the comparison between the proposed and state-of-the-art methods in terms of the number of channels, subjects, and databases, as well as the epoch length, training-testing approach, and average classification metrics. It is worth to be mentioned that we have only considered studies that used EEG signals from the prefrontal cortex.

Table 3.4. The comparison between the proposed and state-of-the-art methods. LOSOCV and LOOCV stand for leave-one-subject-out and leave-one-out cross-validation, respectively.

study	Channel	No. Database	Epoch length	No. Subjects	Training-testing approach	Mean Acc (%)	Mean Sen (%)	Mean Spe (%)
[148]	Fp1	1	20s	15	LOSOCV	68.0	58.0	73.0
[176]	Fp1	1	10s	29	10-fold CV	72.7	88.7	45.2
[153]	Fp1 &Fp2	1	1s	16	10-fold CV	95.3	NA	NA
[177]	Fp1 &Fp2	1	1s	35	LOOCV	94.2	94.0	94.3
[20]	Fp1 &Fp2	1	20s	12	10-fold CV	78.1	80.7	75.2
Ours	Fp1	2 Database A	20s	12	Random sampling	88.4	90.2	87.7
		Database B		16	Random sampling	86.6	87.4	85.5

Although, due to using different databases, epoch length, subjects, and training-testing approach, it is inequitable to quantitatively compare the performance of the proposed method with other studies, the consistency of the obtained results from two different databases using the proposed method cannot be neglected. Indeed, the robustness of our algorithm was proven based on two different databases, which is not the case for the mentioned studies. In addition, studies [153] and [177] employed two prefrontal EEG channels for the driver fatigue detection. According to the best of our knowledge, currently, no such EEG headbands with this channel configuration exist in the market. Nevertheless, it should be mentioned that the reported results from [148] are based on leave-one-subject-out (inter-subject) cross-validation, i.e., verifying the possibility of generalized model establishment, which was not investigate here.

3.2.4. Discussion

The objective of this chapter was to present an algorithm for the detection of driver fatigue based on concurrent analysis of EEG and blinks through a single prefrontal channel, oriented towards the pragmatic limitations of the current studies. The most of the current methods were developed based on multi-channel EEG recordings, not suitable for a practical application, as wearing an EEG cap with several accessories (electrodes and cables) may inconvenience the user for the long-term driving. Furthermore, multi-channel EEG configuration usually covers hair-bearing

areas of the scalp that are more susceptible to noise [148, 178]. Contrastingly, employing a single prefrontal EEG channel provides the user with more comfort as only one electrode is placed on the forehead, which is a hairless area. Moreover, the prefrontal EEG signal contains eye blinks that their changes have been shown to correlate with the transition from the alert to the fatigued state [147,148,180], therefore, blink-related measures can be extracted from the prefrontal EEG channel and used as a complementary information.

On the other hand, a few studies that addressed the fatigue driving detection based on the single or low prefrontal EEG channels only employed one database to develop and test the performance of the proposed algorithms [20, 148, 153, 176, 177]. Unarguably, the interchangeability of methods presented for detecting the driver fatigue while using different databases, which is of great importance for the real-world applications, was undermined in literature. To overcome the mentioned problem, we assessed the effectiveness of the proposed algorithm in detecting the fatigue driving by employing two databases; the first database was used for the parameter tuning and the other for the testing.

Due to both beneficial and detrimental influence of eye blinks on EEG-based fatigue driving detection [20], a hybrid algorithm based on MSD and DWT was used to locate the EBIs, extract blink-related features, and then filter them out from the EEG signal. As displayed in Fig. 3.10, while using different databases, the proposed MSD-DWT showed the comparable performance for eye blink detection and filtering, indicating its robustness for an unseen database.

Considering the fact that the interchangeability of a proposed feature set for other EEG signals recorded with distinctive characteristics plays a vital role for real-world applications, we employed two different databases; one was used for such tuning, whereas the other one was used only for testing. When comparing the obtained results by the AdaBoost classifier from Database A and B, Database A only gained 2.8%, 2.2%, and 1.6% higher mean for the Sen, Spe, and Acc, respectively, indicating the interchangeability of the tuned parameters of the used nonlinear measures. Analogously, the obtained average accuracy results by other models from both databases also showed less than 2% difference. Nevertheless, it should be noted that one cannot deduct that the power of interchangeability of the proposed algorithm is greater than the methods under comparison as such a test has not been done.

Even though [153] and [177] outperformed the proposed algorithm in terms of classification metrics, these studies have some limitations. The former only reported results on male subjects. This is while some studies showed the difference of EEG characteristics between males and females [188]. The latter also used some entropy measures, e.g., fuzzy, which require the tuning of several parameters. As it was

already mentioned, it is important to evaluate the robustness of tuned feature with other databases.

Although the reported results are promising, there are a few issues that must be considered for the future work. Firstly, due to the small number of subjects in each database, the inter-subject variability analysis has not been addressed here. Therefore, the performance of the proposed method should be further investigated with a larger number of subjects. Secondly, we have only investigated 20s-long EEG epochs for the detection of driver fatigue. Although it has been considered as a proper length [104, 148], the analysis of a shorter time interval would be of primary importance for the real-world applications. Thirdly, we have only considered classifiers that are commonly used for the EEG-based brain computer-interface systems [131, 139]. It might be possible to improve the classification results by using advanced classifiers such as XG-Boost and deep neural network. Fourthly, we have not considered the EEG channel configuration based on other available EEG consumer headbands, e.g., Emotive. In the future work, we should investigate the performance of the proposed method based on other consumer EEG headbands in the market. Fifthly, we have only employed the DWT for eye blink removal from EEG. It may be possible to further improve the performance of filtering by using methods such as the wavelet packed decomposition [189]. However, it also increases the computational complexity. Lastly, we have tuned the required parameters of the proposed algorithm based on Database A, which contains only male subjects. One may argue that it would be better to adjust parameters with Database B as it has both genders. Yet, we decided to test the performance of the proposed algorithm on a database with both genders.

3.3. Conclusions of the Chapter

1. Eye blinks serve dual roles as both a source of information and artifacts in detecting driver fatigue by using prefrontal EEG signals. Comparing the synergy of the eye blink and RBP EEG features before and after filtering revealed a notable improvement in the mean accuracy of driver fatigue detection (71.2% vs. 78.1%).

2. The proposed driver fatigue detection algorithm, which relies on simultaneous EEG and eye blink analysis using an Fp1 EEG channel, demonstrated robust performance across two databases with different recording characteristics, achieving comparable accuracy values of (88.4% vs. 86.8%).

3. The combination of RBP and nonlinear features extracted from a single prefrontal EEG channel, in addition to eye blink features, outperformed the RBP features derived from two prefrontal EEG channels for the detection of driver fatigue (88.4% vs. 71.1%).

4. DEPTH OF ANESTHESIA MONITORING

Anesthesia is another critical field for assessing varying levels of consciousness, creating a continuum from full awareness to complete unresponsiveness. The use of low-cost portable EEG systems for anesthesia monitoring is more affordable than the current commercial systems as it eliminates the need for disposable electrodes per subject, leading to a cost-effective and environmentally sustainable alternative.

General anesthesia represents a pharmacologically induced reversible state of unconsciousness, facilitating the secure execution of surgical procedures [190]. Ensuring the proper level of unconsciousness during surgery is essential as there is growing evidence of detrimental effects of excessive hypnotic depth and potentially inadequate hypnosis [10, 191]. While the former is associated with adverse cardiovascular and respiratory effects, delayed recovery, as well as postoperative delirium and postoperative cognitive dysfunction [192], the latter can lead to accidental intraoperative awareness, accompanied by its psychological consequences, including the development of posttraumatic stress disorder [193]. In addition, continuous monitoring of depth of anesthesia (DoA) can provide economic benefits by preventing the wastage of anesthetics, which has been identified as a significant contributor to the overall cost of anesthesia procedures [11, 194]. Thus, DoA monitoring benefits the patient and promotes the efficient use of resources in the healthcare system.

Anesthetics profoundly influence the brain's electrical activity, leading to discernible alterations in EEG oscillations [195]. Consequently, EEG is considered the gold standard method for DoA monitoring [196]. As the use of raw EEG is not a standard practice in an operating room, the demand arose for introducing a processed electroencephalogram, which involves simplifying EEG data into easily interpretable numeric values [197]. To this end, various systems employing different algorithms for EEG-based DoA monitoring have been developed and are being widely utilized in clinical practices and research [198]. These systems aim to quantify the DoA using predominantly EEG signals recorded from the prefrontal cortex and represented on a numerical scale [199]. For example, the bispectral index (BIS) monitor, the first EEG-based commercial DoA device, gauges the DoA on a scale from 0 to 100, where 0 denotes the absence of brain activity, and 100 indicates complete alertness [200]. Nonetheless, these systems may not be accessible to developing countries due to their high cost and reliance on single-use sensors, making them expensive for routine anesthetic practice. Consequently, various algorithms have been developed to monitor the DoA using EEG signals recorded by conventional systems [201].

Generally, two main approaches are commonly employed: feature extraction and deep learning methods. Regarding the feature extraction, several measures have been extracted from EEG signals to monitor DoA. These features aim to capture various aspects of brain activity that can reflect consciousness and DoA. One commonly

utilized feature is the power spectral density, which quantifies power distribution across different frequency bands in the EEG signal [202]. Additionally, entropy measures, such as approximate entropy (AppEn) and SampEn, have been shown to be promising for monitoring the DoA [203]. On the other hand, deep learning architectures have demonstrated promising results in capturing complex temporal and spatial dependencies within the EEG signals for DoA monitoring [204, 205]. In particular, the employment of hybrid deep learning methods showed promising results [206, 207]. Moreover, several other analyses have been explored for DoA monitoring, including functional connectivity [208], microstate analysis [209], unscented Kalman filter-based neural mass modelling [210], amplitude modulation [211], and intrinsic phase-amplitude coupling [212].

4.1. Entropy-based DoA Monitoring

The nonlinear characteristics of EEG signals have made entropy analysis a popular approach for DoA monitoring [203]. This approach is based on the understanding that as DoA increases and consciousness levels decrease, the complexity of the EEG signal changes [205]. Entropy metrics, which quantify the irregularity and complexity of EEG waveforms, are effective for this purpose. As DoA deepens, EEG signals become more predictable and regular, leading to noticeable alternation in entropy values. Thus, entropy analysis provides a promising method for assessing consciousness levels during anesthesia by leveraging the nonlinear dynamics of EEG signals to offer objective DoA measures.

According to the literature, four entropy metrics, namely, SampEn [213], permutation entropy (PeEn) [214], spectral entropy (SpEn) [215], and AppEn [216], have shown promising results for DoA monitoring using EEG. However, the utilization of fuzzy entropy (FuzzEn) and slope entropy (SlopEn) in this context remains insufficiently explored. This is while that these metrics have been proposed to overcome the limitations of the conventional entropy metrics.

On one hand, FuzzEn was initially introduced to alleviate the limitations of SampEn regarding class boundaries and data length [217]. In addition, FuzzEn demonstrates adaptability to data characteristics by allowing computation based on various membership functions [218]. This flexibility may provide a broader modeling range for capturing complex relationships in EEG signals, accommodating variations that may need to be more effectively captured by SampEn and AppEn measures.

On the other hand, SlopEn is designed to address the limitations of SampEn regarding data length and PeEn in terms of disregarding the time series amplitude information [219]. A recent study demonstrated that the spectral slope of EEG decreases during anesthesia induction and increases during recovery [220]. Motivated by above-mentioned study, SlopEn, which uniquely emphasizes variations in the signal

slope, can be employed as an effective index for DoA monitoring. SlopEn quantifies the rate of changes or slope of a signal's variations over time, assessing how quickly the signal values shift. Given that EEG patterns during anesthesia often exhibit a more regular and synchronized activity, the use of SlopEn, which measures shifts in the EEG signal, is expected to be valuable for DoA monitoring.

Here, the objectives are thus, to (i) investigate the performance of FuzzEn and SlopEn for DoA monitoring and (ii) evaluate their effectiveness compared to SampEn, SpEn and AppEn.

4.1.1. The proposed entropy-based algorithm for DoA monitoring

Fig. 4.1 displays the steps for DoA monitoring using different entropy metrics. The details of each step are explained below.

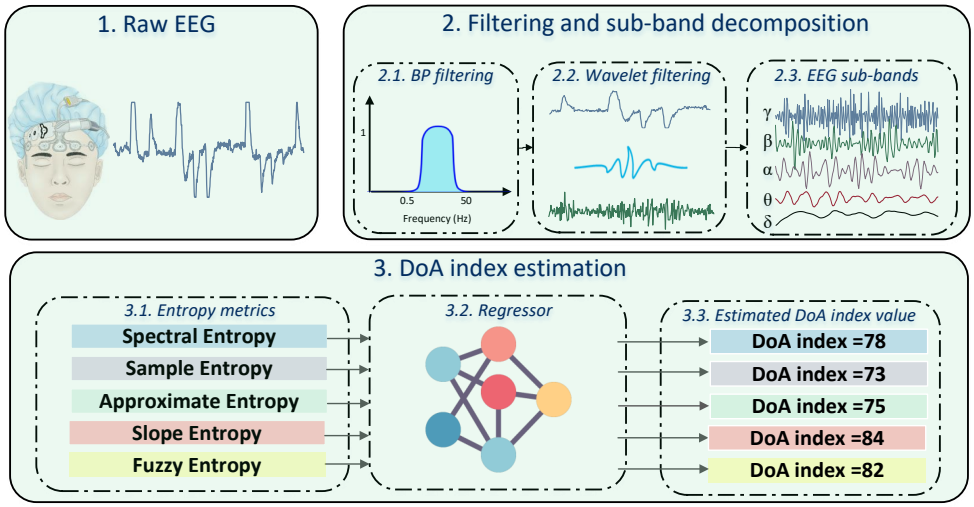

Fig. 4.1. The block diagram of DoA monitoring using different entropy metrics.

Pre-processing and sub-band decomposition

Prior to commencing the analysis, the EEG signals were segmented into 5-second intervals, and segments lacking DoA index values were excluded from consideration. Subsequently, a 4th-order Butterworth band-pass filter with cutoff frequencies at 0.5 Hz and 50 Hz was applied to eliminate very low and high-frequency noise components. Then, artifacts resulting from medical equipment, eye blinks, or muscle movements were removed by using a wavelet transform filter [18]. After the pre-processing phase, the filtered EEG signal underwent decomposition into sub-bands using zero-phase filters, encompassing the following frequency ranges: 0.5–4 Hz (δ), 4–8 Hz (θ),

8–13 Hz (α), 13–30 Hz (β), and 30–50 Hz (γ).

Entropy metrics

After decomposing the EEG signal into its sub-bands, in addition to FuzzEn and SlopEn, we also extracted SampEn, AppEn, SpEn for the quantitative comparison.

FuzzEn

The FuzzEn of a signal with the length of N is defined as follows:

$$\text{FuzzEn}(m, r, d) = -\ln\left(\frac{\sum_{i=1}^{N-m+1} u_i^{(m,d)}}{\sum_{i=1}^{N-m} u_i^{(m+1,d)}}\right), \tag{4.1}$$

where $u_i^{(m,d)}$ and $u_i^{(m+1,d)}$ represent membership values calculated based on the Chebyshev distance. Azami et al. [217] systematically compared FuzzEn using various membership functions (MFs) to discriminate between focal and non-focal EEG signals. The fine-tuning was carried out through the defuzzification process. The results of their study indicated that FuzzEn implemented with Gaussian (Gau): $\exp\left(-\frac{\text{dist}(x_i,x_j)^4}{r\cdot d}\right)$ and Exponential (Exp): $\exp\left(-\frac{\left(\frac{\text{dist}(x_i,x_j)}{\sqrt{2}\cdot r}\right)^2}{d}\right)$ MFs perform the best for such discrimination. As displayed, the process involves tuning three parameters: the embedding dimension denoted as m, which determines the length of sequences for comparison; the threshold represented by r, which balances the accuracy of logarithmic likelihood estimations against potential signal information loss; and the time delay denoted as d, which establishes the gap between successive data points.

SlopEn

Assume $x(n)$ as the EEG signal; the following steps are performed to compute the SlopEn:

- Transform the input signal $x(n)$ into a reconstructed trajectory phase space using time delay (d) embedding dimension (m) as:

$$\mathbf{X}_n = [x(n), x(n-d), \ldots, x(n-(m-1)d)], \tag{4.2}$$

- Compute the slope (S) of the reconstructed trajectory in the phase space based on the following:

$$S = \frac{1}{m-1}\sum_{i=1}^{m-1}\Delta\theta_i, \tag{4.3}$$

$$\Delta\theta_i = \arctan\left(\frac{x(n-id) - x(n-(i+1)d)}{d}\right), \tag{4.4}$$

- Apply an angular threshold (θ) to identify significant changes in the slope.

- Quantize the trajectory based on the identified significant slope changes, resulting in N bins.

- Calculate the probability (p_i) of a data point falling into bin i:

$$p_i = \frac{\text{Number of data points in bin } i}{\text{Total number of data points}}, \tag{4.5}$$

- Compute the SlopEn using only the bins corresponding to significant slope changes:

$$SlopEn = -\sum_{i=1}^{N} p_i \cdot \log_2(p_i), \tag{4.6}$$

Parameter tuning of entropy metrics

Regarding FuzzEn, for simplicity and to align with other entropy metrics, $d = 1$ is used here. However, the fine-tuning of m and r is crucial for the adequate performance of FuzzEn. The results of [217] indicated that FuzzEn implemented with Gau and Exp MFs, using values of $m = 4$ and $r = 0.253$ and 0.0018 multiplied by the standard deviation of the signal, respectively, exhibited the most favorable performance.

The SlopEn requires the fine-tuning of three parameters: embedding dimension m, time delay d, and an angular threshold range $\Delta\theta$. Here, we use an embedding dimension of 6, a time delay of 1, and an angular threshold within the range of [0, 45] degrees, adopted from the EEG analysis conducted in the reference work [219].

Table 4.1 presents the parameter values used for the entropy metrics. It is important to note that the parameters for SampEn, AppEn, and SpEn are chosen from [213], [216], and [215], respectively. These studies utilized these metrics for the DoA monitoring based on a single frontal EEG signal.

Table 4.1. The values of parameters for the other entropy metrics. SD stands for standard deviation.

Entropy metrics	Parameters
SampEn	$m = 2$, $r = 0.2\times SD$, $d = 1$
AppEn	$m = 2$, $r = 0.2 \times SD$, $d = 1$
SpEn	N.A.
Fuzz_{Gau}	$m = 4$, $r = 0.2553$, $d = 1$
Fuzz_{Exp}	$m = 4$, $r = 0.0018 \times SD$, $d = 1$
SlopEn	m = 6, $\Delta\theta = [0\ \ 45^\circ]$, $d = 1$

Regression

To predict DoA index values, we employed a feedforward neural network regression model, where the fine-tuning of its hyperparameters was carried out through the Bayesian optimization technique [186]. The feature vector was randomly divided into two subsets: a training-validation set (70%), and a test set (30%). To ensure the robustness of the results, the training-validation procedure adopted a 10-fold CV approach, while the testing phase was exclusively executed on the previously unseen subset. To assess the model performance, the mean absolute error (MAE) and CC were employed, which are defined as follows:

$$\text{MAE} = \mu(|\text{DoA index}_{\text{Est}} - \text{DoA index}_{\text{Ref}}|), \tag{4.7}$$

$$\text{CC} = \frac{\text{Cov}(\text{DoA index}_{\text{Est}}, \text{DoA index}_{\text{Ref}})}{\sigma_{\text{DoA index}_{\text{Est}}} \sigma_{\text{DoA index}_{\text{Ref}}}}, \tag{4.8}$$

where μ, Cov, σ, Est, and Ref stand for mean, covariance, standard deviation, and estimated and reference DoA index values, respectively.

4.1.2. Data

Here, a publicly accessible database is sourced from [213] is used which includes a single frontal EEG channel and BIS data acquired from a cohort of 24 patients with an average age of 44.5 ± 12.9 years, an average height of 164.2 ± 7.1 centimetres, a mean weight of 63.4 ± 14.8 kilograms, BMI (kg/m²) averaging at 23.4 ± 4.2, and the gender distribution encompassing 14 female and 10 male participants. The surgical procedure's duration was recorded at an average of 126.4 ± 72.9 minutes.

Data recording commenced five minutes prior to induction onset, corresponding to the fully conscious state, and concluded when the patients exhibited purposeful responses to verbal instructions from the attending anesthesiologist. Intermittent BIS measurements were obtained every 5 seconds using an EEG BIS Quatro Sensor (Aspect Medical Systems, Newton, MA, US), while the continuous EEG waveform signal was sampled at a rate of 128 Hz.

4.1.3. Results

Performance of individual entropy

Fig. 4.2 displays scatter plots illustrating the estimated DoA index values compared to the reference values using individual entropy metrics. Upon examining these scatter plots, a noticeable distinction becomes evident in the degree of relationship and variability between the reference and the estimated data points obtained using both FuzzEn metrics and SlopEn in contrast to the others. Notably, a stronger correlation emerges between the reference and the estimated DoA index values

derived from the FuzzEn and SlopEn metrics, with the points clustering more closely around a trendline. This heightened correlation implies a greater alignment between the estimated values and the reference data, indicating a more accurate representation of the underlying relationship. Additionally, the spread or dispersion of points in the plots related to FuzzEn and SlopEn metrics appears to be lower, suggesting a higher degree of consistency in the estimations.

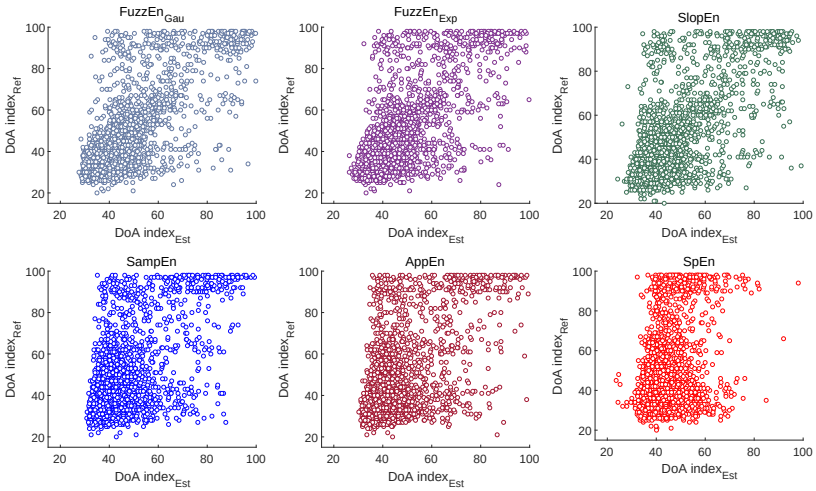

Fig. 4.2. Scatter plots between reference and estimated DoA index values for different entropy metrics.

Table 4.2 compares different entropy metrics based on their performance in terms of MAE and CC.

Table 4.2. The performance of each entropy for regressing the DoA index values.

Entropy type	Metrics ($\mu \pm \sigma$)	
	MAE	CC
FuzzEn (Gau)	6.4 ± 0.7	0.77 ± 0.02
FuzzyEn (Exp)	6.7 ± 0.5	0.75 ± 0.01
SlopEn	6.8 ± 0.6	0.74 ± 0.03
SampEn	8.7 ± 0.9	0.63 ± 0.05
AppEn	8.9 ± 1.1	0.61 ± 0.04
SpEn	10.7 ± 1.8	0.37 ± 0.10

Both variations of FuzzEn and SlopEn exhibit relatively low MAE values of 6.4, 6.7, and 6.8 respectively, along with comparatively high CC values of 0.77, 0.75, and 0.74, indicating strong correlations between the estimated and the reference DoA

index values. Notably, SampEn and AppEn show higher MAE values of 8.7 and 8.9, respectively, with CC values of 0.63 and 0.61, suggesting moderate correlations between the estimated and the reference DoA index values. According to the conducted Mann-Whitney U test, no significant difference was observed between the results obtained from both variations of FuzzEn and SlopEn (p>0.05). However, a statistically significant difference was found between the results of FuzzEn and SlopEn metrics and those of the other metrics (p<0.05).

Fusing both variations of FuzzEn

Fig. 4.3 shows the scatter plot and the histogram of AE for the fusion of both variation of FuzzEn entropy. Interestingly, the utilization of just these two FuzzEn metrics yielded notably favorable outcomes. The correlation was 0.85, indicating a strong alignment between the estimated and the reference DoA index values. Additionally, the MAE was low at 5.4. These findings underscore the efficacy of the combined FuzzEn metrics in accurate DoA monitoring.

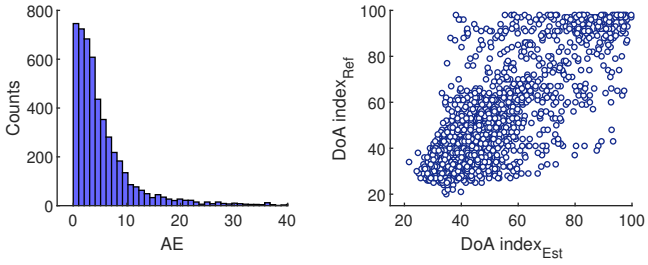

Fig. 4.3. Scatter plots and histograms of AE between reference and estimated DoA index values by employing fused FuzzEn.

4.1.4. Discussion

In this study, the performance of FuzzEn and SlopEn for DoA monitoring using a single frontal EEG channel was investigated and compared against the conventional entropy metrics commonly used in this field. The results indicated that both FuzzEn and SlopEn outperformed the conventional metrics in terms of CC and MAE.

The superior performance of FuzzEn with Gau and Exp membership functions compared to SampEn and AppEn can be attributed to several factors. Firstly, FuzzEn's utilization of membership functions enables a more nuanced representation of uncertainty, capturing varying degrees of uncertainty in the data and offering a more flexible model than the binary distinctions of SampEn and AppEn [221]. Secondly, FuzzEn exhibits adaptability to data characteristics. Gau and Exp membership

functions provide a broader range for modeling complex relationships in EEG signals, accommodating variations not effectively captured by SampEn and AppEn measures [217]. Lastly, combining FuzzEn with suitable membership functions enhances robustness to noise in EEG signals, mitigating the impact of variations [222].

The advantage of SlopEn over metrics such as SampEn, AppEn, and SpEn lies in its unique capability to capture and quantify the rate of changes or slope of a signal. While other entropy metrics focus on various aspects of the signal complexity, SlopEn specifically emphasizes variations in the signal's slope. This characteristic makes SlopEn particularly sensitive to abrupt changes or trends in the signal, offering a distinctive perspective on signal dynamics. In the context of DoA monitoring using EEG, slope entropy may provide a more nuanced and detailed representation of the underlying neural activity. Its proven lower sensitivity to data length compared to SampEn and AppEn potentially enhances the accuracy anesthesia depth assessment, making it a valuable metric in this application.

Although the results are promising, there are a few issues that should be considered for the future work. First, it may be possible to improve the performance by combining entropy metrics from different sub-bands, i.e., a feature selection method can be applied to find the prominent features based on different entropy metrics from all EEG sub-bands. Second, the examination of parameter tuning has yet to be conducted within the scope of this chapter. Instead, we utilized parameters recommended in existing literature. The performance of the employed entropy metrics may vary when subjected to diverse parameter tuning approaches.

4.2. Parameter-Free Feature Set for DoA Monitoring

Despite the promising results reported in the literature, most of the developed algorithms rely on the employment of multi-channel EEG signals analysis, which introduces complexities in wearable instruments, data processing, and interpretation. As an alternative, low-priced wearable EEG systems with a few channels can be utilized for DoA monitoring.

As far as our knowledge extends, only a few studies have explored the viability of such systems for DoA monitoring. Liu *et al.* [213] conducted a study on 24 subjects who underwent general anesthesia, exploring the use of SampEn and multivariate empirical mode decomposition (MEMD) for DoA monitoring. Nsugbe *et al.* [223] introduced a method for DoA monitoring, which involves combining raw EEG signals with handcrafted features, achieving a mean accuracy of 85% using the LDA across ten subjects. Alsafy *et al.* [224] decomposed the EEG signal into four levels using hierarchical dispersion entropy (HDE) and then extracted several features to trace the DoA. Using a balanced dataset, the correlation coefficient of 0.96 between the reference and the estimated DoA index values was reported. Schmierer *et al.* [225]

used empirical wavelet transform (EWT) and SpEn to monitor the DoA and reported an average correlation coefficient of 0.83 between the reference and the estimated DoA index values. Ra *et al.* [215] used the SpEn of 10 EEG sub-bands for DoA monitoring and reported the mean correlation coefficient of 0.80 between the reference and the estimated DoA index values. Kalinichenko *et al.* [216] proposed a combination of AppEn, power spectrum density, and burst suppression ration for DoA monitoring using a single EEG channel and reported the mean correlation of 0.78 between the reference and the estimated DoA index values. Shi *et al.* [226] proposed a deep residual shrinkage network for the DoA monitoring using four EEG channels and reported the correlation of 0.93 between the reference and the estimated DoA index values. Shin *et al.* [202] proposed the phase lag entropy (PLE) as a feature for DoA monitoring. By employing four EEG channels, the correlation of 0.83 between the reference and the estimated DoA index values were reported. Chen *et al.* [195] investigated the EEG variability analysis for DoA monitoring, which was based on extraction of the envelope generated by local maxima of the original EEG signal. The best correlation of 0.72 between the reference and the estimated DoA index values was obtained by the median frequency as the feature.

Nonetheless, utilizing only one database for developing and testing the DoA monitoring algorithm poses a potential limitation for the aforementioned studies. This is especially notable when employing nonlinear features like SampEn that require parameter tuning before the computation [227]. Indeed, the ability to interchange tuned features across different databases, which is crucial for the generality of the proposed method, has been neglected [221, 228].

Here, the objectives are, thus, twofold: (i) to introduce a parameter-free feature set for the DoA monitoring using a single frontal EEG channel, eliminating the need for human intervention in tuning parameters before computation, and (ii) to investigate the performance of the proposed feature set on two different databases, ensuring the generalizability of the proposed feature set when applied to data recorded with distinct characteristics, e.g., varying sampling rates.

4.2.1. The proposed algorithm

In Fig. 4.4, the block diagram of the proposed algorithm for the DoA monitoring is depicted. A detailed explanation of each step is given in the following subsections.

Pre-processing and sub-band decomposition

The pre-processing and sub-band decomposition procedures are similar to those described in Section 4.1.1.

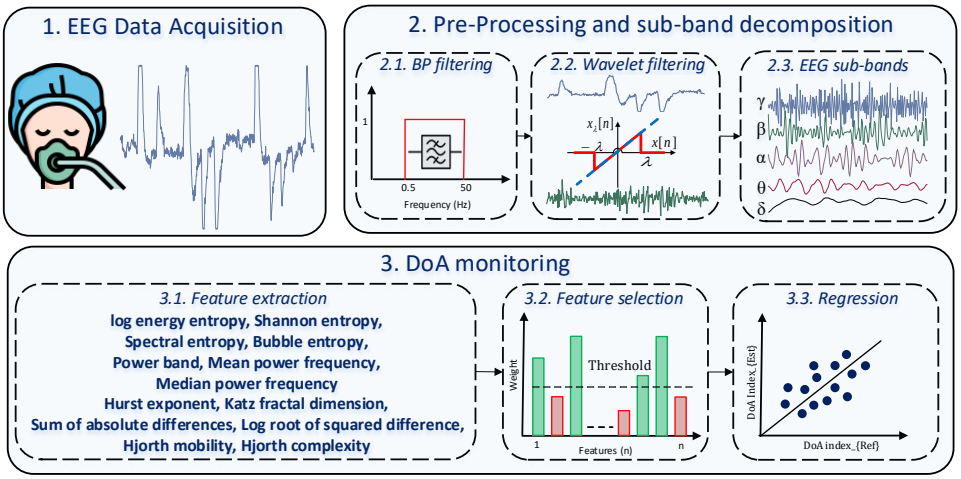

Fig. 4.4. The block diagram of the proposed algorithm for DoA monitoring.

Feature extraction

Here, we utilize four distinct categories of features: entropy, band power and frequency, fractal, and variation-based features.

Entropy-based features

Generally, entropy quantifies the irregularity of the EEG signal, offering a quantitative assessment of the brain's response to anesthesia [229]. Here, we use four entropy measures called LeEn, ShEn, SpEn, and BubbEn, where SpEn is defined as follows:

$$\mathrm{SpEn} = -\sum_{f} P_f \times \log_2(P_f), \tag{4.9}$$

with P_f representing the probability of the signal's power spectral density having a value at the frequency bin f. The first three entropy metrics are parameter-free, and the fourth one only requires the adjustment of the embedding dimension. Nevertheless, it has been shown that the performance of BubbEn is not highly dependent on the embedding dimension [111]; thus, we have used $m = 8$ as investigated in earlier research [27].

Power and frequency band features

As the alternation of consciousness level is linked to different EEG sub- bands, it can be expected that the features which represent the power and frequency of EEG sub-bands be of discriminative power for the DoA monitoring [105]. Here, we use power band (PB), mean power frequency (MPF), and median power frequency (MAPF)

of each sub-band computed as follows:

$$\text{PB} = \sqrt{\frac{1}{N}\sum_{i=1}^{N} B_i^2(n)}, \tag{4.10}$$

$$\text{MPF} = \frac{\sum_{i=1}^{M} f_i P_i}{\sum_{i=1}^{M} P_i}, \tag{4.11}$$

$$\text{MAPF} = f \text{ where } \{CDF(f) = 0.5\}, \tag{4.12}$$

where f_i and P_i are the frequency value and power spectrum at the frequency bin i, M is the length of the frequency bin, and CDF is the cumulative distribution function of the normalized power spectral density of the sub-band.

Fractal-based features

Based on the findings of studies focused on classifying consciousness levels, it has been observed that EEG signals tend to exhibit higher complexity levels when individuals are more alert [230, 231]. This leads to the expectation that complexity measures can serve as robust indicators for DoA monitoring. Here, we utilize a pair of complexity characteristics known as KFD and HE.

Variation-based features

The EEG pattern during anesthesia typically shows a more regular and synchronized activity, resembling the patterns observed during deep sleep [232]. This shift in EEG signals reflects the suppression of conscious awareness and the altered neural dynamics induced by anesthetics. Thus, we expect the features that represent such variations to be helpful for DoA monitoring. Here, we use two features called sum of absolute differences (SAD) and log root of squared difference (LRSD) defined as follows [82]:

$$\text{SAD} = \sum_{i=2}^{N-1} |B(n) - B(n-1)|, \tag{4.13}$$

$$\text{LRSD} = \log_{10}\left(\sqrt{\sum_{n=2}^{N-1} (B(n) - B(n-1))^2}\right), \tag{4.14}$$

In addition, two Hjorth measures, i.e., mobility (M_H) and complexity (C_H), are also computed as follows:

$$M_H = \frac{\sigma_{B'(n)}}{\sigma_{B(n)}}, \tag{4.15}$$

$$C_H = \frac{\sigma^2_{B''(n)} / \sigma^2_{B'(n)}}{\sigma^2_{B'(n)} / \sigma^2_{B(n)}}, \tag{4.16}$$

where σ stands for the standard deviation of the EEG sub-band $B(n)$, $'$ and $''$ express the first and second derivatives, respectively.

Feature selection

To select the prominent features, the NCA algorithm is used. Here, we used a sub-set of Database I for finding the prominent features; then those selected features are used to regress out the DoA index values for the rest of Database I and the whole Database II. For more information regarding the NCA, refer to Section 3.2.1.

Regression

RF and SVM regression models are utilized to predict the DoA index values following the selection of the prominent features, as they have previously demonstrated promising results in DoA monitoring [213]. The fine-tuning of the model's hyperparameters is adjusted based on the Bayesian optimization method. To assess the models' performance, the MAE and CC were employed.

4.2.2. Data

As already stated, we employ two databases to evaluate the performance of the proposed algorithm. It should be noted that a fraction of Database I is used for selecting the prominent features, and Database II is only used for investigating the interchangeability of the selected features.

Database I

Database I used in this section is the same database detailed in the previous section. For more information, refer to Section 4.1.2.

Database II

This database comprises EEG and BIS data from 30 patients undergoing a scheduled surgical procedure at the University Hospital in Krakow, Poland. The study included individuals classified as ASA physical status 1, 2, and 3, with an average age of 48.7 ± 13.3 years, height of 172.5 ±8.6 centimetres, weight of 81.3 ± 16.6 kilograms, BMI (kg/m^2): 27.2 ± 4.9, and a gender distribution of 12 female and 18 male subjects. The duration of the surgery was 74 ± 28.2 minutes.

The intermittent BIS measurements were recorded at 5-second intervals utilizing an EEG BIS Quatro Sensor (Aspect Medical Systems, Newton, MA, US). EEG data acquisition was facilitated through a 64-channel ActiveTwo amplifier system (BioSemi, Amsterdam, NL), with a sampling rate set at 1024 Hz. It is imperative to underscore that, although the recordings were made with a 64-channel EEG system, the present

study exclusively focused on the Fp1 EEG channel to enhance comparability with low-cost portable EEG headbands, akin to the NeuroSky product [16]. It is noteworthy that the analysis was limited to 23 subjects, as the values of one BIS measurement were unavailable, and the EEG signals associated with the Fp1 channel of other 6 participants exhibited significant noise.

Prior to data recording, each subject signed the informed consent form. The study's execution adhered to the principles outlined in the Declaration of Helsinki and secured approval from the local ethics committee, namely, the Bioethical Committee at Jagiellonian University Medical College in Krakow, Poland, under the ethics code 1072.6120.60.2019.

4.2.3. Results

This section presents the results obtained from both databases based on random sampling and leave-one-subject-out cross-validation. Regarding the random sampling, the prominent features are divided into two subsets: training-validation (70%) and testing (30%) randomly. To enhance result robustness, the training-validation process adheres to a 10-fold CV approach, whereas the testing is exclusively conducted on the unseen subset.

Prominent features

To identify the prominent features, we conducted a selection process on the entire recordings of six subjects from Database I. From each sub-band, 13 features were extracted. Subsequently, the NCA was employed to highlight the key features. This was achieved by maximizing an objective function, which evaluated the mean leave-one-out regression across all 65 features extracted from the six recordings above. Here, features receiving a weight exceeding 0.5 were deemed prominent, as depicted in Fig. 4.5. 34 features were identified with weights surpassing 0.5. Notably, MPF, MAPF, and M_H of all sub-bands are amongst the selected features. It is also worth mentioning that these recordings have been excluded from the final regression results.

Regression based on random sampling

After excluding samples with unknown DoA index values, 25198 and 19399 5s EEG signal segments of Databases I and II were used for the analysis. The entire process was repeated ten times to ensure the robustness of the results. Table 4.3 presents the mean and standard deviation of the MAE and CC between the reference and the estimated DoA index values. Although the RF shows slightly better performance, based on the conducted Mann-Whitney U test, no significant difference was found between the obtained results using either model ($p>0.05$).

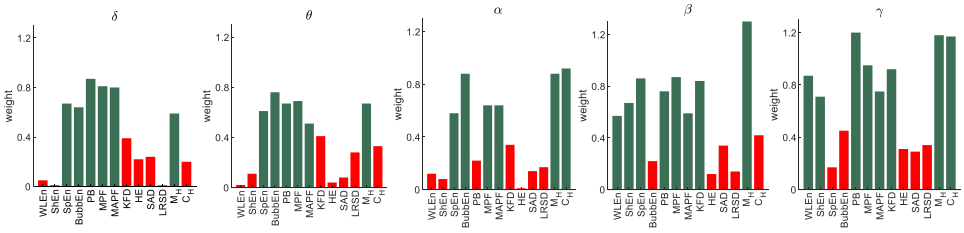

Fig. 4.5. The selected features (green) by the NCA, categorized based on each sub-band.

Table 4.3. The MAE and CC obtained for the random sampling approach using both Databases.

	Regression model	MAE ($\mu \pm \sigma$)	CC ($\mu \pm \sigma$)
Database I	Random forest	5.3 $\pm$ 0.5	0.86 $\pm$ 0.03
	SVM	5.9 $\pm$ 0.7	0.81 $\pm$ 0.02
Database II	Random forest	7.1 $\pm$ 0.8	0.85 $\pm$ 0.02
	SVM	7.3 $\pm$ 1.1	0.83 $\pm$ 0.04

Regression based on LOSOCV

Comparing the results for RF and SVM in Databases I and II (Table 4.4), we observe that the RF generally exhibits higher CC values across subjects, suggesting a stronger linear relationship between the estimated and the reference values. Additionally, the RF tends to have lower MAE values, indicating a better estimation accuracy than SVM. This trend is consistent across most subjects. Overall, the RF model achieved a higher mean CC for Database I (0.80 vs. 0.65) and Database II (0.79 vs. 0.60) and a lower mean MAE for Database I (7.1 vs. 9.3) and Database II (9.01 vs. 12.2).

Table 4.4. The MAE and CC obtained for the LOSOCV approach using both Databases.

	Regression model	MAE ($\mu \pm \sigma$)	CC ($\mu \pm \sigma$)
Database I	Random forest	7.1 $\pm$ 1.4	0.80 $\pm$ 0.05
	SVM	9.3 $\pm$ 1.9	0.65 $\pm$ 0.09
Database II	Random forest	9.0 $\pm$ 1.6	0.79 $\pm$ 0.07
	SVM	12.2 $\pm$ 2.0	0.60 $\pm$ 0.13

Fig. 4.6 illustrates an instance of the reference DoA index values alongside the estimated ones by both models using Database II. The observation reveals that the RF model adeptly captures the trajectory of the reference DoA index values. Indeed, the RF model yielded a more accurate DoA index estimation than the SVM, demonstrating a more robust correlation (0.86 vs. 0.68).

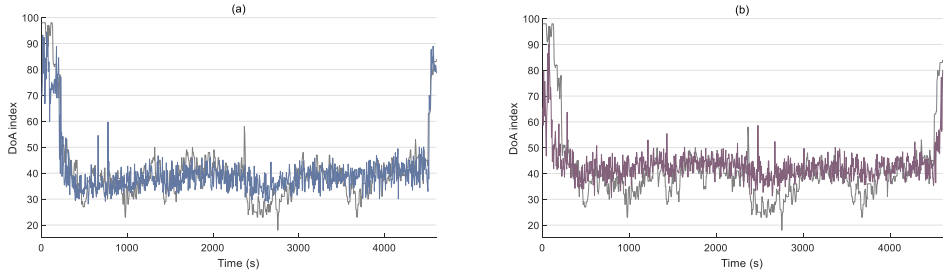

Fig. 4.6. An example on how RF (dark blue) **(a)** and SVM (purple) **(b)** follows the trend of references DoA index values (light gray) for one subject from Database II.

Comparison with state-of-the-art

Table 4.5 compares the proposed algorithm and state-of-the-art approaches, focusing on several aspects, including the number of channels, subjects, databases, the training-testing approach, and the average regression metrics. It is worth noting that our analysis exclusively included studies that utilized EEG data from the frontal cortex with a few channels.

Table 4.5. The comparison between the proposed and state-of-the-art algorithms. LR and LOSOCV represent the linear regression and leave-one-subject-out cross-validation, respectively.

Study	No. databases	No. subjects	No. channels	EEG decomposition	Features	Regressor	Training-testing approach	CC	MAE
[195]	1	56	1	EEG variability	MAPF	N.A.	LOSOCV	0.74	N.A.
[202]	1	34	4	N.A.	PLE	N.A.	LOSOCV	0.84	N.A.
[207]	1	176	2	N.A.	Raw data	CNN	Random sampling	0.80	6.03
[213]	1	24	1	MEMD	SampEn	SVM	LOSOCV	0.90	5.22
[224]	1	37	1	HDE	Entropy	LR	Random sampling	0.96	N.A.
[225]	1	23	2	EWT	SpEn	SVM	LOSOCV	0.83	N.A.
[215]	1	37	1	Sub-bands	SpEn	LR	LOSOCV	0.80	N.A.
[216]	1	54	1	N.A.	AppEn BR BP	LR	LOSOCV	0.78	N.A.
[226]	1	18	4	N.A.	SampEn AppEn BP SEF	DRSN	Random sampling	0.93	N.A.
Ours	Database I	24	1	Sub-bands	Entropy Fractal Power Variation	RF	Random sampling LOSOCV Random sampling LOSOCV	0.86 0.80 0.85 0.79	5.3 7.1 7.1 9.0
	Database II	23	1						

Compared to [195], our feature set yields a higher mean CC for the LOSOCV approach. Although [202] achieved a slightly higher mean CC with LOSOCV, their results were based on the use of four EEG channels, whereas ours are based on a single EEG channel, potentially reducing wearable complexity. Our proposed algorithm shows a higher mean CC for random sampling analysis compared to [207], which utilized two EEG channels. Additionally, our method exhibits lower computational complexity than [213], as we employ simple linear filters for extracting

EEG sub-bands instead of MEMD. While [224] achieved a higher mean CC for random sampling, it is worth noting that they used a balanced dataset. In real-life scenarios, as considered in our study, imbalanced data among DoA index values are typical. Although [225] achieved a slightly higher mean CC for leave-one-subject-out cross-validation, our algorithm stands out by using a single EEG channel, reducing computation and wearable complexity. Regarding [215], our results were comparable, but we demonstrated more consistency by employing two different databases in our evaluation. Compared to [216], we achieved a higher mean CC for LOSOCV. Regarding [226], although their reported mean CC was higher than ours, we stand out by employing only one EEG channel instead of four.

4.2.4. Discussion

Here, we aimed to propose a parameter-free feature set for DoA monitoring using a single frontal EEG channel, specifically tailored to address the pragmatic constraints encountered in existing research. On the one hand, a wide range of methods presented in the literature were designed using multi-channel EEG recordings, which could introduce inconvenience during surgery as it necessitates wearing multiple accessories connected to various regions of the brain. On the contrary, employing a single frontal EEG channel is more convenient since it involves placing just one electrode on the hairless forehead area, thus, potentially reducing susceptibility to noise.

On the other hand, studies that focused on DoA monitoring using a single frontal EEG channel typically utilized only one database to develop and assess the performance of their proposed algorithms. Indisputably, the interchangeability of algorithms presented across different databases, a crucial aspect of real-world applications, has been undermined in the literature. This issue becomes particularly notable when using nonlinear features like approximate or sample entropy, as they require parameter tuning before computation, i.e., optimal performance of these measures is sensitive to the initial calibration [221, 228]. However, our algorithm introduced a feature set that does not require parameter tuning. As a result, there should be less concern about the performance of parameters with other databases, ensuring the feature set's interchangeability and applicability across different databases.

Considering the critical importance of feature set interchangeability for DoA monitoring across different databases in real-world applications, our algorithm involved utilizing two distinct databases. In this process, a portion of Database I was employed to select the prominent features, while the rest of Database I and the whole Database II were exclusively used to test the selected features from the previous stage. When comparing the results obtained for the random sampling approach using the RF regressor between Database I and II, the former achieved only 0.01 higher mean CC and 1.8 lower MAE. Similarly, both databases demonstrated comparable results for the

one-subject-leave-out cross-validation with the RF regressor, as the former only gained 0.01 higher CC and 1.91 lower MAE. These outcomes suggest that the proposed feature set is interchangeable across the two different databases.

Furthermore, based on the best of our knowledge of the current studies in the field, a significant portion of the research that estimated DoA index values from a single EEG channel primarily focused on investigating either random sampling or leave-one-subject-out cross-validation, overlooking the importance of consistent performance for both scenarios [121]. However, in contrast, our study emphasizes the robustness of the proposed feature set by achieving comparable results for both scenarios. Specifically, a comparison between Table 4.3 and Table 4.4 demonstrates comparable mean CC values for Database I (0.86 and 0.80) and Database II (0.85 and 0.79), as well as comparable mean MAE values for Database I (5.3 and 7.1) and Database II (7.1 and 9.01) obtained using the RF model for both scenarios. This also indicates the robustness and consistency of our proposed approach across different databases and evaluation scenarios. Nonetheless, it is essential to acknowledge that the greater power of interchangeability of the proposed feature set compared to other methods cannot be conclusively deduced as no such test has been conducted.

Similar to other research on DoA monitoring, the proposed algorithm has a few limitations that one should take into consideration in future work. Firstly, although the regression results are promising, further investigation on a more extensive database might be necessary for the assessment of the proposed feature set. In particular, the investigation of the performance of the proposed feature set on specific drugs [233] and subjects of different ages [234] should be beneficial. Secondly, exploring more advanced classifiers, such as CNN, for regression could be beneficial, but their implementation requires substantial computational resources and specialized knowledge. Thirdly, for Database II, we only considered the Fp1 EEG channel to test the performance of the feature set. It is possible that the proposed feature set would perform differently on other frontal EEG channels. However, it is essential to highlight that we aimed to propose a method suitable for available consumer frontal EEG headsets; hence, we specifically focused on the Fp1 channel. Fourthly, different feature selection methods could yield varying results. Although we found the NCA approach convenient due to its simplicity and independence from parameter tuning, exploring other feature selection methods might be worthwhile. Lastly, our reference for DoA was solely the BIS, which is acknowledged to possess several limitations, such as sensitivity to certain anesthetics [235, 236], unreliability in cases of hypothermia or neurological impairment, etc. Consequently, it remains plausible that the proposed feature set might exhibit varying performance when aligned with alternative DoA measurement systems as the reference. Notably, prior studies have highlighted disparities in DoA index values across diverse measurement systems [237].

4.3. Conclusions of the Chapter

1. In evaluating individual entropy metrics for DoA monitoring using a single frontal EEG channel, both FuzzEn and SlopEn demonstrated superior performance compared to the conventional SampEn and AppEn with a higher CC of 0.77 and 0.74, respectively, compared to 0.63 and 0.61 for SampEn and AppEn. Additionally, they showed lower MAE, with values of 6.4 and 6.8 compared to 8.7 and 8.9.

2. The combination of both variations of FuzzEn with Gau and Exp membership functions appears to create synergy for the estimation of DoA index values, resulting in a higher CC of 0.85 and a lower MAE of 5.4 between the reference and the estimated DoA index values.

3. The proposed parameter-free feature set for DoA monitoring demonstrated robustness, achieving comparable CC values of 0.86 and 0.85, and MAE values of 5.3 and 7.1 between the reference and the estimated DoA index values for Databases I and II, respectively, despite their different recording characteristics. Moreover, it shows comparable regression results to current state-of-the-art methods, while distinguishing itself through its simplicity by eliminating the necessity for prior calibration of parameters.

5. CONCLUSIONS

1. The proposed SWT-kurtosis algorithm effectively addressed the removal of electrical shift-linear trend artifacts in a short segment of a single EEG signal. It demonstrated superior performance compared to AWICA and EAWICA, with a higher CC of 0.92 versus 0.58 and 0.67, and a NRMSE of 5.4 versus 12.2 and 11.5, respectively, between the artifact-free and filtered EEG signals. Similarly, the VME-DWT proved to be an effective algorithm for detecting and filtering eye blink artifacts in a short segment of a single frontal EEG channel. It outperformed AVMD and DWT, showing a higher CC of 0.92 versus 0.83 and 0.58, and a lower RRMSE of 0.42 versus 0.59 and 0.87. Both algorithms hold significant promise for artifact removal in brain-computer interface and clinical applications, as they do not require the initial calibration or reference artifacts.

2. The effectiveness and versatility of a nonlinear feature set derived from a single frontal EEG channel were demonstrated as a potential solution to address the limitations of the conventional RBP analysis for discriminating wakefulness from Sleep Stage I. Our findings indicate that the proposed nonlinear features, which are based on fractal and entropy analysis of EEG sub-bands, outperform the traditional RBP analysis, showing a higher mean sensitivity to Sleep Stage I across multiple databases: Sleep Telemetry (82.6% vs. 71.8%), DREAMS (87.6% vs. 71.8%), DCSM (91.0% vs. 74.2%), and MESA (82.0% vs. 76.1%). Considering the interchangeability of the proposed feature set, proven by using four databases recorded with different characteristics, it can be concluded that it has the potential to be used for estimating the sleep onset latency in clinical applications.

3. New insights into the significance of eye blinks in EEG-based driver fatigue detection were provided, emphasizing their dual role as both informative signals and potential artifacts. The comparison between the synergy of eye blink and EEG RBP features, before and after filtering, revealed a notable improvement in the mean accuracy of driver fatigue detection (71.2% vs. 78.1%). This underscores the dual role of eye blinks in prefrontal EEG for driver fatigue detection. Building on these findings, a driver fatigue detection algorithm was proposed, based on simultaneous EEG and eye blink analysis using an Fp1 EEG channel. The algorithm's performance was evaluated using two databases with different characteristics. The results obtained from both databases using the AdaBoost classifier, in terms of accuracy (88.4% vs. 86.8%), demonstrated the robustness of the proposed algorithm for detecting driver fatigue. Given the availability of commercial single prefrontal channel EEG headbands, this algorithm shows promise for real-world applications in detecting driver fatigue.

4. A parameter-free feature set for DoA monitoring using a single frontal EEG channel was presented, with its performance evaluated across two databases with

distinct characteristics. The proposed feature set demonstrated robustness, achieving comparable CC values of 0.86 and 0.85, and MAE values of 5.3 and 7.1 between the reference and the estimated DoA index values for Databases I and II, respectively. While parameter-free features exhibit a degree of universality across different EEG databases for DoA monitoring, the employment of specific nonlinear features can enhance the performance. Notably, precise adjustment of certain nonlinear features, such as FuzzEn combined with Exp and Gau variants, produced results comparable to the parameter-free features for estimating the DoA index values for Database I, despite their lower dimensionality. This highlights the importance of optimizing nonlinear feature parameters to maximize the performance in EEG-based DoA monitoring.

6. SANTRAUKA

6.1. ĮVADAS

Tyrimo aktualumas

Sąmonė – tai būsena, kai žmogus suvokia ir gali patirti pojūčius, mintis ir aplinką. Ji apima subjektyvius žmogaus patirties aspektus, įskaitant suvokimą, savimonę ir gebėjimą apdoroti informaciją [1]. Tai yra daugialypė sąvoka, apimanti būsenas, kurioms būdingas reagavimas į išorinius dirgiklius ir kognityvinis aktyvumas, iki pakitusių būsenų, per kurias individai gali patirti sumažėjusią kognityvinę funkciją [2]. Žmogui pereinant iš budrumo į pakitusią sąmonės būseną, pavyzdžiui, nuovargį, miegą ir anesteziją, sąmonė patiria dinaminius pokyčius, susijusius su skirtingais nervų sistemos modeliais ir subjektyvia patirtimi [3]. Dėl šios priežasties analizuoti sąmonės lygį yra ypač svarbu tokiomis aplinkybėmis, kaip miego vertinimas, nuovargio nustatymas ir anestezijos gylio stebėjimas.

Miego vertinimo srityje miego kokybė yra glaudžiai susijusi su sąmonės lygiu, patiriamu poilsio metu ir suteikia įžvalgų apie asmens jauninamojo poilsio gylį ir pobūdį [4]. Neseniai atlikto tyrimo duomenimis, beveik 25% Europos Sąjungos gyventojų kenčia nuo vienokių ar kitokių miego sutrikimo formų, kurios neigiamai veikia fizinę ir psichinę sveikatą [5]. Su tuo susijusios gydymo išlaidos ir asmenų veiklos apribojimai dėl prastos miego kokybės dar labiau įrodo, kad svarbu spręsti su miego sąmone susijusius klausimus.

Nuovargio įvertinimas yra dar viena svarbi pritaikymo sritis, kai sąmonės analizė tampa nepakeičiama. Nuovargis labai sutrikdo kognityvines funkcijas ir budrumą [6]. Apskaičiuota, kad pasaulyje 14–20% eismo įvykių įvyksta dėl vairuotojų nuovargio [7]. Jungtinėse Amerikos Valstijose AAA Eismo saugumo fondo atlikto tyrimo duomenimis, vien tik šioje šalyje dėl vairuotojų nuovargio įvyksta daugiau kaip 328 000 eismo įvykių per metus. Iš jų 109 000 baigiasi sužalojimais, o apie 6 400 – mirtimi [8]. Sąmonės lygio analizė palengvina ankstyvą su nuovargiu susijusių pokyčių nustatymą, leidžiantį laiku įsikišti, kad būtų išvengta nelaimingų atsitikimų. Nagrinėdami sudėtingą sąmonės ir nuovargio sąveiką, mokslininkai gali kurti pažangias vairuotojų stebėsenos sistemas, didinančias kelių eismo saugumą.

Medicinos srityje anestezijos gylio stebėjimas yra gyvybiškai svarbus, siekiant užtikrinti pacientų saugumą per chirurgines procedūras. Skirtingų sąmonės lygių analizė padeda anesteziologams palaikyti tinkamiausią pusiausvyrą tarp pacientų be sąmonės būklės ir galimo šalutinio poveikio mažinimo. Ši subtili pusiausvyra padeda ne tik sėkmingai atlikti chirurgines operacijas, bet ir išvengti komplikacijų, susijusių su nepakankama ar pernelyg gilia anestezija [9, 10]. Be to, nuolatinis sąmonės lygio stebėjimas anestezijos metu gali suteikti ekonominės naudos, užkertant kelią anestetikų švaistymui, kuris, kaip nustatyta, labai prisideda prie bendrų anestezijos procedūrų

sąnaudų [11]. Taigi, tokia stebėsena naudinga pacientui ir skatina veiksmingai naudoti sveikatos priežiūros sistemos išteklius.

Smegenys, pasižyminčios sudėtingais neuroniniais tinklais ir sudėtingomis sąveikomis, yra pagrindinis sąmoningos patirties generavimo centras [12]. Neuromoksliniai įrodymai nuosekliai susieja tam tikrą smegenų veiklą su sąmoningais reiškiniais, išryškindami esminį smegenų vaidmenį. Tyrimai, apimantys neurologinius vaizdus ir nervų stimuliaciją, patvirtina, kad smegenys yra biologinis sąmonės substratas [13]. Elektroencefalografija (EEG) yra labai svarbi analizuojant sąmonės lygius, nes leidžia realiuoju laiku gauti įžvalgas apie įvairias būsenas [14]. Dėl neinvazinio pobūdžio, perkeliamumo ir rentabilumo EEG yra nepakeičiama tiriant sąmonės dinamiką įvairiose srityse – nuo medicininių iki kognityvinių tyrimų.

EEG elektrodai yra strategiškai išdėstyti ant galvos odos pagal standartines sistemas, tokias kaip 10–20 ir 10–10 sistemos, kurios užtikrina nuoseklius ir pakartojamus matavimus. Šie elektrodai, pavadinti pagal jų pagrindines smegenų skiltis, apima svarbias sritis, įskaitant frontalinę (F), temporalinę (T), parietalinę (P), okipitalinę (O) ir centrinę (C) sritis. Padėtis nustatoma pagal sisteminę nomenklatūrą: nelyginiai skaičiai (1, 3, 5, 7) žymi vietas kairiajame pusrutulyje, o lyginiai skaičiai (2, 4, 6, 8) – pozicijas dešinėje. Elektrodai, esantys išilgai galvos odos vidurio linijos, pažymėti raide „z“ (nulis), pvz., Fz (priekinė vidurio linija), Cz (centrinė vidurio linija) ir Pz (parietalinė vidurio linija) (6.1 pav) [15].

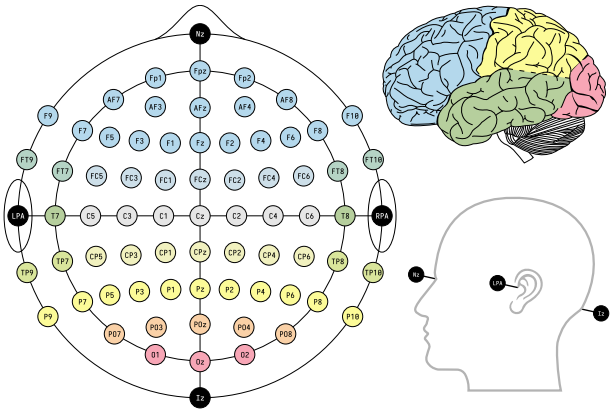

6.1 pav. EEG elektrodų išdėstymas pagal 10–10 sistemą, adaptuota iš [15]

Dabartinių tyrimų spragos ir galimos sprendimo strategijos

Nors literatūroje pateikiami daug žadantys rezultatai tiriant sąmonės lygį naudojant EEG, nemaža šių tyrimų dalis sutelkta į daugiakanalių polisomnografijos įrašų analizę. Toks metodas apsunkina dėvimųjų prietaisų naudojimą ir kelia sunkumų

atliekant ilgalaikius įrašus. Be to, tokia konfigūracija ne tik riboja EEG tyrimų išplečiamumą, bet ir trukdo praktiškai taikyti realaus gyvenimo scenarijuose. Dėl sudėtingo polisomnografijos sistemos montažo ir kvalifikuoto specialisto poreikio jos platesnis naudojimas už kontroliuojamos mokslinių arba klinikinių tyrimų aplinkos ribų nėra praktiškas. Kad EEG pagrįsti sąmonės lygio tyrimai būtų prasmingai taikomi kasdieniame gyvenime, būtina išnagrinėti ir naudoti paprastesnę bei patogesnę konfigūraciją, kuri palengvintų sklandžią integraciją į žmonių kasdienybę.

Viena iš galimų priemonių išspręsti šią problemą – naudoti vartotojo lygio (angl. *consumer grade*) dėvimas vieno frontalinio kanalo EEG galvajuostes. Šios sistemos turi daug privalumų: yra prieinamos, patogios ir praktiškai pritaikomos. Kadangi šiuos prietaisus yra lengva ir patogu naudoti, jie yra supaprastinta, tačiau veiksminga smegenų veiklos stebėsenos priemonė, todėl EEG technologija tampa prieinamesnė platesnei gyventojų grupei. Kadangi yra įperkami, jie ypač patrauklūs, gali būti plačiai naudojami ir atveria galimybes asmenims stebėti savo kognityvines būsenas namuose arba įvairiose kasdienio gyvenimo aplinkybėse. Be to, tai, kad vieno frontalinio kanalo konstrukcija yra paprasta, leidžia sumažinti ne tik bendrą kainą, bet ir iššūkius, susijusius su sudėtingu įrengimu ir specialistų priežiūra. Dėl šios priežasties naudotojams, neturintiems specialaus pasirengimo, nesunku prietaisą naudoti. Be to, įrašinėti EEG nuo frontalinės smegenų skilties gali būti patogiau, nes tai neplaukuota sritis, t. y. geresnis elektrodo kontaktas, patogiau naudotojui, nes jis gali naudoti prietaisą kasdienėje veikloje. Tokios sistemos pavyzdys yra „NeuroSky“ MindWave ausinės, kurios siūlo patogią sąsają švietimo ir tyrimų tikslais, leidžiančią tirti smegenų aktyvumą įvairiose aplinkose (6.2 pav.) [16, 17].

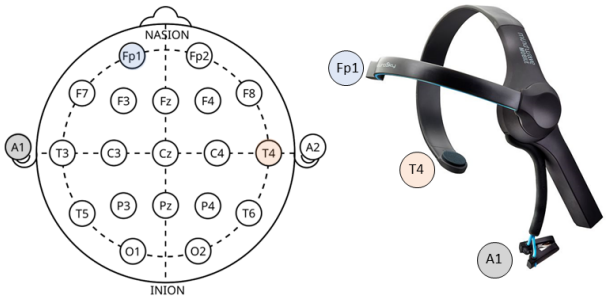

6.2 pav. „NeuroSky“ MindWave ausinių elektrodų išdėstymas pagal 10-20 tarptautinę sistemą, adaptuota iš [16,17]

Mokslinė-technologinė problema

Nepaisant anksčiau minėtų dėvimų EEG sistemų pranašumų, ribota vieno priekinio kanalo erdvinė aprėptis gali sumažinti užregistruotų smegenų signalų detalumą ir specifiškumą, o tai gali pakenkti neuroninės veiklos informacijos,

susijusios su skirtingais sąmonės lygiais, išsamumui.

Tyrimo klausimas: kaip signalų analizės algoritmais kompensuoti smegenų elektrinės veiklos stebėsenos erdvinės aprėpties sumažinimą, siekiant kompromiso tarp sąmonės lygio stebėsenos patikimumo ir prietaiso patogumo naudotojui?

Darbo hipotezė: Vieno priekinio EEG kanalo skaidymas į dažnių juostas ir netiesinės analizės taikymas gali kompensuoti erdvinės aprėpties apribojimą, užfiksuojant skirtingą sudėtingą dinamiką, susijusią su sąmonės lygių pokyčiais.

Tyrimo objektas

Šiame tyrime pagrindinis dėmesys skiriamas signalų apdorojimo algoritmų, skirtų sąmonės lygiui charakterizuoti atliekant miego vertinimą, nuovargio atpažinimą ir anestezijos lygio stebėseną naudojant vieną priekinį EEG kanalą, kūrimui ir tyrimui.

Tyrimo tikslas

Šios daktaro disertacijos tikslas – pasiūlyti sąmonės lygio stebėjimo metodus, naudojant nebrangias dėvimas EEG sistemas aktualiems realaus gyvenimo poreikiams.

Tyrimo uždaviniai

1. Sukurti algoritmų, galinčių veiksmingai sumažinti elektrinius triukšmus, trukdžius, bazinės linijos tendenciją ir akių mirkčiojimo artefaktus, kurie paprastai atsiranda EEG duomenyse, įrašytuose nebrangiomis nešiojamosiomis sistemomis;
2. Pasiūlyti tinkamą požymių rinkinį, pagal kurį būtų galima atpažinti ir atskirti budrumą nuo I miego stadijos, naudojant vieną priekinį EEG kanalą, taip sudarant sąlygas miego pradžios vėlavimui įvertinti, kuris yra labai svarbus, norint pamatuoti miego kokybę;
3. Sukurti algoritmų, specialiai pritaikytų vairuotojų nuovargiui atpažinti, naudojant dabartines komercines nešiojamąsias EEG sistemas;
4. Sukurti anestezijos gylio įvertinimo ir stebėsenos algoritmą, kurio veikimas būtų pagrįstas minimaliu EEG įėjimo kanalų skaičiumi, galimu registruoti nebrangiomis, komercinėmis, vartotojo lygio sistemomis.

Mokslinis naujumas

Pirma, šioje daktaro disertacijoje siūlomi du nauji nesudėtingi algoritmai, skirti bendriesiems artefaktams trumpuose vieno EEG kanalo įrašų segmentuose pašalinti. Šie algoritmai sukurti siekiant sumažinti dėvimų EEG sistemų artefaktus trumpame duomenų segmente, o tai labai svarbu norint užtikrinti, kad duomenų analizė būtų patikima.

Antra, šioje disertacijoje pateikiamas naujas požiūris į akių mirkčiojimo

artefaktus frontaliniuose EEG signaluose vairuotojo nuovargiui nustatyti. Tai pirmasis tyrimas, įrodantis, kad akių mirkčiojimo artefaktai gali turėti tiek teigiamą, tiek neigiamą poveikį EEG signalams, norint aptikti vairuotojo nuovargį.

Galiausiai šiame darbe nagrinėjamas netiesinės EEG dažninių komponenčių analizės potencialas, klasifikuojant skirtingus sąmonės lygius, vertinant miegą, aptinkant vairuotojo nuovargį ir stebint anestezijos gylį, remiantis komercinių dėvimų EEG sistemų kanalų konfigūracijomis.

Skirtingai nei dauguma tyrimų, kuriuose algoritmams kurti ir testuoti buvo naudojama tik viena duomenų bazė, šioje disertacijoje abiem etapams naudojamos kelios. Tai ypač svarbu, kai naudojami netiesiniai požymiai, pavyzdžiui, imties entropija, kurios parametrus reikia derinti. Siekiant užtikrinti siūlomo metodo universalumą, būtina spręsti esminį klausimą dėl suderintų netiesinių požymių pakeičiamumo įvairiose duomenų bazėse, o į šį aspektą dažnai neatsižvelgiama taikant dabartinius pažangiausius metodus.

Praktinė reikšmė

Šio darbo rezultatai turi tokią praktinę reikšmę:

1. Siūlomi artefaktų mažinimo algoritmai gali palengvinti duomenų kokybę dėvimiems, EEG pagrįstiems algoritmams, kurie analizuoja sąmonės lygį kasdienėje veikloje. Be to, siūlomi algoritmai gali būti naudojami EEG signalų kokybei gerinti kitose srityse;
2. Siūlomas požymių rinkinys, skirtas atpažinti ir atskirti budrumą nuo I miego stadijos, gali būti naudojamas miego pradžios vėlavimo laikotarpiui įvertinti, o tai labai svarbus rodiklis, vertinant miego kokybę ir nemigos nustatymą;
3. Siūlomi algoritmai, aptinkantys vairuotojo nuovargį, leidžia išgauti akių mirkčiojimo funkcijas, kartu pašalinant jas iš EEG signalų. Šie algoritmai yra suderinami tiek su vieno, tiek su kelių kanalų EEG sistemomis ir gali būti naudojami įvairiose EEG programose, ypač tose, kuriose tuo pačiu metu reikia analizuoti smegenų veiklą ir akių mirkčiojimą;
4. Siūlomas požymių rinkinys be parametrų, skirtas anestezijos gyliui stebėti, yra efektyvus bei suteikia galimybę lengvai pakartoti eksperimentą ir pagerinti našumą, įtraukiant papildomų funkcijų.

Rezultatų aprobavimas

Daktaro disertacija grindžiama septyniais straipsniais, publikuotais tarptautiniuose mokslo žurnaluose, kurių citavimo indeksas nurodytas *Clarivate Analytics Web of Science* duomenų bazėje, o iš viso rezultatai paskelbti dešimtyje mokslinių straipsnių. Svarbiausi rezultatai pristatyti šešiose tarptautinėse konferencijose.

2021 ir 2022 m. buvo gautos Lietuvos mokslo tarybos skiriamos skatinamosios stipendijos akademiniams tyrimams. 2021, 2022 ir 2023 m. gauti aktyviausio Elektros ir elektronikos inžinerijos mokslo krypties doktoranto apdovanojimai, kuriuos skyrė Kauno technologijos universitetas. 2021 ir 2022 m. buvo gautos trys skatinamosios stipendijos už aukštos kokybės publikacijas, kurias skyrė Kauno technologijos universitetas.

2023 m. gauta viena skatinamoji stipendija už akademinius tyrimus pasauliniame konkurse, kurią skyrė IEEE Signalų apdorojimo draugija (IEEE Signal Processing Society), ir trys stipendijos: (i) moksliniam vizitui į Tokijo žemės ūkio ir technologijų universitetą, kurią skyrė Lietuvos mokslo taryba, (ii) dalyvauti Kompiuterinių neuromokslų akademijos vasaros mokykloje, kurią skyrė Lenkijos nacionalinė akademinių mainų agentūra, ir (iii) dalyvauti 18-ajame IEEE tarptautiniame medicinos matavimų ir taikymų simpoziume, kurią skyrė IEEE Instrumentų ir matavimų draugija (Instrumentation and Measurement Society).

2021 ir 2022 m. du publikuotus šios disertacijos straipsnius IEEE „Transactions on Neural Systems and Rehabilitation Engineering“ ir IEEE „Journal of Biomedical Health and Informatics“ žurnalų redakcinės kolegijos pripažino teminiais (angl. *Featured Articles*).

Ginti pateikti teiginiai

1. Kurtozė ir asimetrija tarnauja kaip labai efektyvūs požymiai, leidžiantys aptikti elektrinių ir tiesinių poslinkų tendenciją bei akių mirkčiojimo artefaktus trumpame vieno EEG kanalo segmente;
2. Vieno frontalinio EEG kanalo netiesiniai požymiai pasirodė patikimesni nei santykinės juostos galios analizė. Pasiūlyti netiesiniai požymiai leidžia atskirti budrumo ir I miego stadiją, kurių laikinės ir spektrinės charakteristikos yra panašios;
3. Akių mirksniai prefrontaliniuose EEG kanaluose turi dvejopą prasmę. Gali tarnauti ir kaip vertingos informacijos šaltinis, ir kaip artefaktas nustatant vairuotojo nuovargį;
4. Pasiūlytas frontalinio EEG signalo požymių rinkinys skirtas anestezijos lygiui stebėti. Požymių rinkinys nereikalauja parametrų optimizavimo, gali būti įgyvendintas nebrangiomis EEG registravimo ir skaičiavimo priemonėmis. Todėl galėtų būti naudingas besivystančių šalių ligoninių operacinėse.

6.2. EEG ARTEFAKTŲ PAŠALINIMAS

6.2.1. ELEKTRINIAI POSLINKIAi IR LINIJINĖS TENDENCIJOS

EEG signaluose, įrašytuose nešiojamosiomis sistemomis, dažniau pasitaiko nefiziologinių artefaktų dėl tiriamųjų judėjimo ir kasdienės veiklos [29]. Nors pagrindiniai tiesiniai filtrai gali sušvelninti daugelį artefaktų, pažangesnių metodų vis tiek reikia tiems, kurie apima visas EEG dažnių juostas [30], pavyzdžiui, elektrinio poslinkio ir linijinės tendencijos artefaktams (ESLT). Jie gali atsirasti dėl elektrodų poslinkių arba dėl to, kad sumažėja laikinasis odos ir elektrodų kontaktas. Esami ESLT šalinimo algoritmai yra skirti apdoroti neprisijungus arba daugiakanaliam apdorojimui, todėl nėra užtektinai veiksmingi trumpiems segmentams, esantiems viename ar keliuose EEG kanaluose, kurie būdingi nešiojamosioms sistemoms. Čia siūlomas stacionariąja bangelių transformacija (SWT) pagrįstas ESLT eliminavimo sprendimas, taip pat sprendžiama problema, susijusi su tinkamiausių dekompozicijos lygių parinkimu skirtingu dažniu parenkamiems signalams [30, 35–37]. Įdiegta kurtozės principu pagrįsta strategija, leidžianti savaime reguliuoti SWT dekompozicijos lygį, taip sumažinant skaičiavimo apkrovą ir pagreitinant filtravimą. Tai, ar siūlomas algoritmas įgyvendinamas, patvirtinama įvairiais atrankos dažniais ir palyginama su automatine bangelių nepriklausomų komponentų analize (AWICA) [31] ir patobulintais AWICA (EAWICA) [34] algoritmais.

Siūloma SWT kurtozė ESLT pašalinti

SWT išskaido signalą į žemo ir aukšto dažnio juostas, aproksimacijos a(n) ir detalės d(n) komponentus atitinkamai per aukšto pralaidumo ir žemo pralaidumo filtrus. SWT reikėjo nustatyti du parametrus: bangelių pagrindo funkciją ir dekompozicijos lygį. db1 pagrindo funkcija pasirinkta dėl jos panašumo į ESLT artefaktus. Dekompozicijos lygio nustatymas yra svarbus kuriant automatinį SWT pagrįstą algoritmą. Kurtozė naudojama kaip kriterijus automatiškai sustabdyti SWT, kai jis pasiekia artefaktų komponentus, o mažesnės nei trys reikšmės rodo ESLT paplitimą dėl jų platikurtinio pasiskirstymo EEG signaluose [33, 45]. Per SWT dekompoziciją aproksimacijos komponentų kurtozė apskaičiuojama kas du lygius, o absoliutus skirtumas naudojamas sprendžiant, ar tęsti, ar sustabdyti procesą. Jis sustoja, jei skirtumas viršija 0,1, o tai rodo, kad dekompozicija yra tinkama artefaktams filtruoti. Paskutinė aproksimacijos komponentė pašalinama, siekiant eliminuoti žemo dažnio artefaktų komponentus, o detalių komponentų triukšmas slopinamas naudojant universalųjį slenkstį [37]. Tada detalių komponentai su nuslopintu triukšmu naudojami atkuriant filtruotą EEG signalą per atvirkštinį SWT.

Eksperimentų rezultatai ir aptarimas

Čia buvo naudojami tiek pusiau imituoti, tiek tikri užteršti EEG duomenys. Naudojant pusiau imituotus duomenis, taip pat buvo galima įvertinti filtravimo veiksmingumą kiekybiškai. Lyginant pusiau imituotus duomenis su AWICA ir EAWICA, pasiūlytas SWT kurtozės algoritmas pasižymi didesniu koreliacijos koeficiento vidurkiu (0,92, palyginti su 0,58, 0,67), didžiausio signalo ir triukšmo santykiu (20,3 dB, palyginti su 13,0, 13,6 dB) ir mažesniu normalizuotos vidutinės kvadratinės paklaidos vidurkiu (5,4, palyginti su 12,2, 11,5) tarp švarių ir filtruotų duomenų, o tai rodo, kad EEG signalai, filtruoti siūlomais duomenimis, geriau aproksimuoja originalius be ESLT.

Kalbant apie tikruosius duomenis, 6.3 pav. pavaizduota penkių sekundžių trukmės 12 užterštų ir filtruotų EEG signalų. Remiantis vizualiniu vertinimu, pasiūlytas algoritmas sėkmingai pašalino ESLT artefakto komponentus. Stebina tai, kad AWICA ir EAWICA negalėjo tinkamai pašalinti artefaktų, o kai kuriuose signaluose (nr. 1 ir nr. 2) netgi modifikavo EEG komponentus.

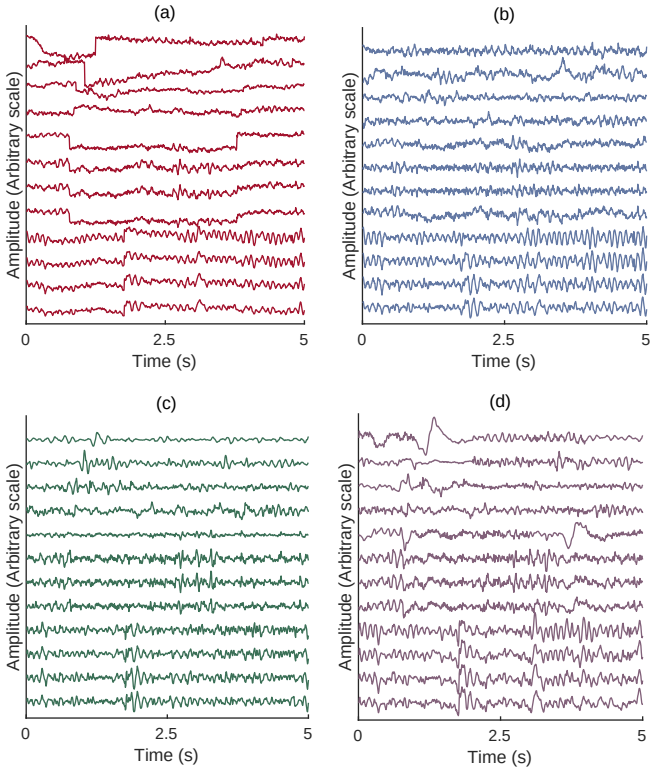

6.3 pav. Tikrų užterštų EEG signalų **(a)** ir filtruotų EEG signalų pavyzdžiai pagal siūlomus SWT kurtozės **(b)**, AWICA **(c)** ir EAWICA **(d)** algoritmus

Pagrindinis pasiūlytos SWT kurtozės privalumas, palyginti su įprastiniais bangelių transformacijos metodais, yra toks, kad, taikant šį algoritmą, nebūtina atlikti užterštų EEG signalų medžio visiškos dekompozicijos. Užtat jis automatiškai nutraukia dekompozicijos procesą pasiekus ESLT komponentus, taip išvengiant nereikalingo apdorojimo ir potencialiai paspartinant triukšmo slopinimo procesą. Be to, šis algoritmas padeda pašalinti keletą dabartinių naujausių metodų apribojimų: gali veiksmingai pašalinti ESLT artefaktus trumpame vieno EEG kanalo segmente, jis nereikalauja didelio žmogaus įsikišimo, nes reikia nustatyti tik vieną parametrą; panašu, kad jis yra sukeičiamas tarp duomenų rinkinių ir jam nereikia pradinio kalibravimo. Dėl šių funkcijų jį puikiai tinka naudoti su nebrangiomis EEG galvajuostėmis.

6.2.2. AKIŲ MIRKČIOJIMO ARTEFAKTAI EEG: APTIKIMAS IR ŠALINIMAS

Akių mirkčiojimo artefaktai dėl savo amplitudės ir dažnio diapazono [50] kelia nemažai problemų EEG įrašuose, ypač frontalinių kanalų. Kadangi jie yra nevalingi ir neišvengiami, tokios strategijos, kaip įrašymas užmerktomis akimis, yra nepraktiškos ilgalaikiam stebėjimui [51]. Be to, tokia strategija gali pakeisti EEG ritmą [52] ir neįmanoma atliekant vizualinio stimuliavimo eksperimentus. Taigi, norint užtikrinti tikslią smegenų veiklos analizę, ypač vieno frontalinio kanalo EEG sistemose, labai svarbu filtruoti akių mirkčiojimą. Dabartiniai pažangiausi jo šalinimo metodai dažniausiai skirti apdoroti neprisijungus arba daugiakanalei EEG konfigūracijai, tačiau juose neatsižvelgiama į gyvybiškai svarbų poreikį realiuoju laiku pašalinti akių mirkčiojimą nešiojamosiose vieno kanalo EEG sistemose. Tam reikalingi ir algoritmai, galintys filtruoti artefaktinius intervalus trumpame segmente.

Čia pristatomas veiksmingas VME-DWT algoritmas, skirtas nekontroliuojamam akių mirkčiojimui aptikti ir filtruoti trumpuose vieno kanalo EEG segmentuose (3 s). Algoritmas naudoja variacinį režimo išskyrimą (VME) akių mirkčiojimo intervalams (EBI) aptikti, o paskui – automatinę diskrečiosios bangos transformaciją (DWT) filtruoti. VME iš užterštos EEG išgauna akies mirkčiojimo signalo aproksimaciją, padedančią nustatyti artefaktinį intervalą. TADA DWT filtruoja tik pasirinktus intervalus, išsaugodamas nefaktinius EEG segmentus be išankstinio kalibravimo ar artefaktų nuorodos. VME-DWT veikimas vertinamas pagal pusiau imituotus ir realiai užterštus EEG duomenis ir lyginamas su automatinio VMD (AVMD) [59] ir DWT [55] algoritmais, skirtais panašioms užduotims trumpuose vieno kanalo EEG segmentuose.

Siūlomas VME-DWT akių mirkčiojimui pašalinti

VME algoritmui, skirtam akies mirkčiojimui aptikti, reikia nustatyti du parametrus: kompaktiškumo koeficientą ir apytikslį centrinį dažnį [65]. Čia taikomas 3000 kompaktiškumo koeficientas ir 3 Hz centrinis dažnis. Tada akies mirkčiojimo

smailės lokalizuojamos VME režimu, nustatant vietinius maksimumus, viršijančius universaliąją ribą. Nustačius piko vietą, užterštoje EEG nustatomi laiko atrankiojo filtravimo intervalai, pasirenkamas 500 ms intervalas, apimantis akių mirkčiojimo trukmę. Sutampantiems akių mirkčiojimo atvejams naudojamas kriterijus, matuojantis atstumą tarp nustatytų smailių, siekiant atitinkamai pataisyti filtravimo langą. Aptikus artefaktinių intervalų, triukšmui slopinti naudojamas DWT, kuris įvesties signalą suskaido į apytikslius ir detalius komponentus. DWT reikia nustatyti du parametrus: bazinę bangelių funkciją ir dekompozicijos lygį. Db4 pasirenkamas kaip pagrindinė bangelė dėl savo panašumo į akių mirkčiojimą. Automatizacijai labai svarbu nustatyti dekompozicijos lygį, o tinkamam lygiui kontroliuoti ir rasti naudojama asimetrija pagrįsta strategija. Akių mirksnių atsiradimas lemia asimetrinį EEG signalo pasiskirstymą, todėl gaunamos didelės DWT komponentų absoliutinės asimetrijos vertės. Absoliutus asimetrijos verčių skirtumas tarp nuoseklių aproksimacijos komponentų naudojamas sprendžiant, ar tęsti, ar nutraukti dekompozicijos procesą, kai slenkstis yra 0,1, nustatant tašką, kuriame pasiekiami mirkčiojimo komponentai.

Eksperimentų rezultatai ir aptarimas

Išanalizavus 912 trijų sekundžių trukmės pusiau imituotų užterštų EEG signalų segmentus, kurių signalo ir triukšmo santykis svyruoja nuo -8 iki +3 dB, VME-DWT aptiko daugiau kaip 95% akių mirksnių. Vertinant akių mirkčiojimo pašalinimo veiksmingumą, VME-DWT pranoko AVMD ir DWT, nes jo vidutinė santykinė kvadratinė paklaida buvo mažesnė (0,42, palyginti su 0,59, 0,87), o vidutinė koreliacijos koeficiento vertė – didesnė (0,92, palyginti su 0,83, 0,58) tarp EEG be akių mirkčiojimo ir filtruotos EEG, o tai rodo jo pranašumą išsaugant originalius EEG signalo komponentus.

6.4 pav. pavaizduoti tikrų užterštų EEG signalų iš keturių duomenų bazių pavyzdžiai su juos atitinkančiais filtruotais EEG signalais. Kaip galima pastebėti, pasiūlytas algoritmas gali daug geriau filtruoti intervalus su akių mirkčiojimo artefaktais.

Kadangi tikrieji artefaktais neužteršti EEG signalai nežinomi, laiko kriterijai buvo skaičiuojami tik tarp tikrųjų ir filtruotų EEG signalų intervalų be akių mirkčiojimo [39]. 6.1 lentelė rodo VME-DWT pranašumą, palyginti su AVMD ir DWT, siekiant išsaugoti intervalus be artefaktų.

Išvados atskleidžia keletą siūlomos VME-DWT pranašumų, palyginti su esamais metodais:

1. Rodo gebėjimą veiksmingai aptikti ir pašalinti akių mirkčiojimą per trumpą vieno EEG kanalo intervalą, net kai skirtingas signalo ir triukšmo santykis;

2. Universalus, gerai veikia naudojant skirtingų charakteristikų įrašytus EEG signalus, o tai rodo jo nepakeičiamumą;

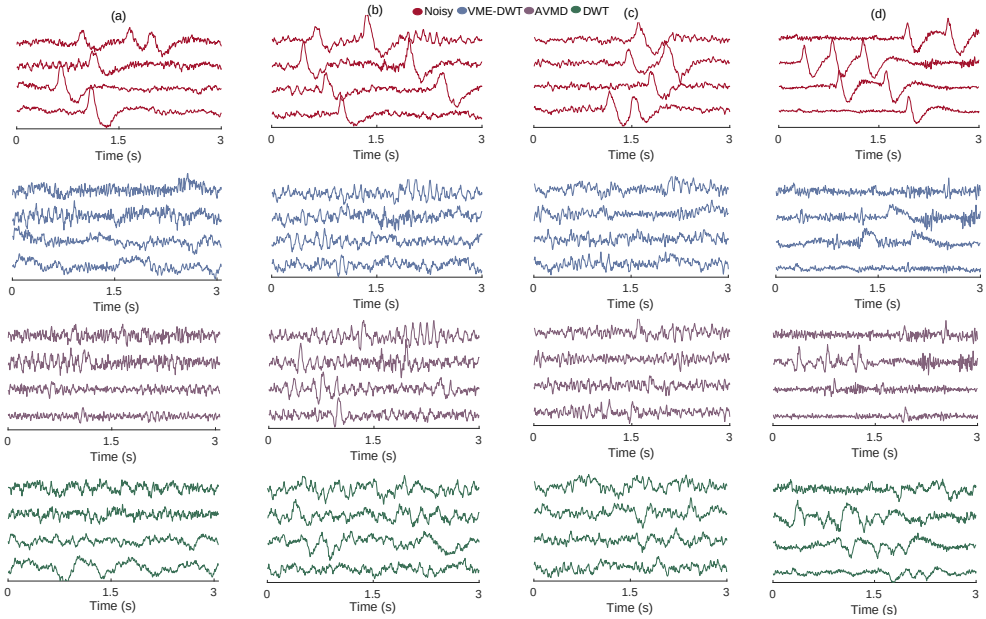

6.4 pav. Stulpeliuose pateikti tikro užteršto EEG signalo pavyzdžiai iš [71] **(a)**, [72] **(b)**, [73] **(c)**, [74] **(d)**, o žemiau – atitinkami filtruoti EEG signalai

6.1 lentelė. Užterštų ir filtruotų EEG signalų bei užterštų ir filtruotų realių duomenų akių nemirkčiojimo intervalų CC ir RRMSE palyginimas (vidurkis ± SD) (CC ir RRMSE reiškia koreliacijos koeficientą ir santykinę vidutinę kvadratinę paklaidą)

Duomenų bazė	VME-DWT		AVMD		DWT	
	CC	RRMSE	CC	RRMSE	CC	RRMSE
[71]	0,94±0,03	0,16±0,04	0,89±0,08	0,18±0,10	0,68±0,11	0,84±0,18
[72]	0,97±0,02	0,14±0,02	0,93±0,04	0,21±0,12	0,73±0,03	0,96±0,03
[73]	0,93±0,04	0,15±0,05	0,88±0,07	0,19±0,06	0,64±0,14	0,76±0,23
[74]	0,98±0,01	0,09±0,04	0,84±0,06	0,19±0,09	0,62±0,14	0,94±0,34

3. Palyginti su kitais dekompozicijos algoritmais, tokiais kaip AVMD ir DWT, yra mažiau invazinis, nes atrankiai filtruoja tik užterštus intervalus, nepakeisdamas neartefaktinių segmentų;

4. Nesiremia artefaktų nuorodomis ir jam nereikia pradinio kalibravimo, o tai dar labiau supaprastina jo įgyvendinimo procesą.

Dėl šių privalumų jis puikiai tinka akių mirkčiojimui šalinti nebrangiose EEG galvajuostėse.

6.3. MIEGO VERTINIMAS: BUDRUMO IR I MIEGO STADIJOS ATPAŽINIMAS

Miego sutrikimai vargina nemažą dalį Europos gyventojų, o tai kelia iššūkių ne tik asmens sveikatai, bet ir ekonominiam produktyvumui bei saugumui [5]. Nors polisomnografija yra auksinis miego stebėsenos standartas, jos klinikiniai reikalavimai ir jutiklių apkrova riboja platų pritaikymą [75]. Reaguodami į tai, tyrėjai sukūrė algoritmų, naudojančių mažos galios dėvimuosius prietaisus, ypač EEG [76], kad būtų galima stebėti miegą namuose ir taip patenkinti prieinamesnių ir nepastebimų sprendimų poreikį. Nepaisant gausios EEG informacijos, reikalingos miego analizei atlikti, dėl panašių EEG charakteristikų vis dar sunku atskirti budrumą nuo I miego etapo [82, 85–90]. Šis atpažinimas yra labai svarbus norint įvertinti miego pradžios vėlavimą, pagrindinį miego kokybės vertinimo rodiklį [91]. Nors pagalbiniai jutikliai, tokie kaip elektrokardiograma [92], elektromiograma ir elektrookulograma [93], gali padidinti atpažinimo tikslumą, jie apsunkina dėvimųjų prietaisų naudojimą.

Nors vis dar ginčijamasi dėl netiesinės EEG prigimties, keli tyrimai parodė netiesinių matavimų pranašumą, palyginti su tiesiniais, įvairiose EEG taikymo srityse [101–103], ypač sąmonės tyrimuose [104, 105]. Motyvuojant tuo, kad budrumo ir I miego stadijos atpažinimas gali būti susijęs su sąmonės lygiu [106] ir priemonių išskyrimo iš EEG pojuosčių veiksmingumu vertinant miegą [82, 85, 86], siūlomas netiesinių priemonių rinkinys, išskirtas iš vieno frontalinio EEG kanalo pojuosčių, siekiant pagerinti budrumo ir I miego stadijos klasifikavimą. Netiesinių priemonių veiksmingumas paprastai priklauso nuo kelių parametrų nustatymo rankiniu būdu, padidinant žmogaus įsikišimą. Šiuo tikslu naudojami EEG signalai iš keturių skirtingų miego duomenų bazių, iš kurių viena skirta netiesinėms funkcijoms derinti, o kita – pakoreguotų priemonių veiksmingumui tirti. Siūlomo priemonių rinkinio efektyvumas taip pat lyginamas su RBP analize, kuri laikoma vienu iš labiausiai paplitusių EEG pagrįstos miego analizės metodų [81–84].

6.3.1. Duomenys

Čia naudojami 20 s trukmės vieno frontalinio kanalo EEG signalai, atspindintys budrumo ir I miego stadijos būsenas iš keturių skirtingų duomenų bazių, t.y. Sleep Telemetry [113], DREAMS [114], DCSM [115] ir MESA [116]. 6.2 lentelėje pateikiamas kiekvienos duomenų bazės balų metodas, mėginių ėmimo dažnis, naudojamas kanalas, miego sutrikimo būsena, tiriamųjų skaičius, budrumo (W) ir I miego stadijos (S) būsenos.

6.2 lentelė. Naudojamų duomenų bazių aprašymo santrauka

Duomenų bazė	Sleep Telemetry	DREAMS	DCSM	MESA
Taškai	R&K	R&K	AASM	AASM
Fs (Hz)	100	200	256	256
Miego sutrikimai	Yra	Nėra	Yra	Yra
Kanalas	Fpz-Cz	Fp1-A1	F3-A1	Fz-Cz
Tiriamųjų skaičius	22	20	20	27
Nr. W	4920	4576	3921	7000
Nr. S	4604	1788	2142	4122

6.3.2. Siūloma budrumo ir I miego stadijos atpažinimo sistema

6.5 pav. pateikta blokinė diagrama apibūdina algoritmo struktūrą, kurią sudaro pirminio apdorojimo, EEG pojuosčių dekompozicijos, priemonių išskyrimo ir klasifikavimo etapai.

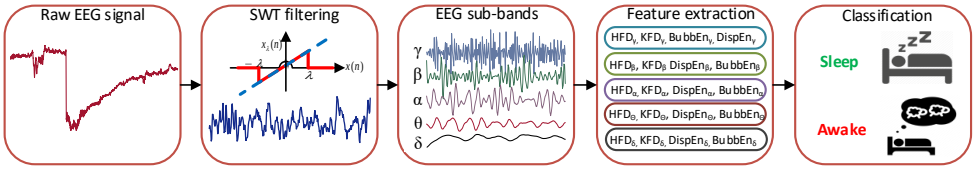

6.5 pav. Siūlomo budrumo ir I miego stadijos atvejų klasifikavimo, naudojant vieną EEG kanalą, algoritmo blokinė schema

Per pirminį apdorojimą įrašyti EEG signalai filtruojami naudojant kurtozės principu pagrįstą kietąjį universalų SWT slenkstį, kad būtų pašalinti artefaktai su žemo ir aukšto dažnio komponentais. Vėliau DWT išskaido EEG signalą į detalius ir apytikslius komponentus, leidžiančius išgauti skirtingų dažnių diapazonams būdingus pojuosčių signalus. Keturi DWT lygiai naudojami EEG signalui išskaidyti į gama, beta, alfa, teta ir delta juostas. Po dekompozicijos iš kiekvienos pojuostės išrenkami keturi netiesiniai matai – Higuchi ir Katzo fraktaliniai matmenys (HFD, KDF), burbulinė entropija (BubbEn) ir dispersinė entropija (DispEn) – ir suformuojamas funkcijų vektorius, kurį sudaro 20 matų. Galiausiai budrumo ir I miego stadijos atvejai klasifikuojami naudojant pagalbinę vektorių mašiną (SVM) su radialinės bazinės funkcijos branduoliu.

6.3.3. Eksperimentų rezultatai ir aptarimas

Taikomų netiesinių funkcijų parametrai, t. y. didžiausias HFD intervalas, įterpimo dimensija BubbEn ir įterpimo dimensija, klasių skaičius ir laiko delsa DispEn, taisomi naudojant miego telemetrijos duomenų bazę. Šioje duomenų bazėje galima

rasti įvairią kohortą, kuri palengvina patikimą parametrų derinimą. Koregavimai atliekami remiantis Vilkoksono rangų sumos testu tarp budrumo ir I miego stadijos atvejų.

Taikant Sleep Telemetry duomenų bazei (6.6 pav., a), pasiūlytas funkcijų rinkinys buvo pranašesnis už RBP, atitinkamai 10,71%, 10,93% ir 10,76% didesnės vidutinės Sen, Spe ir Acc vertės. DREAMS duomenų bazėje (6.6 pav., b), nors abiejuose funkcijų rinkiniuose buvo panašios SPE vertės, pasiūlytasis pranoko RBP pagal Sen (87%, palyginti su 71%) ir Acc (92%, palyginti su 88%). Kalbant apie DCSM duomenų bazę (6.6 pav., c), pasiūlytasis funkcijų rinkinys įgijo 16,79%, 2,53% ir 7,86% didesnes vidutines Sen, Spe ir Acc reikšmes. Kalbant apie MESA duomenų bazę (6.6 pav., d), nors abu funkcijų rinkiniai turėjo panašias Spe ir Acc reikšmes, pasiūlytasis požymių rinkinys turėjo 5,88% didesnį Sen vidurkį. Pagal atliktą nepriklausomą dviejų imčių t-testą nustatytas statistiškai reikšmingas skirtumas tarp pasiūlytojo ir RBP funkcijų rinkinių gautų Sen reikšmių ($p < 0,05$).

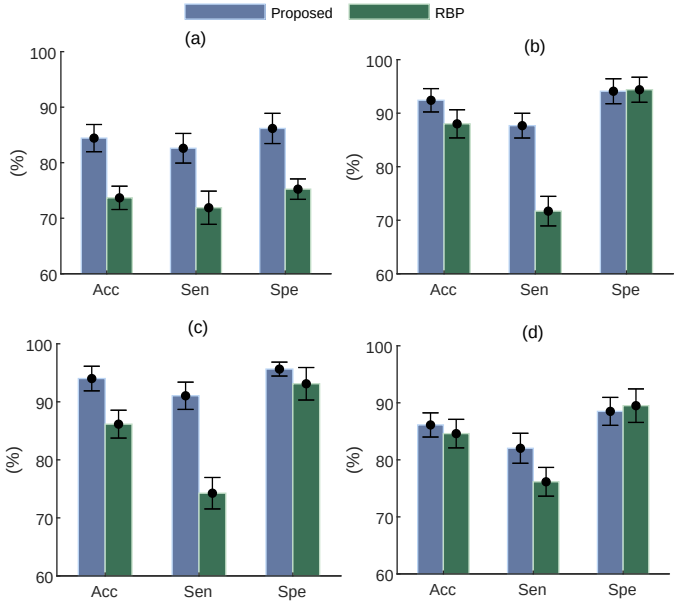

6.6 pav. SVM gautų Acc, Sen ir Spe verčių (vidurkis ± SD) palyginimas, abiem funkcijų rinkiniams naudojant miego telemetrijos **(a)**, DREAMS **(b)**, DCSM **(c)** ir MESA **(d)** duomenų bazes

Šio tyrimo svarbą lemia miego pradžios vėlavimo analizė, atspindinti bendrą mieguistumą ir miego kokybę, kuri taip pat gali būti naudojama atsigavimui nuo komos prognozuoti. Šiuo tikslu buvo tiriami HFD, KFD, BubbEn ir DispEn, išskirti iš EEG pojuosčių. KFD matuoja sudėtingumo ir savipanašumo laipsnį pagal tai, kaip greitai signalas didėja ar mažėja, keičiant mastelį. Kadangi tikimasi, kad EEG bus

sudėtingesnė, kai žmogus budrus, manoma, kad FD reikšmės bus didesnės. Kita vertus, entropija kiekybiškai įvertina tai, kiek signalas neapibrėžtas. Taigi, manoma, kad, žmogui esant budriam, pastebimas didesnis neapibrėžtumas [106].

Palyginti su šiuolaikiniais algoritmais, siūlomo algoritmo privalumus galima aptarti dviem būdais. Pirma, nors dauguma tyrimų vertino tik vieną ar dvi duomenų bazes rezultatams pranešti [76, 83, 84, 86, 88–90, 95, 97–99], siūlomo algoritmo veikimas buvo vertinamas naudojant keturias duomenų bazes, tad čia pateikti rezultatai yra patikimesni, nes buvo naudojamos skirtingos duomenų bazės, pasižyminčios išskirtinėmis savybėmis. Antra, siūlomam algoritmui reikia mažiau skaičiavimo galios ir išteklių, palyginti su gilaus mokymosi metodais [49, 98, 99]. Be to, giliuoju mokymusi grindžiamiems metodams sukurti ir įgyvendinti reikia daug pradinių žinių ir patirties.

6.4. VAIRUOTOJO NUOVARGIO PATIKRINIMAS

6.4.1. AKIŲ MIRKČIOJIMO VAIDMUO NUSTATANT VAIRUOTOJO NUOVARGĮ PREPRIEKINĖS EEG PAGRINDU

Mokslininkai pripažino akių mirkčiojimo analizės svarbą nustatant vairuotojo nuovargį [143–145]. Tradiciškai akių mirkčiojimas registruojamas naudojant šalia akies esančius elektrodus, o tai gali būti sudėtinga tiriamiesiems ir riboti jų regėjimo lauką [146]. Alternatyvus metodas, orientuotas į su mirkčiojimu susijusių funkcijų išgavimą iš frontalinių EEG kanalų, siūlo paprastesnę dėvimąją sąrangą ir yra perspektyvus, nustatant vairuotojų nuovargį [134, 146, 147]. Nors ankstesniuose tyrimuose buvo išfiltruoti akių mirkčiojimai siekiant pagerinti EEG analizę [139, 140, 150–153] arba išskirtos su mirkčiojimu susijusios funkcijos kartu su užteršta EEG analize [134, 146, 148, 149], nebuvo ištirtas akių mirkčiojimo EEG potencialas kaip informacijos šaltinis ir artefaktas. Čia pristatomas naujas algoritmas, skirtas tuo pačiu metu išgauti akių mirkčiojimo funkcijas ir jas pašalinti iš žemo kanalo prepriekinės EEG signalų. Šis algoritmas, kuriam nereikia artefaktų nuorodos, sintetinių duomenų generavimo ar pradinio kalibravimo, susideda iš EBI identifikavimo naudojant VME iš Fp1 EEG kanalo, šių intervalų projektavimo į kitus EEG kanalus ir pagrindinių komponentų analizės (PCA)-DWT naudojimo akių mirkčiojimo komponentams pašalinti. Tada išvestos su mirkčiojimu susijusios funkcijos derinamos su filtruotų EEG signalų juostų galios funkcijomis, kad būtų galima klasifikuoti vairuotojo būseną.

Vienalaikis akių mirkčiojimo apibūdinimas ir pašalinimas iš EEG, siekiant nustatyti vairuotojo nuovargį

Siūlomo algoritmo blokinė schema, pavaizduota 6.7 pav., apibūdina pagrindinius jo etapus, tai: EBI identifikavimas iš EEG, naudojant VME, su mirkčiojimu susijusių funkcijų išgavimas, mirkčiojimo dažnis (BR) ir jo amplitudė (BA), EBI filtravimas iš EEG per PCA-DWT ir mirkčiojimo bei juostos galios funkcijų panaudojimas iš filtruotų EEG signalų vairuotojo būsenai klasifikuoti. Pašalinus akių mirkčiojimą, apskaičiuojamos EEG juostos galios funkcijos, sutelkiant dėmesį į teta, alfa ir beta juostas, bet ne į delta juostą, susijusią su gilaus miego stadijomis. Vėliau budrumo ir nuovargio būsenos klasifikuojamos naudojant SVM su radialine bazine funkcija, kurios hiperparametrai optimizuojami taikant tinklelio paiešką ir dešimties kartų kryžminį patvirtinimą.

Eksperimentų rezultatai ir aptarimas

6.8 pav. rodo, kad vairuotojo nuovargio nustatymas pagerėjo naudojant BR ir BA kaip papildomas funkcijas, be EEG signalų dažnių juostos galios funkcijų, prieš ir po akių mirkčiojimo pašalinimo siūlomu algoritmu. Kaip parodyta, didesnis Sen vidurkis (80,7%, palyginti su 72,1%), Spe (75,2%, palyginti su 70,1%) ir Acc (78,1%, palyginti

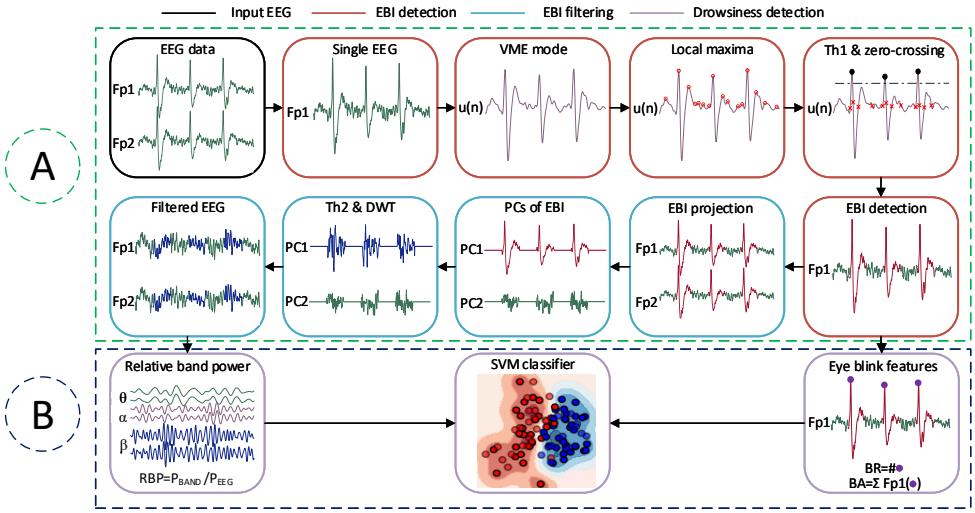

6.7 pav. Siūlomo algoritmo, skirto tuo pačiu metu išskirti ir pašalinti akių mirkčiojimo funkcijas, siekiant pagerinti vairuotojo būklės stebėjimo kokybę, blokinė schema. Blokeliuose, pažymėtuose žaliomis brūkšninėmis linijomis (apskritimas A), parodyti siūlomo akių mirkčiojimo aptikimo (raudona spalva) ir filtravimo (žydra spalva) iš EEG algoritmo etapai, o blokeliuose, pažymėtuose tamsiai mėlynomis brūkšninėmis linijomis (apskritimas B), – vairuotojo nuovargio aptikimo procedūra naudojant mirkčiojimo ir filtruotų EEG juostų galios funkcijas pagal SVM (violetinė spalva)

su 71,2 %) buvo pasiektas, tuo pačiu metu išskiriant ir pašalinant akių mirkčiojimo funkciją.

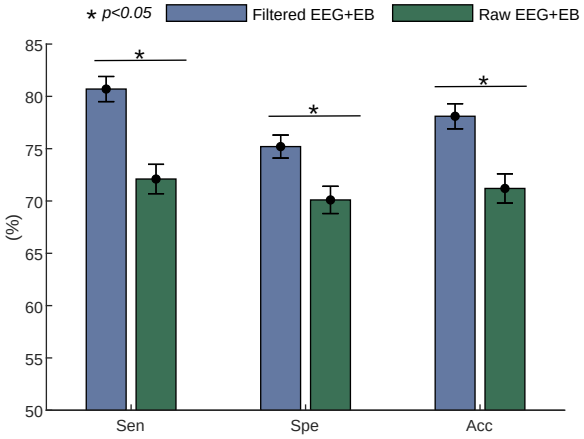

6.8 pav. Vairuotojo nuovargio aptikimo naudojant BR ir BA kokybės pagerėjimas prieš ir po akių mirkčiojimo pašalinimo siūlomu algoritmu. EB reiškia akių mirkčiojimą

Dabartiniuose naujausiuose tyrimuose akių mirkčiojimas laikomas informacijos

šaltiniu [148, 149] arba artefaktais [139, 140], o tai paneigia galimybę, kad akių mirkčiojimas gali būti ir vienas, ir kitas šaltinis. Iš tiesų, mes parodėme, kad mirkčiojimo funkcijų išskyrimas, o paskui jo pašalinimas iš žemo kanalo prepriekinės EEG signalų gali padėti dar tiksliau nustatyti vairuotojo nuovargį, palyginti su tais, kurie jį laiko tik artefakto arba informacijos šaltiniu.

6.4.2. EEG IR AKIŲ MIRKČIOJIMO ANALIZĖS SINTEZĖ VAIRUOTOJŲ NUOVARGIUI NUSTATYTI

Nors keliuose EEG grindžiamuose tyrimuose daugiau kaip 90% tikslumu nustatytas vairuotojo nuovargis, daugumoje jų buvo atsižvelgta į daugiakanalius EEG įrašus, pavyzdžiui, [131, 135, 171–173], o tai didina dėvimų prietaisų sudėtingumą [174] ir yra nepatogu ilgalaikiam vairavimui. Tačiau, atsiradus nebrangioms nešiojamosioms vieno kanalo EEG galvajuostėmis, atsirado ir nauja galimybė nustatyti vairuotojo nuovargį tikroviškomis sąlygomis [140, 175]. Viena vertus, įrašinėti EEG iš prepriekinės žievės gali būti patogiau, nes tai neplaukuota sritis, t. y. mažiau trukdžių, triukšmo [139], be to, tai gali suteikti naudotojui daugiau komforto, nes vairuojant galima naudotis galvos atrama [148]. Kita vertus, akių mirkčiojimas frontaliniuose EEG signaluose taip pat gali būti naudojamas vairavimo nuovargiui apibūdinti [147]. Dėl šios priežasties pirmenybė turėtų būti teikiama algoritmams, kuriais galima nustatyti vairuotojo nuovargį, naudojant vieną prepriekinės EEG kanalą.

Nepaisant daug žadančių rezultatų, gautų atlikus keletą tyrimų vairuotojų nuovargiui nustatyti, kuriuose jis buvo nustatytas naudojant vieną prepriekinės EEG kanalą, tik vienos duomenų bazės naudojimas yra galimas apribojimas. Ypač svarbu, kad, naudojant netiesines priemones, pavyzdžiui, entropiją, būtų galima tarpusavyje sukeisti pritaikytas funkcijas kitose duomenų bazėse. Čia pateikiamas naujas metodas vairuotojo nuovargiui nustatyti naudojant vieną Fp1 EEG kanalą, kurio veiksmingumą vertina dvi skirtingos duomenų bazės; pirmoji naudojama pasiūlyto metodo parametrams tikslinti, o antroji – sureguliuotų parametrų veiksmingumui įvertinti.

EEG ir akių mirkčiojimo analizės integravimas

Apskritai, nuovargio pradžią EEG gali geriau atskleisti jos subjuostų analizė [126, 148, 176, 178]. Kita vertus, kaip rodo sąmonės būsenų klasifikavimo tyrimų kontekstas, EEG gali būti sudėtingesnė, kai tiriamasis yra budrus [104, 137, 179], galima tikėtis, kad sudėtingumo priemonės bus geri rodikliai vairuotojo nuovargiui nustatyti. Be to, įrodyta, kad mirkčiojimas turi ir teigiamą, ir neigiamą poveikį, EEG nustatant vairuotojo nuovargį [20]. Remiantis minėtomis prielaidomis, mūsų siūlomu metodu pirmiausia nustatome EEG EBI, taikydami judančio standartinio nuokrypio (MSD) algoritmą, kad išskirtume su mirkčiojimu susijusias funkcijas. Antra, EBI

filtruojami iš EEG taikant DWT. Trečia, išfiltruota EEG suskirstoma į pojuostes, kad būtų galima išgauti skirtingas funkcijas. Galiausiai išskirtinės funkcijos atrenkamos taikant kaimynystės komponentų analizės (NCA) algoritmą ir perduodamos įvairiems klasifikatoriams, kad būtų galima atskirti nuovargį ir budrų vairavimą (6.9 pav.).

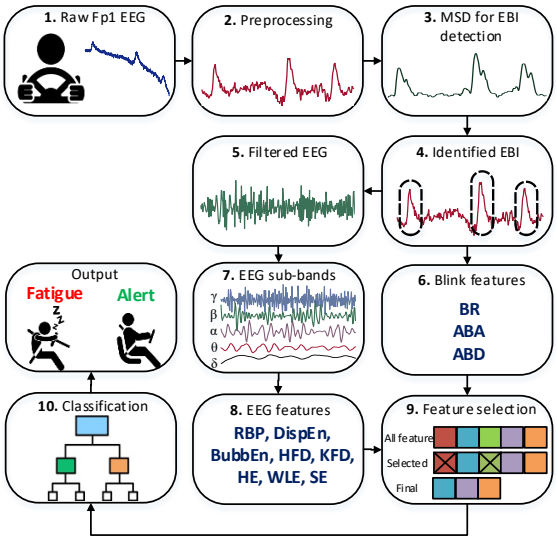

6.9 pav. Siūlomo metodo, skirto nuovargiui ir budriam vairavimui klasifikuoti, naudojant vieną Fp1 EEG kanalą, blokinė schema

EEG ir akių mirkčiojimo funkcijos

Visuotinai žinoma, kad kai tiriamieji atlieka regimojo dėmesio reikalaujančias užduotis, pavyzdžiui, vairuoja, jie mažiau mirksi, kad išliktų labiau susikaupę [180, 181]. Todėl, atsižvelgiant į tai, kad pavargus sumažėja dėmesio koncentracija, su mirkčiojimu susijusios priemonės gali padėti atpažinti ir atskirti budrumo ir nuovargio būsenas. Visų pirma, buvo įrodyta, kad nors pavargus BR padidėja, BA sumažėja [148]. Panašiai apskaičiuojami trys mirkčiojimo matai: BR, BA ir vidutinis atstumas tarp mirksnių (ABD). Pašalinus akių mirksnius ir suskirsčius EEG į pojuostes, iš kiekvienos išskiriamos aštuonios funkcijos, t. y. RBP, logaritminė energijos (LeEn) bei Šenono (SE) entropijos, DispEn, BubbEn, HFD, KFD ir Hursto eksponentas (HE).

Eksperimentų rezultatai ir aptarimas

EEG netiesinių funkcijų parametrų derinimas

Norėdami suderinti naudojamų netiesinių priemonių, kurias reikėjo optimizuoti, t. y. DispEn, BubbEn ir HFD, parametrus, atsižvelgėme į mažiausią atlikto Wilcoxon Rank-Sum testo p reikšmę tarp budraus ir pavargusio vairuotojo atvejų [107]. Kalbant

apie HFD, didžiausio laiko intervalo, *Kmax*, per kurį apskaičiuojamos FD vertės, reikšmės buvo įvairios, nuo 2 iki 10, o *Kmax* = 4 buvo nustatyta kaip tinkamiausia reikšmė. Kalbant apie BubbEn įterpimo dimensiją, buvo išbandytos vertės nuo 4 iki 16. Kaip tinkamą pasirinkome įterpimo matmenį 8. Kalbant apie DispEn, išbandytos kelios konfigūracijos ir nustatyta, kad gerai tinka 4 įterpimo dimensija, 2 klasių skaičius ir viena laiko delsa.

Funkcijų pasirinkimas

6.3 lentelėje parodytos svertinės funkcijos naudojant NCA, optimizuotus stochastiniu gradientinio nusileidimo algoritmu. Klasifikacijai pasirenkamos funkcijos, kurių svorio vertė yra didesnė nei 0,5 (18 priemonių).

6.3 lentelė. Svertinės funkcijos, naudojant NCA (pasirinktos funkcijos paryškintos)

Funkcijos	Svoris				
	EEG juostos				
	Delta	Teta	Alfa	Beta	Gama
RBP	**0,59**	0,13	0,21	**1,84**	0,31
DispEn	**0,74**	0,12	0,05	0,31	**0,56**
BubbEn	0,07	0,08	0,14	0,01	**0,74**
HFD	0,11	0,34	**0,86**	**1,42**	**0,85**
KFD	0,09	**1,26**	**1,71**	0,33	**1,16**
HE	0,02	0,36	0,01	0,01	**1,14**
WLE	**1,38**	**1,73**	0,35	0,13	**1,98**
SE	0,08	**0,88**	0,04	0,24	0,37
Mirktelėjimas					
BR	**1,12**				
BA	**0,79**				
ABD	0,05				

Klasifikavimo rezultatai

6.10 pav. rodo visų keturių modelių nematytų bandymų duomenų klasifikavimo rezultatus pagal Acc, Sen, Spe ir AUC. Palyginimas patvirtina, kad AdaBoost yra pranašesnis už kitus modelius.

Kai į modelius buvo pateiktas pasirinktas duomenų bazės A funkcijų rinkinys, AdaBoost klasifikatorius pasiekė geresnių rezultatų nei kiti – jo vidutiniai Acc, Sen, Spe ir AUC atitinkamai yra 88,4%, 90,2%, 87,7% ir 0,94. Antrasis geriausias modelis buvo SVM, kurio vidutinis Acc buvo 83,7% (4.6 a-b). Remiantis atliktu nepriklausomu dviejų imčių t-testu, nustatytas statistiškai reikšmingas skirtumas tarp AdaBoost ir kitų klasifikatorių Acc, Sen ir Spc reikšmių ($p < 0,05$). Kalbant apie B duomenų bazę (4.6 c-d), kaip ir A duomenų bazės atveju, AdaBoost modelis pasiekė didžiausias vidutines

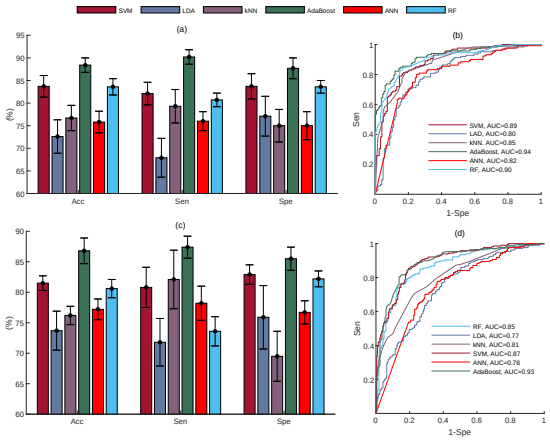

6.10 pav. Klasifikavimo rezultatai, nustatant vairuotojo nuovargį pagal visus modelius. A duomenų bazė **(a)-b)**, B duomenų bazė **(c)-d)**

Acc, Sen, Spe ir AUC vertes, atitinkamai 87,4%, 85,5%, 86,8% ir 0,93. Išskyrus AdaBoost, SVM ir RF SPE vertes, pastebimas statistiškai reikšmingas skirtumas tarp gautų rezultatų pagal AdaBoost ir kitus klasifikatorius ($p < 0,05$).

Diskusija

Šis metodas, pagrįstas vienalaike EEG ir mirksnių analize per vieną prepriekinį kanalą, yra sukurtas būtent tam, kad būtų galima pašalinti praktinius dabartinių tyrimų apribojimus. Sutelkiant dėmesį į vieną prepriekinį EEG kanalą ir sumažinant priedų skaičių, siekiama pateikti patogesnį ir praktiškesnį vairuotojo nuovargio nustatymo sprendimą. Iš tiesų, naudojant vieną prepriekinės EEG kanalą, naudotojui suteikiama daugiau komforto, nes ant kaktos, kuri yra beplaukė, dedamas tik vienas elektrodas. Be to, prepriekinės EEG signale yra akių mirkčiojimo pokyčių, kurie, kaip įrodyta, koreliuoja su perėjimu iš budrumo būsenos į nuovargio [147, 148, 180]. Dėl šios priežasties su mirkčiojimu susijusios priemonės gali būti išskirtos iš prefrontalinio EEG kanalo ir naudojamos kaip papildoma informacija.

Kita vertus, keliuose tyrimuose, kuriuose buvo nagrinėjamas nuovargio vairuojant nustatymas, remiantis vienu arba mažu prefrontaliniu EEG kanalu, buvo naudojama tik viena duomenų bazė siūlomiems metodams kurti ir jų veiksmingumui išbandyti [20, 148, 153, 176, 177]. Neabejotina, kad literatūroje buvo sumenkintas pateiktų vairuotojų nuovargio nustatymo metodų pakeičiamumas naudojant skirtingas duomenų bazes, kurios yra labai svarbios tikram pritaikymui. Siekiant išspręsti minėtą problemą, pasiūlyto metodo veiksmingumas nustatant vairuotojų nuovargį buvo įvertintas naudojant dvi duomenų bazes; pirmoji duomenų bazė buvo naudojama parametrams derinti, o antroji – testavimui.

6.5. ANESTEZIJOS STEBĖJIMO GYLIS

6.5.1. EEG ENTROPIJOS ANALIZĖ ANESTEZIJOS GYLIUI STEBĖTI

Entropijos analizė tapo populiariu anestezijos gylio (angl. *Depth of Anesthesia, DoA*) stebėjimo metodu dėl netiesinių EEG signalų charakteristikų [203]. Pagrindinis principas yra tas, kad, gilėjant anestezijai, sąmonės aktyvumas mažėja, todėl keičiasi tai, kiek sudėtingas yra EEG signalas [205]. Entropijos rodikliai, tokie kaip SampEn, permutacijos entropija (PeEn), spektrinė entropija (SpEn) ir apytikslė entropija (AppEn), kiekybiškai įvertina EEG bangų formų netolygumą ir sudėtingumą ir yra perspektyvūs vertinant DoA [213–216]. Visgi šiame kontekste išsklaidytos entropijos (FuzzEn) ir nuolydžio entropijos (SlopEn) tyrimai tebėra riboti, nepaisant jų potencialo įveikti įprastinių entropijos metrikų trūkumus.

FuzzEn suteikia galimybę prisitaikyti prie skirtingų duomenų charakteristikų, nes leidžia skaičiuoti pagal įvairias narystės funkcijas, tad gali veiksmingiau nei SampEn ir AppEn atspindėti sudėtingus EEG signalų ryšius [217, 218]. Kita vertus, SlopEn sprendžia SampEn ir PeEn trūkumus, kiekybiškai įvertindamas EEG signalų nuolydžio pokyčius laikui bėgant, kurie gali rodyti anestezijos gylio pokyčius [219, 220]. Atsižvelgiant į per anesteziją stebimus EEG aktyvumo modelius, kuriems būdingas padidėjęs reguliarumas ir sinchronizacija, SlopEn dėmesys EEG signalo verčių pokyčiams leidžia tikėtis patikimo DOA stebėjimo. Šio skyriaus tikslai – ištirti FuzzEn ir SlopEn veiksmingumą DoA stebėsenai ir jį įvertinti, palyginti su pripažintomis entropijos metrikomis, tokiomis kaip SampEn, SpEn ir AppEn, naudojant A duomenų bazę, kaip aptarta [213].

Metodologinė strategija

DoA stebėsenos metodologinė strategija naudojant skirtingas entropijos metrikas pateikta 6.11 pav. Iš pradžių EEG signalai iš anksto apdorojami segmentuojant juos į penkių sekundžių intervalus, taikant „Butterworth“ juostos pralaidumo filtrą ir pašalinant artefaktus bangelių transformacijos filtru [18]. Tada, naudojant nulinės fazės filtrus, signalai išskaidomi į pojuostes nuo delta iki gama. Vėliau iš pojuosčių išskiriami SampEn, AppEn, SpEn, FuzzEn ir SlopEn kiekybiniam palyginimui.

FuzzEn, apskaičiuotas naudojant Gauso (Gau) ir eksponentinę (Exp) narystės funkcijas, parodo, kad jį galima pritaikyti prie skirtingų duomenų charakteristikų. SlopEn taip pat kiekybiškai įvertina EEG signalų nuolydžio poslinkius laikui bėgant, galimai užfiksuodamas poslinkius, rodančius anestezijos gylio pokyčius [217, 219]. FuzzEn ir SlopEn bei parametrai kartu su kitomis entropijos metrikomis yra kruopščiai sureguliuoti, siekiant tinkamiausio veikimo. Galiausiai DoA indekso reikšmėms prognozuoti taikomas neuroninio tinklo regresijos modelis, kurio hiperparametrai tikslinami, naudojant Bajeso optimizavimą ir modelio vertinimą, pagrįstą vidutine absoliučiąja paklaida ir koreliacijos koeficientu tarp apskaičiuotų ir referencinių DoA

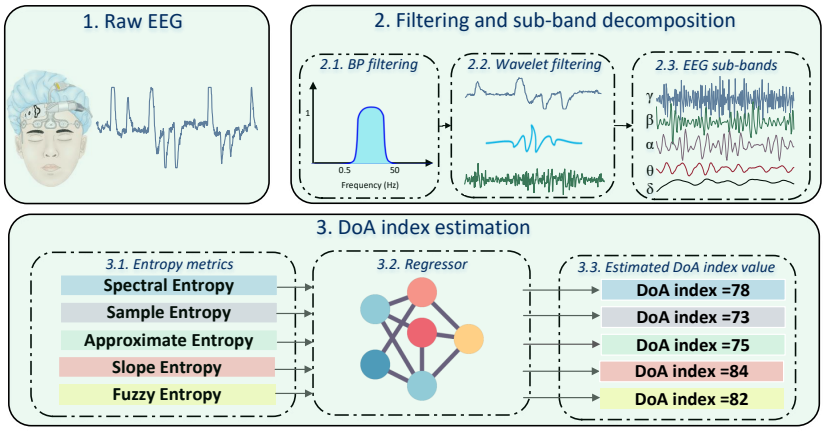

6.11 pav. DoA stebėjimo, naudojant skirtingus entropijos rodiklius, blokinė diagrama

indekso reikšmių.

DoA stebėsenos naudojant skirtingas entropijos metrikas blokinė diagrama

Rezultatų patikimumas užtikrinamas taikant 10-ies kartų kryžminio patikrinimo strategiją per mokymo patvirtinimą ir vertinimą atskiroje bandomojoje aibėje. 6.4 lentelėje. kiekybiškai įvertinamas kiekvienos entropijos metrikos veiksmingumas, remiantis vidutine absoliučiąja paklaida ir koreliacijos koeficientu, kai tiek FuzzEn, tiek SlopEn variacijose yra santykinai mažos vidutinės absoliučiosios paklaidos vertės (6,4, 6,7 ir 6,8) ir didelės koreliacijos koeficiento vertės (0,77, 0,75 ir 0,74). Tai rodo tikslesnį etaloninių DoA indekso reikšmių įvertinimą. Ir, atvirkščiai – SampEn ir AppEn rodo didesnes vidutines absoliutinės paklaidos vertes (8,7 ir 8,9) ir vidutines koreliacijos koeficiento vertes (0,63 ir 0,61). Pažymėtina, kad reikšmingo skirtumo tarp FuzzEn ir SlopEn metrikų rezultatų nenustatyta, tačiau buvo pastebėtas statistiškai reikšmingas skirtumas, palyginti su kitomis metrikomis.

6.4 lentelė. Kiekvienos entropijos rezultatai, regresuojant DoA indekso reikšmes

Entropijos tipas	Metrika ($\mu \pm \sigma$)	
	MAE	CC
FuzzEn (Gau)	6,4 $\pm$ 0,7	0,77 $\pm$ 0,02
FuzzyEn (Exp)	6,7 $\pm$ 0,5	0,75 $\pm$ 0,01
SlopEn	6,8 $\pm$ 0,6	0,74 $\pm$ 0,03
SampEn	8,7 $\pm$ 0,9	0,63 $\pm$ 0,05
AppEn	8,9 $\pm$ 1,1	0,61 $\pm$ 0,04
SpEn	10,7 $\pm$ 1,8	0,37 $\pm$ 0,10

Be to, sujungus abu FuzzEn variantus gaunami palankūs rezultatai – koreliacija

yra 0,85, o vidutinė absoliučioji paklaida – 5,4. Tai rodo kombinuotų FuzzEn metrikų veiksmingumą siekiant tiksliai stebėti DoA (6.12 pav.).

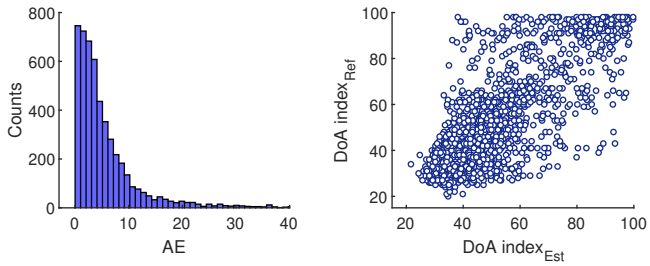

6.12 pav. AE sklaidos diagramos ir histogramos tarp atskaitos ir apskaičiuotų DoA indekso verčių, naudojant sulietą FuzzEn

Geresnį FuzzEn su Gau ir eksponentine Exp narystės funkcijomis veiksmingumą, palyginti su SampEn ir AppEn, galima paaiškinti keliais veiksniais:

1. FuzzEn narystės priemonių panaudojimas leidžia geriau atspindėti neapibrėžtumo niuansus. Jis užfiksuoja skirtingus duomenų neapibrėžtumo laipsnius ir siūlo lankstesnį modelį nei dvejetainiai SampEn ir AppEn skirtumai;

2. FuzzEn pasižymi gebėjimu prisitaikyti prie duomenų charakteristikų, o Gau ir Exp narystės funkcijos suteikia platesnį spektrą sudėtingiems EEG signalų santykiams modeliuoti pritaikant variantus, atsižvelgiant į skirtumus, kurių SampEn ir AP-PEN priemonės veiksmingai neužfiksuoja;

3. Derinant FuzzEn su tinkamomis narystės funkcijomis, padidėja atsparumas EEG signalų triukšmui ir sumažėja svyravimų poveikis.

SlopEn pranašumas, palyginti su tokiomis metrikomis, kaip SampEn, ApEn ir SpEn, yra jo savita galimybė užfiksuoti ir kiekybiškai įvertinti signalo pokyčio greitį ar nuolydį. Kitose entropijos metrikose daugiausia dėmesio skiriama įvairiems signalo sudėtingumo aspektams, o nuolydžio entropija pabrėžia signalo nuolydžio pokyčius. Dėl šios savybės nuolydžio entropija yra ypač jautri staigiems signalo pokyčiams ar tendencijoms, todėl suteikia savitą požiūrį į signalo dinamiką. Atliekant DoA stebėseną, kai naudojama EEG, nuolydžio entropija gali suteikti daugiau niuansų ir išsamiau atspindėti pagrindinį nervinį aktyvumą. Įrodytas mažesnis jos jautrumas duomenų ilgiui, palyginti su SampEn ir AppEn, gali padidinti anestezijos gylio vertinimo tikslumą, todėl ji yra vertinga metrika šioje srityje.

6.5.2. DĖVIMASIS EEG PAGRĮSTAS ANESTEZIJOS STEBĖJIMO GYLIS: NEPARAMETRINIS FUNKCIJŲ RINKINYS

Bendroji anestezija, būtina saugioms chirurginėms procedūroms atlikti, reikalauja tikslios kontrolės, kad būtų išvengta tokių komplikacijų, kaip širdies ir kraujagyslių įtampa ir pooperacinės kognityvinės problemos. Anestezijos gylio (DoA) stebėsena, daugiausia pagrįsta EEG signalais, padeda palaikyti tinkamą sąmonės netekimo lygį, užtikrindama tiek paciento saugą, tiek ekonominę naudą. Siekiant supaprastinti EEG duomenis į skaitines skales, buvo sukurtos įvairios sistemos, pavyzdžiui, bispektrinio indekso (BIS) monitorius, tačiau dėl didelių sąnaudų ir priklausomybės nuo vienkartinių elektrodų jos sunkiai prieinamos. Dėl šios priežasties reikia ieškoti alternatyvių, ekonomiškai veiksmingų metodų, pavyzdžiui, tokių, kurie naudoja įprastas vieno kanalo EEG sistemas.

Nepaisant to, naudojant tik vieną duomenų bazę DoA stebėjimo algoritmui kurti ir išbandyti, galima apriboti tyrimus, kuriuose naudojamos tokios sistemos. Tai ypač pastebima naudojant netiesines funkcijas, pavyzdžiui, SampEn, kurioms prieš skaičiavimą reikia sureguliuoti parametrus [227]. Iš tiesų, nebuvo atsižvelgta į galimybę keisti sureguliuotas funkcijas skirtingose duomenų bazėse, nors ji yra labai svarbi siūlomo metodo bendrumui [221, 228]. Taigi, siekiama dviejų tikslų: (i) įdiegti naują, parametrų neturintį funkcijų rinkinį, skirtą DoA stebėsenai, naudojant vieną frontalinį EEG kanalą, pašalinant žmogaus įsikišimo poreikį, derinant parametrus prieš skaičiavimą, ir ii) ištirti pasiūlyto požymių rinkinio veikimą dviejose skirtingose duomenų bazėse, užtikrinant pasiūlyto funkcijų rinkinio apibendrinimą, kai jis taikomas duomenims, įrašytiems su skirtingomis charakteristikomis, pavyzdžiui, skirtingu mėginių ėmimo dažniu.

Siūlomas algoritmas

Siūlomas DoA stebėsenos algoritmas pavaizduotas 6.13 pav., jis susideda iš pirminio apdorojimo, pojuosčių dekompozicijos, funkcijų išskyrimo, funkcijų atrankos ir regresijos etapų. Išankstinio apdorojimo ir pojuostės dekompozicijos etape EEG signalas segmentuojamas ir filtruojamas, siekiant pašalinti triukšmą ir artefaktus. Paskui, naudojant nulinės fazės filtrus, išvedamos EEG pojuostės. Funkcijų išskyrimas apima entropija pagrįstas galios ir dažnių juostas, fraktalais ir variacijomis pagrįstas funkcijas, atspindinčias įvairius EEG signalo savybių aspektus, svarbius DoA stebėsenai. Entropijos priemonės kiekybiškai įvertina EEG netolygumus, o galios ir dažnių juostos funkcijos suteikia įžvalgų apie pojuosčių veiklos dinamiką. Fraktalais pagrįsti požymiai atspindi EEG sudėtingumą, o variacijomis pagrįstos funkcijos parodo su anestezija susijusius EEG modelio pokyčius.

Po funkcijų išskyrimo funkcijoms atrinkti taikomas NCA metodas, kad būtų galima nustatyti svarbias funkcijas, kurios reikšmingai prisideda prie to, kaip

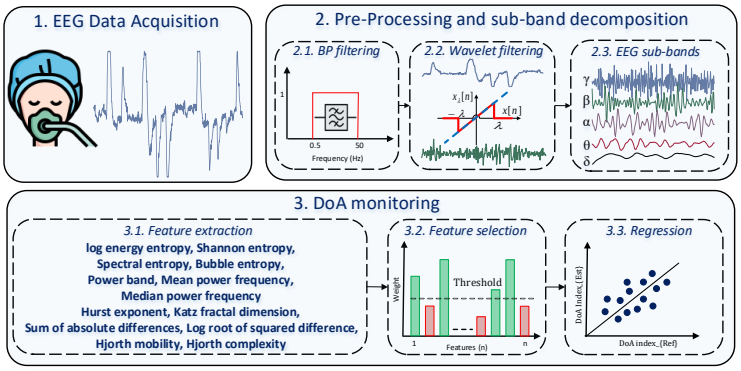

6.13 pav. Siūlomo DoA stebėsenos algoritmo blokinė schema

prognozuojama DoA indekso vertė. Tada DoA indekso prognozei naudojami atsitiktinio miško ir SVM regresijos modeliai, kurių hiperparametrai tikslinami Bajeso optimizavimo būdu. Veiksmingumo vertinimas apima vidutinės absoliutinės paklaidos ir koreliacijos koeficiento apskaičiavimą, siekiant įvertinti, kiek tikslus ir patikimas yra DoA indeksas, palyginti su pamatinėmis vertėmis.

Eksperimentų rezultatai ir aptarimas

Funkcijos atrankos procese visos 65-ios funkcijos, išskirtos iš šešių I duomenų bazės subjektų, įvertinamos naudojant NCA, siekiant nustatyti svarbias DoA stebėsenos funkcijas. Iš jų 34-ims funkcijoms buvo priskirti svoriai, viršijantys 0,5, o tai rodo jų svarbą prognozuojant DoA. Tarp atrinktų svarbių funkcijų yra tokios funkcijos, kaip vidutinis galios dažnis (MPF), vidutinis galios dažnis (MAPF) ir mobilumas (MH) visose EEG pojuostėse. Šios funkcijos, pavaizduotos 6.14 pav., buvo laikomos labai svarbiomis dėl jų atpažinimo galios apibūdinant anestezijos būseną ir prisidėjo prie tolesnės regresijos analizės. Pažymėtina, kad, siekiant išvengti tyrimo šališkumo, į galutinę regresiją nebuvo įtraukti funkcijų atrankai naudoti įrašai.

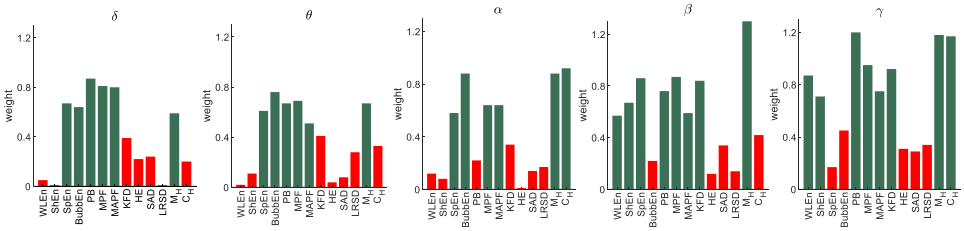

6.14 pav. NKI pasirinktos funkcijos (žalios), suskirstytos į kategorijas pagal kiekvieną pojuostę

Regresijos analizei buvo panaudoti 25198 ir 19399 penkių sekundžių EEG

signalo segmentai iš I ir II duomenų bazių, atitinkamai atmetus segmentus su nežinomomis DoA indekso vertėmis.

6.15 pav. pateiktas etaloninių DoA indekso verčių pavyzdys kartu su abiejų modelių įvertintomis vertėmis, naudojant II duomenų bazę. Stebėjimas atskleidžia, kad atsitiktinio miško modelis tiksliai atspindi etaloninių DoA indekso verčių trajektoriją. Iš tiesų, atsitiktinio miško modelis leido tiksliau įvertinti DoA indeksą nei SVM ir parodė patikimesnę koreliaciją (0,86 ir 0,68).

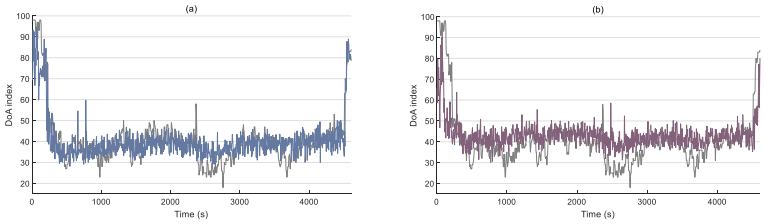

6.15 pav. Pavyzdys, kaip atsitiktinio miško (tamsiai mėlyna) **(a)** ir SVM (violetinė) **(b)** modeliai atkartoja vieno II duomenų bazės tiriamojo DoA indekso verčių tendenciją (šviesiai pilka)

Diskusija

Čia buvo pasiūlytas naujas, parametrų neturintis DoA stebėsenos naudojant vieną priekinį EEG kanalą funkcijų rinkinys, specialiai pritaikytas pragmatiniams apribojimams, su kuriais susiduriama atliekant esamus tyrimus, spręsti. Viena vertus, daugybė literatūroje pateiktų metodų buvo sukurti naudojant daugiakanalius EEG įrašus. Tai gali sukelti nepatogumų operacijos metu, nes reikia kelių priedų, prijungtų prie įvairių smegenų sričių. Priešingai, naudoti vieną priekinį EEG kanalą yra patogiau, nes ant beplaukės kaktos srities reikia uždėti tik vieną elektrodą, o tai gali sumažinti imlumą triukšmui.

Kita vertus, tyrimuose, kuriuose daugiausia dėmesio buvo skiriama DoA stebėjimui naudojant vieną priekinį EEG kanalą, paprastai buvo naudojama tik viena duomenų bazė, skirta jų siūlomų algoritmų veikimui sukurti ir įvertinti. Neabejotina, kad įvairiose duomenų bazėse pateiktų algoritmų pakeičiamumas, esminis tikrojo pasaulio taikomųjų programų aspektas, literatūroje buvo sumenkintas. Ši problema ypač išryškėja naudojant netiesines funkcijas, tokias kaip SampEn, nes prieš skaičiuojant reikia suderinti jų parametrus, t. y. tinkamas šių priemonių veikimas yra jautrus pradiniam kalibravimui [221,228]. Vis dėlto čia įdiegtam funkcijų rinkiniui nereikia derinti parametrų. Dėl to turėtų būti mažiau rūpesčių dėl parametrų veiksmingumo su kitomis duomenų bazėmis, užtikrinant, kad funkcijų rinkinys būtų pakeičiamas ir pritaikomas įvairiose duomenų bazėse.

6.6. IŠVADOS

1. Siūlomas SWT-kurtozės algoritmas veiksmingai pašalino elektrinių poslinkių tiesinės tendencijos artefaktus trumpame vieno EEG signalo segmente. Jis pasirodė labai našus, palyginti su AWICA ir EAWICA, su didesniu kroskoreliacijos koeficientu – 0,92, palyginti su 0,58 ir 0,67, o NRMSE – atitinkamai 5,4, palyginti su 12,2 ir 11,5, tarp EEG signalų be artefaktų ir filtruoto EEG. Panašiai pasirodė, kad VME-DWT yra veiksmingas algoritmas, leidžiantis aptikti ir filtruoti akių mirksėjimo artefaktus trumpame vieno frontalinio EEG kanalo segmente. Jis pralenkė AVMD ir DWT, turėdamas didesnį 0,92 kroskoreliacijos koeficientą, palyginti su 0,83 ir 0,58, ir mažesnį RRMSE - 0,42, palyginti su 0,59 ir 0,87. Abu algoritmai gali būti panaudoti šalinant artefaktus smegenų ir kompiuterio sąsajose bei klinikinėse programose, nes jiems nereikia pradinio kalibravimo ar etaloninių artefaktų.

2. Netiesinių požymių rinkinio, gauto iš vieno frontalinio EEG kanalo, efektyvumas ir universalumas buvo įrodytas kaip galimas sprendimas, leidžiantis pašalinti įprastinės RBP analizės apribojimus, skirtus atskirti budrumui nuo I miego stadijos. Netiesiniai požymiai, pagrįsti EEG dažninių komponenčių fraktalinės ir entropijos analizės rezultatais, lenkia tradicinę RBP analizę, rodydami didesnį vidutinį jautrumą I miego stadijai keliose duomenų bazėse: Miego telemetrija (82,6 % ir 71,8 %), DREAMS (87,6 % ir 71,8 %), DCSM (91,0 % palyginti su 74,2 %) ir MESA (82,0 % ir 76,1 %).

3. Pateiktos naujos įžvalgos apie akių mirksėjimo svarbą EEG pagrįsto vairuotojo nuovargio aptikimo metu, pabrėžiant jų dvejopą, kaip informacinių signalų ir galimų artefaktų, vaidmenį. Akių mirksėjimo ir EEG RBP funkcijų sinergijos palyginimas prieš ir po filtravimo atskleidė pastebimą vidutinį vairuotojo nuovargio nustatymo tikslumo pagerėjimą (71,2 %, palyginti su 78,1 %). Tai pabrėžia dvigubą akių mirksėjimo vaidmenį frontaliniame EEG signale nustatant vairuotojo nuovargį. Remiantis šiais duomenimis, buvo pasiūlytas vairuotojo nuovargio atpažinimo algoritmas, pagrįstas tuo pačiu metu atliekama EEG ir akių mirksėjimo analize naudojant Fp1 EEG kanalą. Algoritmo veikimas buvo įvertintas naudojant dvi skirtingų charakteristikų duomenų bazes. Rezultatai, gauti iš abiejų duomenų bazių naudojant AdaBoost klasifikatorių, pagal tikslumą (88,4 % vs. 86, 8 %), parodė siūlomo algoritmo, skirto vairuotojo nuovargiui nustatyti, patikimumą. Atsižvelgiant į komercinių vieno prefrontalinio kanalo EEG galvos juostų prieinamumą, šis algoritmas yra perspektyvus aptinkant vairuotojo nuovargį realiomis aplinkybėmis.

4. Anestezijos lygiui stebėti buvo pasiūlytas požymių rinkinys, nereikalaujantis parametrų derinimo skirtingoms duomenų bazėms. Vėlgi, algoritmo įėjimo duomenys yra vienas frontalinis EEG kanalas. Algoritmo veikimas buvo įvertintas dviejose duomenų bazėse, turinčiose skirtingas charakteristikas. Siūlomas funkcijų rinkinys

pasirodė atsparus skirtingai duomenų bazių kilmei, pasiekdamas palyginamas 0,86 ir 0,85 kroskoreliacijos vertes ir 5,3 ir 7,1 vidutinės absoliutinės klaidos vertes tarp I ir II duomenų bazių etaloninių ir apskaičiuotų anestezijos gylio indekso verčių. Tai pabrėžia netiesinių požymių parametrų optimizavimo svarbą, siekiant maksimaliai padidinti EEG pagrįsto anestezijos gylio stebėjimo patikimumą.

REFERENCES

[1] CHALMERS, D. *The Conscious Mind: In Search of a Fundamental Theory*. Oxford University Press, 1996.

[2] TINDALL, S. C., *Clinical Methods: The History, Physical, and Laboratory Examinations*. 3rd ed. Boston: Butterworths, 1990, ch. 57. Level of Consciousness.

[3] LIU, X., YANAGAWA, T., LEOPOLD, D. A., CHANG, C., ISHIDA, H. *et al.* Arousal transitions in sleep, wakefulness, and anesthesia are characterized by an orderly sequence of cortical events. *NeuroImage*. 2015, 116, 222–231.

[4] GOMES, G., PASSOS, M., SILVA, H., OLIVEIRA, V., NOVAES, W. *et al.* Sleep quality and its association with psychological symptoms in adolescent athletes. *Rev. Paul. Pediatr.* 2017, 35(3), 316–321.

[5] RAKUSA, M., SIEMINSKI, M., RAKUSA, S., FALUP-PECURARIU, C., FRONCZEK, R. *et al.* Awakening to sleep disorders in europe: Survey on education, knowledge and treatment competence of european residents and neurologists. *Eur. J. Neurol.* 2021, 28(9), 2863–2870.

[6] VAN DER LINDEN, D., MASSAR, S., SCHELLEKENS, A., ELLENBROEK, B., and VERKES, R. Disrupted sensorimotor gating due to mental fatigue: preliminary evidence. *Int. J. Psychophysiol.* 2006, 62(1), 168–174.

[7] BAKKER, B., ZABŁOCKI, B., BAKER, A., RIETHMEISTER, V., MARX, B. *et al.* A multi-stage, multi-feature machine learning approach to detect driver sleepiness in naturalistic road driving conditions. *IEEE Trans. Intell. Transp. Syst.* 2022, 23(5), 4791–4800.

[8] TEFFT, B. C., Prevalence of motor vehicle crashes involving drowsy drivers united states 2009–2013, AAA Foundation for Traffic Safety, Washington, DC, USA, Tech. Rep., 2014.

[9] BROWN, E., LYDIC, R., and SCHIFF, N. General anesthesia, sleep, and coma. *N. Engl. J. Med.* 2010, 363(27), 2638–2650.

[10] CHEW, W. Z., TEOH, W. Y., SIVANESAN, N., LOH, P. S., SHARIFFUDDIN, I. I. *et al.* Bispectral index (bis) monitoring and postoperative delirium in elderly patients undergoing surgery: A systematic review and meta-analysis with trial sequential analysis. *J. Cardiothorac. Vasc. Anesth.* 2022, 36(12), 4449–4459. Epub 2022 Jul 8.

[11] CHAUDHARY, K., GARG, R., BHALOTRA, A., ANAND, R., and GIRDHAR, K. Anesthetic drug wastage in the operation room: A cause for concern. *J. Anaesthesiol Clin. Pharmacol.* 2012, 28(1), 56–61.

[12] GAZZANIGA, M. Brain and conscious experience. *Adv. Neurol.* 1998, 77, 181–92; discussion 192–3.

[13] SATTIN, D., MAGNANI, F., BARTESAGHI, L., CAPUTO, M., FITTIPALDO, A. *et al.* Theoretical models of consciousness: A scoping review. *Brain Sci.* 2021, 11(5), 535.

[14] NARO, A., CALABRÒ, R., and NAGAMINE, T. Frontiers in detecting consciousness: The growing use of eeg analysis. *Innov. Clin. Neurosci*. 2020, 17(7-9), 8–9.

[15] Eeg 10-10 electrodes placement. 2024. [Online]. Available: https://commons.wikimedia.org

[16] Neurosky. 2022. [Online]. Available: http://neurosky.com/biosensors/eeg-sensor/biosensors/

[17] Eeg 10-20 electrodes placement. 2010. [Online]. Available: https://commons.wikimedia.org

[18] SHAHBAKHTI, M., RODRIGUES, A. S., AUGUSTYNIAK, P., BRONIEC-WÓJCIK, A., SOLOŠENKO, A. *et al.* Swt-kurtosis based algorithm for elimination of electrical shift and linear trend from eeg signals. *Biomed. Signal Process. Control*. 2021, 65, 102373.

[19] SHAHBAKHTI, M., BEIRAMVAND, M., NAZARI, M., BRONIEC-WÓJCIK, A., AUGUSTYNIAK, P. *et al.* Vme-dwt: An efficient algorithm for detection and elimination of eye blink from short segments of single eeg channel. *IEEE Trans. Neural Syst. Rehabil. Eng.* 2021, 29, 408–417.

[20] SHAHBAKHTI, M., BEIRAMVAND, M., REJER, I., AUGUSTYNIAK, P., BRONIEC-WOJCIK, A. *et al.* Simultaneous eye blink characterization and elimination from low-channel prefrontal eeg signals enhances driver drowsiness detection. *IEEE J. Biomed. Health Inform.* 2022, 26(3), 1001–1012.

[21] SHAHBAKHTI, M., BEIRAMVAND, M., NASIRI, E., FAR, S. M., CHEN, W. *et al.* Fusion of eeg and eye blink analysis for detection of driver fatigue. *IEEE Trans. Neural Syst. Rehabil. Eng.* 2023, 31, 2037–2046.

[22] SHAHBAKHTI, M., BEIRAMVAND, M., NASIRI, E., CHEN, W., SOLE-CASALS, J. *et al.* The importance of gender specification for detection of driver fatigue using a single eeg channel. In *2022 14th Biomedical Engineering International Conference (BMEiCON)*. Songkhla, Thailand, 2022, 1–3.

[23] SHAHBAKHTI, M., BEIRAMVAND, M., EIGIRDAS, T., SOLÉ-CASALS, J., WIERZCHON, M. *et al.* Discrimination of wakefulness from sleep stage i using nonlinear features of a single frontal eeg channel. *IEEE Sens. J.* 2022, 22(3), 6975–6984.

[24] SHAHBAKHTI, M., KRYCINSKA, R., BEIRAMVAND, M., HAKIMI, N., LIPPING, T. *et al.* Wearable eeg-based depth of anesthesia monitoring: A non-parametric feature set. *IEEE Sens. J.* 2024, 24(11), 1–10.

[25] SHAHBAKHTI, M., BEIRAMVAND, M., HAKIMI, N., REJER, I., LIPPING, T. *et al.* Fusing fuzzy entropy with gaussian and exponential membership functions outperforms traditional entropy metrics in monitoring the depth of anesthesia using a single frontal eeg channel. *IEEE Sens. Lett.* 2024, 8(3), 1–4.

[26] SHAHBAKHTI, M., BEIRAMVAND, M., FAR, S. M., SOLE-CASALS, J., LIPPING, T., and AUGUSTYNIAK, P. Utilizing slope entropy as an effective index for wearable eeg-based depth of anesthesia monitoring. In *2024 46th Annual International Conference of the IEEE Engineering in Medicine and Biology, EMBC 2024*. Florida, USA, 2024, 1–4.

[27] SHAHBAKHTI, M., BEIRAMVAND, M., KRYCINSKA, R., NASIRI, E., CHEN, W. *et al.* A reliable method to estimate the bispectral index value using a single frontal eeg channel for intra and inter subject variability. In *Proc. 2023 IEEE Int. Symp. Med. Meas. Appl. (MeMeA)*. 2023.

[28] S. E.A. GREGORYA, H. W. and KESSLER, K. A dataset of eeg recordings from 47 participants collected during a virtual reality working memory task where attention was cued by a social avatar and non-social stick cue. *Data in Brief*. 2022, 41, 1–9.

[29] TATUM, W. *Ambulatory EEG monitoring*. Springer Publishing Company, 2017.

[30] GUARNIERI, R., MARINO, M., BARBAN, F., GANZETTI, M., and MANTINI, D. Online eeg artifact removal for bci applications by adaptive spatial filtering. *J. Neural Eng*. 2018, 15, 1–12.

[31] MAMMONE, N., FORESTA, F., and MORABITO, F. Automatic artifact rejection from multichannel scalp eeg by wavelet ica. *IEEE Sens. J.* 2012, 12, 533–542.

[32] GIRI, B., SARKAR, S., MAZUMDER, S., and DAS, K. A computationally efficient order statistics based outlier detection technique for eeg signals. *Conf. Proc. IEEE Eng. Med. Biol. Soc., Milan*. 2015, 4765–4768.

[33] DELORME, A., SEJNOWSKI, T., and MAKEI, S. Enhanced detection of artifacts in eeg data using higher-order statistics and independent component analysis. *NeuroImage*. 2007, 34, 1443–1449.

[34] MAMMONE, N. and MORABITO, F. Enhanced automatic wavelet independent component analysis for electroencephalographic artifact removal. *Entropy*. 2014, 16, 6553–6572.

[35] STONE, D., TAMBURRO, G., FIEDLER, P., HAUEISEN, J., and COMANI, S. Automatic removal of physiological artifacts in eeg: the optimized fingerprint method for sports science applications. *Front. Hum. Neurosci.* 2018, 21, 1–15.

[36] BLUM, S., JACOBSEN, N., BLEICHNER, M., and DEBENER, S. A riemannian modification of artifact subspace reconstruction for eeg artifact handling. *Front. Hum. Neurosci.* 2019, 13, 1–10.

[37] BAJAJ, N., CARRIÓN, J., BELLOTTI, F., BERTA, R., and GLORIA, A. Automatic and tunable algorithm for eeg artifact removal using wavelet decomposition with applications in predictive modeling during auditory tasks. *Biomed. Signal Process. Control*. 2020, 55, 1–13.

[38] CHANG, C., HSU, S., PION-TONACHINI, L., and JUNG, T. Evaluation of artifact subspace reconstruction for automatic artifact components removal in multi-channel eeg recordings. *IEEE Trans. Biomed. Eng*. 2020, 67, 1114–1121.

[39] SOMERS, B., FRANCART, T., and BERTRAND, A. A generic eeg artifact removal algorithm based on the multi-channel wiener filter. *J. Neural Eng*. 2018, 15, 1–13.

[40] CHAVEZ, M., GROSSELIN, F., BUSSALB, A., FALLANI, F., and NAVARRO-SUNE, X. Surrogate-based artifact removal from single-channel eeg. *IEEE Trans. Neural Syst. Rehabil. Eng*. 2018, 26, 540–550.

[41] GHANDEHARION, H. and ERFANIAN, A. A fully automatic ocular artifact suppression from eeg data using higher order statistics: Improved performance by wavelet analysis. *Med. Eng. Phys.* 2020, 32, 720–729.

[42] SINGHA, B. and WAGATSUMA, H. Two-stage wavelet shrinkage and eeg-eog signal contamination model to realize quantitative validations for the artifact removal from multiresource biosignals. *Biomed. Signal Process. Control*. 2019, 47, 94–114.

[43] ZIKOV, T., BIBIAN, S., DUMONT, G., HUZMEZAN, M., and RIES, C. A wavelet based de-noising technique for ocular artifact correction of the electroencephalogram. In *Proc. Second Joint EMBS/BMES Conf.* 2002, 98–105.

[44] BRYCHTA, R., TUNTRAKOOL, S., APPALSAMY, M., KELLER, N., ROBERTSON, D. *et al.* A wavelet methods for spike detection in mouse renal sympathetic nerve activity. *IEEE Trans. Biomed. Eng*. 2007, 54, 82–93.

[45] MAHJAN, R. and MORSHED, B. Unsupervised eye blink artifact denoising of eeg data with modified multiscale sample entropy, kurtosis, and wavelet-ica. *IEEE J. Biomed. Health Informt.* 2015, 19, 158–165.

[46] KLADOS, M. and BAMIDIS, P. A semi-simulated eeg/eog dataset for the comparison of eog artifact rejection techniques. *Data in Brief*. 2016, 8, 1004–1006.

[47] SHOEB, A., Application of machine learning to epileptic seizure onset detection and treatment, Ph.D. dissertation, 2009.

[48] DELORME, A. and MAKEIG, S. Eeglab: an open source toolbox for analysis of single-trial eeg dynamics including independent component analysis. *J. Neurosci. Methods*. 2004, 134, 9–21. Available: http://sccn.ucsd.edu/eeglab/.

[49] CHEN, X., CHEN, Q., ZHANG, Y., and WANG, Z. A novel eemd-cca approach to removing muscle artifacts for pervasive eeg. *IEEE Sens. J.* 2019, 19, 8420–8431.

[50] URIGÜEN, J. and GARCIA-ZAPIRAIN, B. Eeg artifact removal—state-of-the-art and guidelines. *J. Neural Eng.* 2015, 12, 1–23.

[51] JAFARIFARMAND, A. and BADAMCHIZADEH, M. Eeg artifacts handling in a real practical brain–computer interface controlled vehicle. *IEEE Trans. Neural Syst. Rehabil. Eng.* 2019, 27(6), 1200–1280.

[52] BARRY, R. J., CLARKE, A. R., JOHNSTONE, S., MAGEE, C., and RUSHBY, J. Eeg differences between eyes-closed and eyes-open resting conditions. *Clin. Neurophysiol*. 2007, 118(12), 2765–2773.

[53] JINDAL, K., UPADHYAYA, R., and SINGH, H. Application of hybrid glct-pica de-noising method in automated eeg artifact removal. *Biomed. Signal Process. Control*. 2020, 60, 1–16.

[54] SAI, C., MOKHTAR, N., AROF, H., CUMMING, P., and IWAHASHI, M. Automated classification and removal of eeg artifacts with svm and wavelet-ica. *IEEE J. Biomed. Health Informt.* 2018, 22, 664–670.

[55] KHATUN, S., MAHAJAN, R., and MORSHED, B. Comparative study of wavelet-based unsupervised ocular artifact removal techniques for single-channel eeg data. *IEEE. J. TRANSL. ENG. HE.* 2016, 4.

[56] MAJMUDAR, C. and MORSHED, B. Autonomous oa removal in real-time from single channel eeg data on a wearable device using a hybrid algebraic-wavelet algorithm. *ACM. T. EMBED. COMPUT. S.* 2016, 16(1).

[57] PATEL, R., JANAWADKAR, M., SENGOTTUVEL, S., GIREESAN, K., and RADHAKRISHNAN, T. Suppression of eye-blink associated artifact using single channel eeg data by combining cross-correlation with empirical mode decomposition. *IEEE Sens J*. 2016, 16(18), 6947–6954.

[58] SAINI, M., PAYAL, and SATIJA, U. An effective and robust framework for ocular artifact removal from single-channel eeg signal based on variational mode decomposition. *IEEE Sens J*. 2020, 20(1), 369–376.

[59] DORA, C. and BISWAL, P. K. An improved algorithm for efficient ocular artifact suppression from frontal eeg electrodes using vmd. *Biocybern. Biomed. Eng*. 2019, 40(1).

[60] STERN, J. *Atlas of EEG patterns*. Lippincott Williams & Wilkins, 2005.

[61] AARABI, A., KAZEMI, K., GREBE, R., MOGHADDAM, H., and WALLOIS, F. Detection of eeg transients in neonates and older children using a system based on dynamic time-warping template matching and spatial dipole clustering. *NeuroImage*. 2009, 48, 50–62.

[62] KLEIN, A. and SKRANDIES, W. A reliable statistical method to detect eyeblink artefacts from electroencephalogram data only. *Brain Topogr*. 2013, 26, 558–568.

[63] CHANG, W., CHA, H., KIM, K., and IM, C. Detection of eye blink artifacts from single prefrontal channel electroencephalogram. *Comput. Methods Programs Biomed.* 2016, 124, 19–30.

[64] VALDERRAMA, J., A.TORRE, and DUN, B. An automatic algorithm for blink-artifact suppression based on iterative template matching: application to single channel recording of cortical auditory evoked potentials. *J. Neural Eng*. 2018, 15, 1–15.

[65] NAZARI, M. and SAKHAEI, S. Variational mode extraction: a new efficient method to derive respiratory signals from ecg. *IEEE J. Biomed. Health Inform.* 2018, 22(4), 1059–1067.

[66] FATT, I. and WEISSMAN, B. *Physiology of the eye: an introduction to the vegetative functions*. 2nd ed. Boston: MA: Butterworth-Heinemann, a division of Reed Publishing (USA) Inc, 1992.

[67] BULLING, A., WARD, J., GELLERSEN, H., and TROSTER, G. Eye movement analysis for activity recognition using electrooculography. *IEEE Trans Pattern Anal Mach Intell.* 2011, 33(4), 741–753.

[68] KANOGA, S., NAKANISHI, M., and MITSUKURA, Y. Assessing the effects of voluntary and involuntary eyeblinksin independent components of electroencephalogram. *Neurocomputing*. 2016, 193, 20–32.

[69] SANEI, S. and CHAMBERS, J. *EEG Signal Processing*. West Sussex PO19 8SQ, England: John Wiley and Sons Ltd, 2007.

[70] DAMMERS, J., SCHIEK, M., BOERS, F., SILEX, C., ZVYAGINTSEV, M. *et al.* Integration of amplitude and phase statistics for complete artifact removal in independent components of neuromagnetic recordings. *IEEE. Trans. Biomed. Eng*. 2008, 55(10), 2353–2361.

[71] CHO, H., AHN, M., AHN, S., KWON, M., and JUN, S. Eeg datasets for motor imagery brain–computer interface. *GigaScience*. 2017, 6(7).

[72] KAYA, M., BINLI, M., OZBAY, E., YANAR, H., and MISHCHENKO, Y. A large electroencephalographic motor imagery dataset for electroencephalographic brain computer interfaces. *Scientific Data*. 2018, 5, 1–16.

[73] TORKAMANI-AZAR, M., KANIK, S., AYDIN, S., and CETIN, M. Prediction of reaction time and vigilance variability from spatio-spectral features of resting-state eeg in a long sustained attention task. *IEEE J. Biomed. Health Inform.* 2020, 24(9), 2550–2558.

[74] REICHERT, C., CEJA, I. T., SWEENEY-REED, C., HEINZE, H., HINRICHS, H., and DÜRSCHMID, S. Impact of stimulus features on the performance of a gaze-independent brain-computer interface based on covert spatial attention shifts. *Front. Neurosci.* 2020, 14.

[75] VAN GILST, M. and ET AL. Protocol of the somnia project: an observational study to create a neurophysiological database for advanced clinical sleep monitoring. *BMJ. Open*. 2019, 9(11), 1–9.

[76] CASCIOLA, A. and ET AL. A deep learning strategy for automatic sleep staging based on two-channel eeg headband data. *Sensors*. 2021, 21(10), 1–17.

[77] RAHMAN, M., BHUIYAN, M., and HASSAN, A. Sleep stage classification using single-channel eog. *Comput. Biol. Med.* 2018, 102, 211–220.

[78] KIM, J., CHU, C., and KANG, M. Iot-based unobtrusive sensing for sleep quality monitoring and assessment. *IEEE Sens. J.* 2021, 21(3), 3799–3809.

[79] LI, F., VALERO, M., CLEMENTE, J., TSE, Z., and SONG, W. Smart sleep monitoring system via passively sensing human vibration signals. *IEEE Sens. J.* 2021, 21(13), 14 466–14 473.

[80] KIM, D., LEE, E., KIM, J., PARK, P., and CHO, S. A sleep apnea monitoring ic for respiration, heart-rate, spo2 and pulse-transit time measurement using thermistor, ppg and body-channel communication. *IEEE Sens. J.* 2021, 20(4), 1997–2007.

[81] IMTIAZ, S. A systematic review of sensing technologies for wearable sleep staging. *Sensors*. 2021, 21, 1–21.

[82] JAIN, R. and GANESAN, R. Reliable sleep staging of unseen subjects with fusion of multiple eeg features and rusboost. *Biomed. signal Process. control*. 2021, 70, 1–18.

[83] AN, P., YUAN, Z., and ZHAO, J. Unsupervised multi-subepoch feature learning and hierarchical classification for eeg-based sleep staging. *Expert Syst. Appl.* 2021, 186, 1–15.

[84] ZHANG, T. and ET AL. Sleep staging using plausibility score: a novel feature selection method based on metric learning. *IEEE J. Biomed. Health Inform.* 2021, 25(2), 577–590.

[85] LIU, C. and ET AL. Automatic sleep staging with a single-channel eeg based on ensemble empirical mode decomposition. *Physica A Stat. Mech. Appl.* 2021, 567, 1–12.

[86] MEMAR, P. and FARADJI, F. A novel multi-class eeg-based sleep stage classification system. *IEEE Trans. Neur. Sys. Reh. Eng.* 2018, 26(1), 84–95.

[87] ELDELE, E. and ET AL. An attention-based deep learning approach for sleep stage classification with single-channel eeg. *IEEE Trans. Neur. Sys. Reh. Eng.* 2021, 29, 809–818.

[88] JADHAV, P., RAJGURU, G., DATTA, D., and MUKHOPADHYAY, S. Automatic sleep stage classification using time–frequency images of cwt and transfer learning using convolution neural network. *Biocybern. Biomed. Eng.* 2020, 40(1), 494–504.

[89] YANG, B., ZHU, X., LIU, Y., and LIU, H. A single-channel eeg based automatic sleep stage classification method leveraging deep one-dimensional convolutional neural network and hidden markov model. *Biomed. Signal Process. Control*. 2021, 68(1), 1–11.

[90] KHALILI, E. and ASL, B. M. Automatic sleep stage classification using temporal convolutional neural network and new data augmentation technique from raw single-channel eeg. *Comput. Meth. Prog. Bio*. 2021, 204, 1–10.

[91] ALMAAS, M. and ET AL. Sleep patterns and insomnia among adolescents receiving child welfare services: A population-based study. *Sleep Health*. 2021, 652, 1–7.

[92] MIKUTTA, C. and ET AL. Co-ordination of brain and heart oscillations during non-rapid eye movement sleep. *J. Sleep Res.* 2021, 1–11.

[93] LAJNEF, T. and ET AL. Learning machines and sleeping brains: Automatic sleep stage classification using decision-tree multi-class support vector machines. *J. Neurosci. Methods*. 2015, 250, 94–105.

[94] ČIĆ, M., ŠODA, J., and BONKOVIĆ, M. Automatic classification of infant sleep based on instantaneous frequencies in a single-channel eeg signal. *Comput. Biol. Med.* 2013, 43(12), 2110–2117.

[95] SHARMA, M., GOYAL, D., ACHUTH, P., and ACHARYA, U. R. An accurate sleep stages classification system using a new class of optimally time-frequency localized three-band wavelet filter bank. *Comput. Biol. Med.* 2018, 98, 58–75.

[96] PAUL, J., IYPE, T., R, D., HAGIWARA, Y., KOH, J., and ACHARYA, U. R. Characterization of fibromyalgia using sleep eeg signals with nonlinear dynamical features. *Comput. Biol. Med.* 2019, 1–7.

[97] MICHIELLI, N., ACHARYA, U. R., and MOLINARI, F. Cascaded lstm recurrent neural network for automated sleep stage classification using single-channel eeg signals. *Comput. Biol. Med.* 2019, 106, 71–78.

[98] SUPRATAK, A., DONG, H., WU, C., and GUO, Y. Deepsleepnet: A model for automatic sleep stage scoring based on raw single-channel eeg. *IEEE Trans. Neur. Sys. Reh. Eng*. 2017, 25(11), 1998–2008.

[99] MOUSAVI, S., AFGHAH, F., and ACHARYA, U. Sleepeegnet: Automated sleep stage scoring with sequence to sequence deep learning approach. *PLoS ONE*. 2019, 14(5), 1–5.

[100] CHEN, Z., WU, M., CUI, W., LIU, C., and LI, X. An attention based cnn-lstm approach for sleep-wake detection with heterogeneous sensors. *IEEE J. Biomed. Health Inform.* 2021, 25(9), 3270–3277.

[101] MULLER, M. and ET AL. Linear and nonlinear interrelations show fundamentally distinct network structure in preictal intracranial eeg of epilepsy patients. *Hum. Brain Mapp.* 2020, 41(1), 1–16.

[102] TALEBI, N., NASRABADI, A., MOHAMMAD-REZAZADEH, I., and COBEN, R. ncreann: Nonlinear causal relationship estimation by artificial neural network; applied for autism connectivity study. *IEEE Trans. Med. Imaging*. 2019, 38(12), 2883–2890.

[103] GUO, H. and BURRUS, C. Convolution using the undecimated discrete wavelet transform. In *Proc. IEEE Int. Conf. Acoust., Speech, Signal Process*. 1996, 3, 1291–1294.

[104] ZHANG, C., WANG, H., and FU, R. Automated detection of driver fatigue based on entropy and complexity measures. *IEEE Trans. Intell. Transp. Syst.* 2014, 15(1), 168–177.

[105] LI, F. and OTHERS. Identification of the general anesthesia induced loss of consciousness by cross fuzzy entropy-based brain network. *IEEE Trans. Neur. Sys. Reh. Eng*. 2021, 29, 2281–2291.

[106] SCHARTNER, M. and OTHERS. Global and local complexity of intracranial eeg decreases during nrem sleep. *Neurosci. Conscious.* 2017, 2017(1), 1–12.

[107] AMEZQUITA-SANCHEZ, J., MAMMONE, N., MORABITO, F., and ADELI, H. A new dispersion entropy and fuzzy logic system methodology for automated classification of dementia stages using electroencephalograms. *Clin. Neurol. Neurosurg*. 2021, 201, 1–9.

[108] KESIC, S. and SPASIC, S. Application of higuchi's fractal dimension from basic to clinical neurophysiology: A review. *Comput. Meth. Prog. Bio.* 2016, 133, 55–70.

[109] HIGUCHI, T. Approach to an irregular time series on the basis of the fractal theory. *Phys. D: Nonlinear Phenom.* 1988, 31(2), 277–283.

[110] KATZ, M. Fractals and the analysis of waveforms. *Comput. Biol. Med.* 1988, 18(13), 145–156.

[111] MANIS, G., AKTARUZZAMAN, M., and SASSI, R. Bubble entropy: an entropy almost free of parameters. *IEEE Trans. Biomed.* 2017, 64(11), 2711–2718.

[112] ROSTAGHI, M. and AZAMI, H. Dispersion entropy: a measure for time-series analysis. *IEEE Signal Process. Lett.* 2016, 23(5), 610–614.

[113] KEMP, B. and OTHERS. Analysis of a sleep-dependent neuronal feedback loop: the slow-wave microcontinuity of the eeg. *IEEE. Trans. Biomed.* 2000, 47(9), 1185–1194.

[114] DEVUYST, S. The dreams databases and assessment algorithm. 2005. https://doi.org/10.5281/zenodo.2650142.

[115] PERSLEV, M. and OTHERS. U-sleep: resilient high-frequency sleep staging. *npj. Digit. Med.* 2021, 4(72), 1–12.

[116] DENNIS, D. and OTHERS. Scaling up scientific discovery in sleep medicine: the national sleep research resource. *Sleep*. 2016, 39(5), 1151–1164.

[117] RECHTSCHAFFEN, A. and KALES, A. *A manual of standardized terminology, techniques and scoring systems for sleep stages of human subjects*. Los Angeles, CA: UCLA Brain Information Service. Brain Research Institute, 1968.

[118] IBER, C. and OTHERS. *The AASM Manual for the scoring of sleep and associated events: rules, terminology and technical specifications*. Westchester, IL: Acad. Sleep Med., 2007, 176.

[119] SOLAZ, J. and OTHERS. Drowsiness detection based on the analysis of breathing rate obtained from real-time image recognition. *Transport. Res. Proc.* 2016, 14, 3867–3876.

[120] PHAN, H. and OTHERS. Personalized automatic sleep staging with single-night data: a pilot study with kullback–leibler divergence regularization. *Physiol. Meas.* 2020, 41(6), 1–11.

[121] BANLUESOMBATKUL, N. and OTHERS. Metasleeplearner: A pilot study on fast adaptation of bio-signals-based sleep stage classifier to new individual subject using meta-learning. *IEEE J. Biomed. Health Inform.* 2021, 25(6), 1949–1963.

[122] CHEN, C. and OTHERS. Personalized sleep staging system using evolutionary algorithm and symbolic fusion. In *38th Annual International Conference of the IEEE Engineering in Medicine and Biology Society (EMBC)*. 2016, 2266–2269.

[123] LI, G., LEE, B., and CHUNG, W. Smartwatch-based wearable eeg system for driver drowsiness detection. *IEEE Sens. J.* 2015, 15(12), 7169–7180.

[124] ET AL., R. C. Driver fatigue classification with independent component by entropy rate bound minimization analysis in an eeg-based system. *IEEE J. Biomed. Health Informat.* 2017, 21(3), 715–724.

[125] TEFFT, B. Prevalence of motor vehicle crashes involving drowsy drivers, united states, 2009 – 2013. *AAA Foundation for Traffic Safety*. 2014, 1–10.

[126] CUI, Y., XU, Y., and WU, D. Eeg-based driver drowsiness estimation using feature weighted episodic training. *IEEE Trans. Neural Syst. Rehabil. Eng.* 2019, 27(11), 2263–2273.

[127] HASAN, M., WATLING, C., and LARUE, G. Physiological signal-based drowsiness detection using machine learning: Singular and hybrid signal approaches. *J. Safety Res.* 2022, 80, 215–225.

[128] KAPLAN, S., GUVENSAN, M., YAVUZ, A., and KARALURT, Y. Driver behavior analysis for safe driving: A survey. *IEEE Trans. Intell. Transp. Syst.* 2015, 16(6), 3017–3032.

[129] WANG, J., WANG, Y., DAI, Y., ZHANG, F., and YU, X. Cooperative detection method for distracted and fatigued driving behaviors with readily embedded system implementation. *IEEE Trans. Instrum. Meas.* 2021.

[130] ANSARI, S., NAGHDY, F., DU, H., and PAHNWAR, Y. N. Driver mental fatigue detection based on head posture using new modified relu-bilstm deep neural network. *IEEE Trans. Intell. Transp. Syst.* 2022.

[131] SUBASI, A., SAIKIA, A., BAGEDO, K., SINGH, A., and HAZARIKA, A. Eeg based driver fatigue detection using fawt and multiboosting approaches. *IEEE Trans. Industr. Inform.* 2022.

[132] LI, Y., LI, K., WANG, S., CHEN, X., and WEN, D. Pilot behavior recognition based on multi-modality fusion technology using physiological characteristics. *Biosensors*. 2022, 12(6), 404.

[133] CHOI, M., KOO, G., SEO, M., and KIM, S. W. Wearable device-based system to monitor a driver's stress, fatigue, and drowsiness. *IEEE Trans. Instrum. Meas.* 2018, 67(3), 634–645.

[134] ET AL., W. Z. Vigilance estimation using a wearable eog device in real driving environment. *IEEE Trans. Intell. Transp. Syst.* 2020, 21(1), 170–184.

[135] ET AL., Z. G. Relative wavelet entropy complex network for improving eeg-based fatigue driving classification. *IEEE Trans. Instrum. Meas.* 2019, 68(7), 2491–2497.

[136] HARVY, J., BEZERIANOS, A., and LI, J. Reliability of eeg measures in driving fatigue. *IEEE Trans. Neural Syst. Rehabil. Eng.* 2022, 2743–2753.

[137] LI, G. and CHUNG, W. Electroencephalogram-based approaches for driver drowsiness detection and management: A review. *Sensors*. 2022, 22(3), 1100.

[138] ROCCO, J., LE, M., and PAENG, D. A systemic review of available low-cost eeg headsets used for drowsiness detection. *Front. Neuroinform.* 2020, 14, 1–14.

[139] WEI, C., WANG, Y., LIN, C., and JUNG, T. Toward drowsiness detection using non-hairbearing eeg-based brain-computer interfaces. *IEEE Trans. Neural Syst. Rehabil. Eng.* 2018, 26(2), 400–406.

[140] FOONG, R., ANG, K., ZHANG, Z., and QUEK, C. An iterative cross-subject negative-unlabeled learning algorithm for quantifying passive fatigue. *J. Neural Eng*. 2019, 16, 15.

[141] HAGEMANN, D. and NAUMANN, E. The effects of ocular artifacts on (lateralized) broadband power in the eeg. *Clin. Neurophysiol.* 2001, 112, 215–231.

[142] ET AL., S. H. Online artifact removal for brain-computer interfaces using support vector machines and blind source separation. *Comput. Intel. Neurosc.* 2007, 2007, 1–11.

[143] SCHLEICHER, R., GALLEY, N., BRIEST, S., and GALLEY, L. Blinks and saccades as indicators of fatigue in sleepiness warnings: looking tired? *Ergonomics*. 2008, 51(7), 982–1010.

[144] SCHMIDT, J., LAAROUSI, R., STOLZMANN, W., and KARRER, K. Eye blink detection for different driver states in conditionally automated driving and manual driving using eog and a driver camera. *Behav. Res.* 2018, 50, 1088–1101.

[145] CORI, J., ANDERSON, C., SHEKARI, S., JACKSON, M., and HOWARD, M. Narrative review: Do spontaneous eye blink parameters provide a useful assessment of state drowsiness? *Sleep Med. Rev.* 2019, 45, 95–104.

[146] ZHENG, W. and LU, B. A multimodal approach to estimating vigilance using eeg and forehead eog. *J. Neural Eng.* 2017, 14(2), 1–14.

[147] ROY, R. N., CHARBONNIER, S., and BONNET, S. Eye blink characterization from frontal eeg electrodes using source separation and pattern recognition algorithms. *Biomed. Signal Process. Control*. 2014, 14, 256–264.

[148] KO, L., KOMAROV, O., LAI, W., LIANG, W., and JUNG, T. Eyeblink recognition improves fatigue prediction from single-channel forehead eeg in a realistic sustained attention task. *J. Neural Eng.* 2020, 17, 1–12.

[149] MEHREEN, A., ANWAR, S., HASEEB, M., MAJID, M., and ULLAH, M. A hybrid scheme for drowsiness detection using wearable sensors. *IEEE Sens. J.* 2019, 19(13), 5119–5126.

[150] LIN, C. and ET AL. Wireless and wearable eeg system for evaluating driver vigilance. *IEEE Trans. Biomed. Circuits. Syst.* 2014, 8(2), 165–176.

[151] BARUA, S., AHMED, M., AHLSTROM, C., BEGUM, S., and FUNK, P. Automated eeg artifact handling with application in driver monitoring. *IEEE J. Biomed. Health Informat.* 2018, 22(5), 1350–1361.

[152] MIN, J., WANG, P., and HU, J. Driver fatigue detection through multiple entropy fusion analysis in an eeg-based system. *PLoS ONE*. 2018, 12, 1–19.

[153] LUO, H., QIU, T., LIU, C., and HUANG, P. Research on fatigue driving detection using forehead eeg based on adaptive multi-scale entropy. *Biomed. Signal Process. Control*. 2019, 51, 50–58.

[154] ISLAM, M., RASTEGARNIA, A., and YANG, Z. A wavelet-based artifact reduction from scalp eeg for epileptic seizure detection. *IEEE J. Biomed. Health Informat.* 2016, 20(5), 1321–1332.

[155] SUN, Y. and YU, X. An innovative nonintrusive driver assistance system for vital signal monitoring. *IEEE J. Biomed. Health Informat.* 2014, 16(6), 1932–1939.

[156] SLOOTEN, J., JAHFARI, S., and THEEUWES, J. Spontaneous eye blink rate predicts individual differences in exploration and exploitation during reinforcement learning. *Sci. Rep.* 2019(9), 1–13.

[157] MAGLIACANOA, A., FIORENZAB, S., ESTRANEOC, A., and TROJANOA, L. Eye blink rate increases as a function of cognitive load during an auditory oddball paradigm. *Neurosci. Lett.* 2020, 736, 1–7.

[158] ET AL., P. R. Comparison of the use of blink rate and blink rate variability for mental state recognition. *IEEE Trans. Neural Syst. Rehabil. Eng*. 2019, 27(5), 867–875.

[159] PAPROCKI, R. and LENSKIY, A. What does eye-blink rate variability dynamics tell us about cognitive performance? *Front. Hum. Neurosci.* 2017, 11, 1–9.

[160] ET AL., N. S. Joint analysis of eye blinks and brain activity to investigate attentional demand during a visual search task. *Brain Sci.* 2021, 11(5), 1–21.

[161] BRAACK, E., JONGE, B., and PUTTEN, M. Reduction of tms induced artifacts in eeg using principal component analysis. *IEEE Trans. Neural Syst. Rehabil. Eng*. 2013, 21(3), 376–382.

[162] ET AL., R. P. Ocular artifact suppression from eeg using ensemble empirical mode decomposition with principal component analysis. *Comput. Electr. Eng*. 2016, 54, 78–86.

[163] JAVED, E., FAYE, I., MALIK, A., and ABDULLAH, J. Removal of bcg artefact from concurrent fmri-eeg recordings based on emd and pca. *J. Neurosci. Methods*. 2017, 291, 150–165.

[164] Ibva brainmachine. [Accessed: 28-March-2021]. [Online]. Available: https://ibvabrainmachine.wordpress.com/

[165] DORA, C., PATRO, R., ROUT, S., BISWAL, P., and BISWAL, B. Adaptive ssa based muscle artifact removal from single channel eeg using neural network regressor. *IRBM*. 2020.

[166] ZHANG, H., ZHAO, M., WEI, C., MANTINI, D., LI, Z., and LIU, Q. Eegdenoisenet: A benchmark dataset for deep learning solutions of eeg denoising. *ArXiv*. 2021.

[167] ET AL., S. S. Analyzing driver drowsiness: From causes to effects. *Sustainability*. 2020, 12, 1–12.

[168] OBST, P., ARMSTRONG, K., SMITH, S., and BANKS, T. Age and gender comparisons of driving while sleepy: Behaviours and risk perceptions. *Transp. Res. Part F.* 2011, 14, 539–542.

[169] MILLEVILLE-PENNEL, I. and MARQUEZ, S. Comparison between elderly and young drivers' performances on a driving simulator and self-assessment of their driving attitudes and mastery. *Accid. Anal. Prev.* 2020, 135, 1–16.

[170] ET AL., C. L. Age and road safety performance: Focusing on elderly and young drivers. *IATSS Research*. 2020, 44(3), 212–219.

[171] HSU, S. and JUNG, T. Monitoring alert and drowsy states by modeling eeg source nonstationarity. *J. Neural Eng.* 2017, 14, 1–14.

[172] PAULO, R., PIRES, G., and NUNES, U. J. Cross-subject zero calibration driver's drowsiness detection: exploring spatiotemporal image encoding of eeg signals for convolutional neural network classification. *IEEE Trans. Neural Syst. Rehabil. Eng.* 2021, 29, 905–915.

[173] TUNCER, T., DOGAN, S., ERTAM, F., and SUBASI, A. A dynamic center and multi threshold point based stable feature extraction network for driver fatigue detection utilizing eeg signals. *Cognitive Neurodynamics*. 2021, 15, 223–237.

[174] TUNCER, T., DOGAN, S., and SUBASI, A. Eeg-based driving fatigue detection using multilevel feature extraction and iterative hybrid feature selection. *Biomed. Signal Process. and Control*. 2021, 68.

[175] GANGADHARAN, S. and VINOD, A. Drowsiness detection using portable wireless eeg. *Comput. Meth. Prog. Bio.* 2022, 214.

[176] OGINO, M. and MITSUKURA, Y. Portable drowsiness detection through use of a prefrontal single-channel electroencephalogram. *Sensors*. 2018, 18(12), 4477.

[177] MIN, J., XIONG, C., ZHANG, Y., and CAI, M. Driver fatigue detection based on prefrontal eeg using multi-entropy measures and hybrid model. *Biomed. Signal Process. Control*. 2021, 69, 1–10.

[178] WEI, C., WANG, Y., LIN, C., and JUNG, T. Toward drowsiness detection using non-hair-bearing eeg-based brain-computer interfaces. *IEEE Trans. Neural Syst. Rehabilitation Eng.* 2018, 26(2), 400–406.

[179] ZUO, X., ZHANG, C., CONG, F., ZHAO, J., and HÄMÄLÄINEN, T. Driver distraction detection using bidirectional long short-term network based on multiscale entropy of eeg. *IEEE Trans. Intell. Transp. Syst.* 2022.

[180] BORGHINI, G., ASTOLFI, L., VECCHIATO, G., MATTIA, D., and BABILONI, F. Measuring neurophysiological signals in aircraft pilots and car drivers for the assessment of mental workload, fatigue and drowsiness. *Neurosci. Biobehav. Rev.* 2014, 44, 58–75.

[181] ET AL., Y. P. Changes of eeg phase synchronization and eog signals along the use of steady state visually evoked potential-based brain computer interface. *J. Neural Eng.* 2020, 17, 1–20.

[182] PARIKH, P. and MICHELI-TZANAKOU, E. Detecting drowsiness while driving using wavelet transform. In *IEEE 30th Annual Northeast Bioengineering Conference*. 2004, 79–80.

[183] CHAUDHURI, A. and ROUTRAY, A. Driver fatigue detection through chaotic entropy analysis of cortical sources obtained from scalp eeg signals. *IEEE Trans. Intell. Transp. Syst.* 2020, 21(1), 185–198.

[184] GOLDBERGER, J., HINTON, G., ROWEIS, S., and SALAKHUTDINOV, R. Neighbourhood components analysis. *Adv. Neural Inf. Process Syst.* 2005, 17, 513–520.

[185] WANG, P., MIN, J., and HU, J. Ensemble classifier for driver's fatigue detection based on a single eeg channel. *IET Intell. Transp. Syst.* 2018, 12, 1322–1328.

[186] MOČKUS, J. On bayesian methods for seeking the extremum. *Lecture Notes in Computer Science*. 1975, 27.

[187] ET AL., A. S.-P. Quantification of signal-to-noise ratio in cerebral cortex recordings using flexible meas with co-localized platinum black, carbon nanotubes, and gold electrodes. *Front. Neurosci.* 2018, 12.

[188] HU, J. An approach to eeg-based gender recognition using entropy measurement methods. *Knowl. Based Syst.* 2018, 140, 134–141.

[189] ALICKOVIC, E., KEVRIC, J., and SUBASI, A. Performance evaluation of empirical mode decomposition, discrete wavelet transform, and wavelet packed decomposition for automated epileptic seizure detection and prediction. *Biomed. Signal Process. and Control*. 2018, 39, 94–102.

[190] SIDDIQUI, B. A. and KIM, P. Y., Anesthesia stages, Treasure Island, FL, 2024.

[191] SHALBAF, A., SAFFAR, M., SLEIGH, J. W., and SHALBAF, R. Monitoring the depth of anesthesia using a new adaptive neurofuzzy system. *IEEE J. Biomed. Health Inform.* 2018, 22(3), 671–677.

[192] KIM, Y. S. and OTHERS. Differential effects of sevoflurane and desflurane on frontal intraoperative electroencephalogram dynamics associated with postoperative delirium. *J. Clin. Anesth.* 2024, 93(5), 111368.

[193] ABDELAZIZ, H. A., DEAN, Y. E., and ELSHAFIE, A. M. A. Effect of three modalities on emergence agitation among post-traumatic stress disorder patients undergoing laparoscopy: a randomized controlled study. *BMC Psychiatry*. 2024, 78, 24.

[194] BOCSKAI, T. and OTHERS. Cost-effectiveness of anesthesia maintained with sevoflurane or propofol with and without additional monitoring: A prospective, randomized controlled trial. *BMC Anesthesiol.* 2018, 18(1), 1–8.

[195] CHEN, Y. F., FAN, S. Z., ABBOD, M. F., SHIEH, J. S., and ZHANG, M. Electroencephalogram variability analysis for monitoring depth of anesthesia. *J. Neural Eng*. 2021, 18(6), 066015.

[196] KLEIN, A. A. and OTHERS. Recommendations for standards of monitoring during anaesthesia and recovery 2021: Guideline from the association of anaesthetists. *Anaesthesia*. 2021, 76(9), 1212–1223.

[197] LAFERRIERE-LANGLOIS, P. and OTHERS. Depth of anesthesia and nociception monitoring: Current state and vision for 2050. *Anesth. Analg*. 2024, 138(2), 295–307.

[198] JIANG, Y. and SLEIGH, J. W. Consciousness and general anesthesia: challenges for measuring the depth of anesthesia. *Anesthesiology*. 2024, 140(2), 313–328.

[199] ZITANE, M. A. Z. H. and TORRES, D. F. M. Pharmacokinetic/pharmacodynamic anesthesia model incorporating psi-caputo fractional derivatives. *Comput. Biol. Med.* 2023, 167, 107679.

[200] KLOPMAN, M. A. and SEBEL, P. S. Cost-effectiveness of bispectral index monitoring. *Curr. Opin. Anesthesiol.* 2021, 24(2), 177–181.

[201] YOUSEFZADEH, S. H. Z. and OTHERS. Machine learning-guided anesthesiology: A review of recent advances and clinical applications. *J. Cell. Mol. Anesth.* 2024, 9(1), e145369.

[202] SHIN, H. W. and OTHERS. Monitoring of anesthetic depth and eeg band power using phase lag entropy during propofol anesthesia. *BMC Anesthesiol.* 2020, 20, 49.

[203] LIANG, Z. and OTHERS. Eeg entropy measures in anesthesia. *Front. Comput. Neurosci.* 2015, 9, 16.

[204] LIU, X. H. J. and OTHERS. Research on artificial intelligence based computer-assisted anesthesia intelligent monitoring and diagnostic methods in health care. *Neural Comput. Appl.* 2023, 2023.

[205] DUTT, M. I. and SAADEH, W. Monitoring level of hypnosis using stationary wavelet transform and singular value decomposition entropy with feed-forward neural network. *IEEE Trans. Neural Syst. Rehabil. Eng.* 2023, 31, 1963–1973.

[206] LIU, Q. W. F. and OTHERS. Inference of brain states under anesthesia with meta learning based deep learning models. *IEEE Trans. Neural Syst. Rehabil. Eng.* 2022, 30, 1081–1091.

[207] AFSHAR, S., BOOSTANI, R., and SANEI, S. A combinatorial deep learning structure for precise depth of anesthesia estimation from eeg signals. *IEEE J. Biomed. Health Inform.* 2021, 25(9), 3408–3415.

[208] BI, H. and OTHERS. Resting state functional connectivity analysis during general anesthesia: A high-density eeg study. *IEEE/ACM Trans. Comput. Biol. Bioinformatics*. 2022, 19(1), 3–13.

[209] LIU, Z. and OTHERS. Characteristics of eeg microstate sequences during propofol-induced alterations of brain consciousness states. *IEEE Trans. Neural Syst. Rehabil. Eng.* 2022, 30, 1631–1641.

[210] LIANG, Z. and OTHERS. Tracking the effects of propofol, sevoflurane and (s)-ketamine anesthesia using an unscented kalman filter-based neural mass model. *J. Neural Eng.* 2023, 20(2), 026023.

[211] LIU, J. and OTHERS. Analysis of amplitude modulation of eeg based on holo-hilbert spectrum analysis during general anesthesia. *IEEE Trans. Biomed. Eng.* 2024.

[212] DONG, K. and OTHERS. Intrinsic phase–amplitude coupling on multiple spatial scales during the loss and recovery of consciousness. *Comput. Biol. Med.* 2022, 147, 105687.

[213] LIU, Q., MA, L., and OTHERS. Sample entropy analysis for the estimating depth of anaesthesia through human eeg signal at different levels of unconsciousness during surgeries. *PeerJ*. 2018, 6, e4817.

[214] HIGHT, D., OBERT, D., KRATZER, S., SCHNEIDER, G., SEPULVEDA, P. *et al.* Permutation entropy is not an age-independent parameter for eeg-based anesthesia monitoring. *Front. Aging Neurosci.* 2023, 15, 1173304.

[215] RA, J. S., LI, T., and LI, T. A novel spectral entropy-based index for assessing the depth of anaesthesia. *Brain Informatics*. 2021, 8, 10.

[216] KALINICHENKO, A. N., MANILO, L. A., and NEMIRKO, A. P. Analysis of anesthesia stages based on the eeg entropy estimation. *Pattern Recognit. Image Anal.* 2015, 25, 632–641.

[217] AZAMI, H., LI, P., ARNOLD, S., ESCUDERO, J., and HUMEAU-HEURTIER, A. Fuzzy entropy metrics for the analysis of biomedical signals: Assessment and comparison. *IEEE Access*. 2019, 7, 104 833–104 847.

[218] NIERADKA, G. and BUTKIEWICZ, B. A method for automatic membership function estimation based on fuzzy measures. In *Proceedings of the International Fuzzy Systems Association World Congress Eds.* Berlin, Heidelberg: Springer, 2007, 4529, 45–53.

[219] CUESTA-FRAU, D. Slope entropy: a new time series complexity estimator based on both symbolic patterns and amplitude information. *Entropy*. 2019, 21(12), Art no, 1167.

[220] ZHANG, Y., WANG, Y., CHENG, H., YAN, F., LI, D. *et al.* Eeg spectral slope: A reliable indicator for continuous evaluation of consciousness levels during propofol anesthesia. *NeuroImage*. 2023, 283, 120426.

[221] SIMONS, S., ESPINO, P., and ABASOLO, D. Fuzzy entropy analysis of the electroencephalogram in patients with alzheimer's disease: is the method superior to sample entropy? *Entropy*. 2018, 20(1), 21.

[222] JOHNY ELTON, R., VASUKI, P., and MOHANALIN, J. Voice activity detection using fuzzy entropy and support vector machine. *Entropy*. 2016, 18(8), 298.

[223] NSUGBE, E. and CONNELLY, S. Multiscale depth of anaesthesia prediction for surgery using frontal cortex electroencephalography. *Healthc. Technol. Lett.* 2022, 9(3), 43–53.

[224] ALSAFY, I. and DIYKH, M. Developing a robust model to predict depth of anesthesia from single channel eeg signal. *Phys. Eng. Sci. Med.* 2022, 45, 793–808.

[225] SCHMIERER, T., LI, T., and LI, Y. A novel empirical wavelet sodp and spectral entropy based index for assessing the depth of anaesthesia. *Health Inf. Sci. Syst.* 2022, 10, 10.

[226] SHI, M. and OTHERS. Estimating the depth of anesthesia from eeg signals based on a deep residual shrinkage network. *Sensors*. 2023, 23(2), 1008.

[227] ACHARYA, U. R., FUJITA, H., and OTHERS. Application of entropies for automated diagnosis of epilepsy using eeg signals: A review. *Knowl.-Based Syst.* 2015, 88, 85–96.

[228] YENTES, J. M. and OTHERS. The appropriate use of approximate entropy and sample entropy with short data sets. *Ann. Biomed. Eng.* 2013, 41, 349–365.

[229] DONG, K. and OTHERS. An integrated information theory index using multichannel eeg for evaluating various states of consciousness under anesthesia. *Comput. Biol. Med.* 2023, 153, 106480.

[230] LI, Y. and OTHERS. Identification of the general anesthesia induced loss of consciousness by eeg spectrum analysis. *Int. J. Psychophysiol.* 2021, 168, 224–225.

[231] WANG, Z. and OTHERS. Cortical complexity and connectivity during isoflurane-induced general anesthesia: a rat study. *J. Neural Eng.* 2022, 19(3), 036009.

[232] HAGIHIRA, S. Brain mechanisms during course of anesthesia: what we know from eeg changes during induction and recovery. *Front. Syst. Neurosci.* 2017, 11, 39.

[233] KASHKOOLI, K. and OTHERS. Improved tracking of sevoflurane anesthetic states with drug-specific machine learning models. *J. Neural Eng.* 2020, 17(4), 046020.

[234] AKEJU, O. and OTHERS. Age-dependency of sevoflurane-induced electroencephalogram dynamics in children. *Br. J. Anaesth.* 2015, 115, 66–76.

[235] BLAIN-MORAES, S., LEE, U., and OTHERS. Electroencephalographic effects of ketamine on power, cross-frequency coupling, and connectivity in the alpha bandwidth. *Front. Syst. Neurosci.* 2014, 8, 114.

[236] MATEJCEK, M. and OTHERS. Effect of morphine on the electroencephalogram and other physiological and behavioral parameters. *Neuropsychobiology*. 1988, 19(4), 202–211.

[237] HIGHT, D. and OTHERS. Five commercial' depth of anaesthesia' monitors provide discordant clinical recommendations in response to identical emergence-like eeg signals. *Br. J. Anaesth.* 2023, 130(5), 536–545.

CURRICULUM VITAE

Mohammad Shahbakhti
mohammad.shahbakhti@ktu.edu

Education:

2009–2013	BSc in Biomedical Engineering, Faculty of Engineering, Dezful Branch, Islamic Azad University, Dezful, Iran
2018–2020	MSc in Biomedical Engineering, Kaunas University of Technology, Kaunas, Lithuania
2020–2024	Ph.D. in Electrical and Electronic Engineering, Kaunas University of Technology, Kaunas, Lithuania

Professional experience:

2014–2018	Head of the Biomedical Engineering Department, Mehr Private Hospital, Ahwaz, Iran
2021–2021	Digital Signal Processing Engineer, MXLabs, Wrocław, Poland
2022–Now	Researcher, Artinis Medical Systems B.V., Elst, the Netherlands

Areas of research interest:

Biomedical Signal Processing, Wearable, Filter Design, Sleep Analysis, DoA Monitoring, Brain Imaging, Nonlinear Analysis.

Awards and Honors:

#	Award	Issuer	Date
1	One-time incentive scholarship for high quality publications	KTU	Mar & Jun 2021, Jun 2022
2	The most active PhD students (Electrical and Electronic Engineering)	KTU	Dec 2021, Dec 2022, Dec 2023
3	LMT scholarship for study results	LMT	Mar 2022, Sep 2023
4	LMT travel grant	LMT	Feb 2023
5	STSM grant for mobility (Japan)	Cost-Action (CA18106)	Jan 2023
6	Conference travel grant (MeMeA 2023)	Cost-Action (CA18106)	Mar 2023
7	Publication grant (IEEE TNSRE)	Cost-Action (CA18106)	Apr 2023
8	Travel grant for the CNA 2023 summer school	NAWA	May 2023
9	Student Travel Grant for the MeMeA 2023 conference	IEEE IMS	Apr 2023
10	IEEE signal processing society scholarship for research activities	IEEE SPS	Sep 2023
11	Featured Articles	IEEE TNSRE & IEEE J-BHI	Mar 2021 & Mar 2022

The list of scientific papers and conferences related to the topic of the dissertation is given below.

LIST OF PUBLICATIONS ON THE DOCTORAL THESIS SUBJECT

Publications in the journals referred in the *Clarivate Analytics Web of Science* database with impact factor

1. **Shahbakhti, Mohammad**; Santos Rodrigues, Ana; Augustyniak, Piotr; Broniec-Wójcik, Anna; Sološenko, Andrius, Beiramvand, Matin; Marozas, Vaidotas. SWT-Kurtosis Based Algorithm for Elimination of Electrical Shift and Linear Trend from EEG Signals. *Biomedical Signal Processing and Control*. 2021. Art. no. 102373. vol. 65. [IF 5.076; Q2 2021].

2. **Shahbakhti, Mohammad**; Beiramvand, Matin; Nazari, Mojtaba; Broniec-Wójcik, Anna; Augustyniak, Piotr; Santos Rodrigues, Ana; Wierzchon, Michal; Marozas, Vaidotas. VME-DWT: An Efficient Algorithm for Detection and Elimination of Eye Blink from Short Segments of Single EEG Channel. *IEEE Transactions on Neural Systems and Rehabilitation Engineering*. 2021. vol. 29. p. 408-417. [IF 4.528; Q1 2021].

3. **Shahbakhti, Mohammad**; Beiramvand, Matin; Rejer, Izabela; Augustyniak, Piotr; Broniec-Wójcik, Anna; Wierzchon, Michal; Marozas, Vaidotas. Simultaneous Eye Blink Characterization and Elimination From Low-Channel Prefrontal EEG Signals Enhances Driver Drowsiness Detection. *IEEE Journal of Biomedical and Health Informatics*. 2022. vol. 29. no. 3. p. 1001-1012. [IF 7.7; Q1 2022].

4. **Shahbakhti, Mohammad**; Beiramvand, Matin; Eigirdas, Tomas; Solé-Casals, Jordi; Wierzchon, Michal; Broniec-Wójcik, Anna; Augustyniak, Piotr; Marozas, Vaidotas. Discrimination of Wakefulness From Sleep Stage I Using Nonlinear Features of a Single Frontal EEG Channel. *IEEE Sensors Journal*. 2022. vol. 22. no. 7, p. 6975-6984. [IF 4.3; Q1 2022].

5. **Shahbakhti, Mohammad**; Beiramvand, Matin; Nasiri, Erfan; Mohammadi Far, Somayeh; Chen, Wei; Solé-Casals, Jordi; Wierzchon, Michal; Broniec-Wójcik, Anna; Augustyniak, Piotr; Marozas, Vaidotas. Fusion of EEG and Eye Blink Analysis for Detection of Driver Fatigue. *IEEE Transactions on Neural Systems and Rehabilitation Engineering*. 2023. vol. 31. p. 2037-2046. [IF 4.800; Q1 2023].

6. **Shahbakhti, Mohammad**; Beiramvand, Matin; Hakimi, Naser; Rejer, Izabela; Lipping, Tarmo; Broniec-Wójcik, Anna; Solé-Casals, Jordi. Fusing Fuzzy Entropy With Gaussian and Exponential Membership Functions Outperforms Traditional Entropy Metrics in Monitoring the Depth of Anesthesia Using a

Single Frontal EEG Channel. *IEEE Sensors Letters*. 2024. vol. 8. no. 3. p. 1-4. [IF 2.200; Q2 2024]

7. **Shahbakhti, Mohammad**; Krycinska, Roza; Beiramvand, Matin; Hakimi, Naser; Lipping, Tarmo; Chen, Wei; Broniec-Wójcik, Anna; Augustyniak, Piotr; Tanaka, Toshihisa; Solé-Casals, Jordi; Wierzchon, Michal; Wordliczek, Jerzy. Wearable EEG-Based Depth of Anesthesia Monitoring: A Non-Parametric Feature Set. *IEEE Sensors Journal*. 2024. vol. 24. no. 11. p. 18098-18107. [IF 4.300; Q1 2024]

Publications referred in the *Clarivate Analytics Web of Science* database without impact factor

1. **Shahbakhti, Mohammad**; Beiramvand, Matin; Nasiri, Erfan; Chen, Wei; Solé-Casals, Jordi; Wierzchon, Michal; Broniec-Wójcik, Anna; Augustyniak, Piotr; Marozas, Vaidotas. The Importance of Gender Specification for Detection of Driver Fatigue using a Single EEG Channel. In *Proceedings of 14th Biomedical Engineering International Conference (BMEiCON)*. 2022. p. 1-3.

2. **Shahbakhti, Mohammad**; Beiramvand, Matin; Krycinska, Roza; Nasiri, Erfan; Chen, Wei; Solé-Casals, Jordi; Wierzchon, Michal; Broniec-Wójcik, Anna; Augustyniak, Piotr; Marozas, Vaidotas. A Reliable Method to Estimate the Bispectral Index Value Using a Single Frontal EEG Channel for Intra and Inter Subject Variability. In *Proceedings of 18th IEEE International Symposium on Medical Measurements and Applications (MeMeA)*. 2023. p. 1-5.

3. **Shahbakhti, Mohammad**; Beiramvand, Matin; Mohammadi Far, Somayeh; Solé-Casals, Jordi; Lipping, Tarmo; Augustyniak, Piotr. Utilizing Slope Entropy as an Effective Index for EEG-Based Depth of Anesthesia Monitoring. In *46th Annual International Conference of the IEEE Engineering in Medicine and Biology Society (EMBC)*. 2024. p. 1-4.

Conference presentation abstracts

1. **Shahbakhti, Mohammad**. Eye Blink Elimination in Short Segments of EEG. In *Polish IEEE Signal Processing Society Meeting*. 2020.

2. **Shahbakhti, Mohammad**. Detection of Driver Fatigue from Low and Single Prefrontal EEG Channel. In *Polish IEEE Signal Processing Society Meeting*. 2022.

3. **Shahbakhti, Mohammad**; Krycinska, Roza; Sole-Casals,Jordi; Wierzchon, Michal; Marozas, Vaidotas. Monitoring the Depth of Anesthesia Using

Parameter-free Features of a Single Prefrontal EEG Channel. In *Computational Neuroscience Academy*. 2023. p. 02.

LIST OF PUBLICATIONS WHICH ARE NOT DIRECTLY RELATED TO THE TOPIC OF DOCTORAL DISSERTATION

Publications in the journals referred in the *Clarivate Analytics Web of Science* database with impact factor

1. Mohammadi Far, Somayeh; Beiramvand, Matin; **Shahbakhti, Mohammad**; Augustyniak, Piotr. Prediction of Preterm Delivery from Unbalanced EHG Database. *Sensors*. 2022. Art. no. 1507. vol. 22. [IF 3.9; Q2 2022].

2. Hakimi, Naser; **Shahbakhti, Mohammad**; Sappia, Sofia; Horschig, Jörn M; Bronkhorst, Mathijs; Floor-Westerdijk, Marianne; Valenza, Gaetano; Dudink, Jeroen; Colier, Willy N. J. M. Estimation of Respiratory Rate from Functional Near-Infrared Spectroscopy (fNIRS): A New Perspective on Respiratory Interference. *Biosensors*. 2022. Art. no. 1170. vol. 12, [IF 5.4, Q1 2022].

3. **Shahbakhti, Mohammad**; Hakimi, Naser; Horschig, Jörn M; Floor-Westerdijk, Marianne; Claassen, Jurgen; Willy N. J. M. Estimation of Respiratory Rate during Biking with a Single Sensor Functional Near-Infrared Spectroscopy (fNIRS) System, *Sensors*. 2023. Art. no. 3632. vol. 23. no. 7. [IF 3.9; Q2 2023]

4. Mohammadi Far, Somayeh; Beiramvand, Matin; **Shahbakhti, Mohammad**; Augustyniak, Piotr. Prediction of Preterm Labor from the Electrohysterogram Signals Based on Different Gestational Weeks. *Sensors*. 2023. Art. no. 5965. vol. 23. no. 13. [IF 3.9; Q2 2023].

5. Beiramvand, Matin; **Shahbakhti, Mohammad**; Karttunen, Nina; Koivula, Reijo; Turunen, Jari; Lipping, Tarmo. Assessment of Mental Workload Using a Transformer Network and Two Prefrontal EEG Channels: An Unparameterized Approach. *IEEE Transactions on Instrumentation and Measurement*. 2024. Art. no. 4007010. vol. 73. [IF 5.6; Q1 2024].

Publications referred in the *Clarivate Analytics Web of Science* database without impact factor

1. Beiramvand, Matin; **Shahbakhti, Mohammad**; Lipping, Tarmo. Evaluating Mental Workload Through Cross-Entropy Analysis of Two Prefrontal EEG Channels. In *9th European Medical and Biological Engineering Conference*. 2024, p. 43-53.

2. Mohammadi Far, Somayeh; Beiramvand, Matin; **Shahbakhti, Mohammad**;

Augustyniak, Piotr. Combination of Empirical Mode Decomposition and Hjorth Parameters for Prediction of Preterm Labor Using Electrohysterogram Signals. In *46th Annual International Conference of the IEEE Engineering in Medicine and Biology Society (EMBC)*. 2024, p. 1-4.

ACKNOWLEDGMENTS

I guess George Ezra nailed it! Time does fly by in the yellow and green. As I write this, it is hard to believe that it has been nearly four years since I started my PhD adventure. I still remember my folks back in Iran thinking I was nuts when I said I am going to quit my hospital job as the Head of Biomedical Engineering Department to keep on my education abroad. Well, I went for it, and now I am rocking a gig as a full-time researcher at a top-notch company. It is great, innit?

When I hit this road, I casually mentioned to Vaidotas that KTU allows defending PhD without writing a whole dissertation if I publish four journal papers instead of two. He suggested I give it a shot, but I shrugged it off, thinking it is just not possible. Fast forward to today, and here I am, prepping my dissertation based on a whopping seven journal papers and six conference presentations while being cited more than 150 times. Crazy, right?

Along the way, I had the pleasure of collaborating with researchers from all corners of the globe, and let me tell you, building such a network was the best thing I achieved during my PhD. Looking back, I cannot believe all this unfolded. Well, as big Snoopy would say, big thanks to me for putting in the hard work and always believing in, well, me! Anyroad, let's not be self-centred and thank people who really had my back on this wild ride.

Though she is no longer me, my mother (RIP) was my main cheerleader pushing me to keep at it with my education. I bet she would be thrilled to see her son grabbing that PhD, and she could proudly call him Dr. Pitty you ain't here to see it, Ma. This thesis is for you, Narges Jan.

To my amazing wife Somayeh, who wholeheartedly made a massive sacrifice by backing my crazy plan to leave our country and study abroad. There were times I felt terribly guilty for putting you in such an uncomfortable spot. Trust me, surviving in dorms for three years ain't a walk in the park. Obviously, words cannot quite capture how thankful I am for your support and patience. Thanks a million, Hababeh.

To my best friend Matin, who, despite being a sleepy koala bear, burned the midnight oil with me while coding the algorithms we were developing together. Look, Matin, do not get me wrong—I still believe you have serious attitude problems, but this thesis would not be finished without having you by my side. Hope you find Finland as your new home, my anti-social homie!

To my gal pal Ana, who played a crucial role in crafting my first two papers. Her writing style rubbed off on me, and I've stuck with it ever since. Ana, I am still waiting for the day you lift 300 Kg. Your determination is off the charts, and I am confident you will nail it. Keep rocking sister!

To my wonderful Bi (Birute), a huge shoutout for her magnificent assistance in fine-tuning my applications for the LMT grants. It takes real guts to chase your

dreams instead of sticking to the same job you have been doing for the past six years. Wishing you nothing but massive success on your Data Science journey, although you are already killing it!

To my beloved Catalan amic, Jordi, you are the real MVP who turned my dream of seeing cherry blossoms in Japan into reality. I cannot thank you enough. The support you provided for my travels is truly priceless. I genuinely hope our paths cross again someday.

To the wonderful professor Augustyniak, who has been an avid supporter of my work since we first crossed paths during my internship under his supervision. Believe me, I have tried many times, but it is still challenging for me to call you by your first name. Hopefully, we go to the Szalone Widelce together soon. By the way, so far, Krakow is still the best city I have ever lived in.

To my awesome work mentors, Willy and Jorn, big thanks for having my back! You guys took a chance on me, offering a full-time researcher gig while I was still a student. Let me tell you, it was a game-changer. Knowing I had a solid plan for the future made diving into a stress-free PhD journey all the better. Your support has paved the way for Somayeh and me to kick-start a new chapter here in the Netherlands. Cheers to you both!

To Alma and Vaidotas, who warmly welcomed Somayeh and me into their home on multiple occasions, even though we were exotic foreigners :D. BTW, Vaidotas, the BBQ chicken was awesome! I hope we can reciprocate the hospitality by hosting you here in the Netherlands someday.

Last but certainly not least, I want to express my gratitude to my father and three beautiful, albeit a bit crazy, sisters for their unwavering support. When I had no one else to cover the expenses for my research, you generously funded it with your own money. I am at a loss for words to convey my heartfelt thanks.

I sincerely adore you all.

UDK 616.831-073:004.9+616.8-009.83](043.3)

SL 344. 2024-09-10, 20 leidyb. apsk. l. Tiražas 14 egz. Užsakymas 157.
Išleido Kauno technologijos universitetas, K. Donelaičio g. 73, 44249 Kaunas
Spausdino leidyklos „Technologija“ spaustuvė, Studentų g. 54, 51424 Kaunas